GAMMA-RAY SPECTROSCOPY

with particular reference to detector and computer evaluation techniques

P. QUITTNER, Ph.D., C.Sc.

ADAM HILGER LTD
LONDON

English text revised by

D. A. Durham, Ph.D.

Joint edition with Akadémiai Kiadó, Budapest

Published in Great Britain by

ADAM HILGER LTD
Rank Precision Industries Ltd
31 Camden Road
London NW1 9LP

SBN 85274 227 4

Printed in Hungary

CONTENTS

PREFACE

In the late forties and early fifties it was widely thought not only by the man in the street but also by well-known futurologists that the second half of the twentieth century would be identified as the nuclear age. However, in the sixties the use of computers became so common and indispensable in nearly every part of our lives that the expression 'nuclear age' has been more and more often replaced by 'the era of the computer'. It is impossible to predict whether people of later centuries will label our decades as the years of nuclear energy, computerization, or the beginning of space exploitation.

Nuclear pwer stations and computers liberate man from most of his physical and non-essential but time-consuming intellectual work and give him the possibility to concentrate his efforts on solving the most important and exciting problems of nature, life and society. Space vehicles free man from his home planet and open up dimensions inconceivable a few years ago. How fruitful will be this liberty brought by modern science to mankind, depends on man himself.

In the early days of nuclear physics, evaluation of measurements did not need sophisticated numerical calculations. The total number of observed flashes on a scintillating screen, or later the accumulated counts of a GM tube, both representing the intensity of radiation, were the main available experimental data. The technical development of nuclear devices proceeded nearly parallel with the construction of computers, and nuclear measuring equipment has become more and more sophisticated. First scintillation and later semiconductor detectors coupled to multi-channel analysers yielded a tremendous amount of information from even one measurement. To evaluate this mass of data computers were needed, and since then computers have had an important role in nuclear physics. A decade ago, they were used only to perform numerical calculations for rapid evaluation of measured data or to solve numerically the complicated equations of theoretical physicists. But at present besides performing these tasks, computers have become an essential integral part of the modern experimental physicist's laboratory. They help to plan his experiment, control the whole experimental set-up during his measurements, continually evaluate the recorded data and from these decide what to do next, and at the end of the experiments give the final answer to the problem.

With such an arsenal of technical apparatus, the only task of the physicist seems to be to find a suitable, scientifically interesting problem, to program the computer to control and evaluate the experiment, to summarize the results in a form understandable to his colleagues, and obtain funds to

purchase all the necessary equipment. Anyone who has worked in the field of physics, however, knows that sometimes a completely satisfactory solution of these 'slight' problems may not be very easy.

In the present book the use of computers in modern scintillation and semiconductor gamma-ray spectrometry is described. Besides a compilation of the author's own experiences in the Nuclear Physics and Nuclear Chemistry Laboratories of the Central Research Institute for Physics, Budapest, in the National Bureau of Standards, Washington, D.C. and at Texas A. and M. University, College Station, Texas, the literature has been reviewed till the end of 1969, but some of the later papers published during the writing of the manuscript have also been incorporated into the text.

The author is very grateful to Prof. R. E. Wainerdi at Texas A. and M. University with whom he prepared his first summary on computerized gamma-ray spectroscopy. His thanks are also due to Dr. A. Simonits at the Central Research Institute for Physics, Budapest, and Dr. D. Kiss for their valuable comments and suggestions while preparing the manuscript, and to Dr. D. A. Durham for the revision of the English text.

P. QUITTNER

1. INTRODUCTION

The vast amount of information collected by modern semiconductor and scintillation detectors has led to the wide-spread use of computers in the interpretation and evaluation of spectral data. Nuclear levels and decay schemes have been determined by measuring the energy and intensity (and sometimes correlations) of the emitted gamma-rays. Instrumental activation analysis, based upon the use of gamma-ray spectrometry, has been developed into a rapid, non-destructive analytical method. Gamma-ray spectrometers have reached the point in reliability and cost where their use has become economical in several practical applications. Whole conferences, or complete sections of large conferences, have been devoted to the applications of computers in the measurement of nuclear radiation, e.g. refs. [1–4].

Despite the rapid growth of interest in computer methods in nuclear physics, only a few reviews have been published on this topic. Among these should be mentioned Lindenbaum's summary of the on-line applications [5], Gelertner's review of bubble and spark chamber data evaluation [6], and the book of Matalin, Csubarov and Náray [7].

Review studies devoted to some aspects of the computer evaluation of gamma-ray spectra have been published in the last few years, but except for the relatively short paper of Quittner and Wainerdi [8] they have not covered the whole subject. Gibbons [9] and Yule [10] summarized computer methods in activation analysis, Heath reviewed automated gamma-ray spectrometers [11], and Schonfeld, Kibbey and Davis' paper [12] can be regarded as a summary of the different methods of least-squares techniques for scintillation spectra resolution.

This review gives the main applications of computers to modern gamma-ray spectrometry, coupled with a short theoretical outline of the different methods, and refers to illustrative practical applications.

Due to the statistical nature of nuclear disintegrations and detection processes, counts in the individual energy intervals of observed gamma-ray spectra can differ considerably from their expected values. Chapter 2 deals with the statistics of nuclear measurements and with spectrum smoothing. Properly performed, spectrum smoothing removes most of the statistical fluctuations while retaining virtually all the significant features of the original data.

Chapter 3 describes in brief the main features of gamma-ray spectra and the determination of detector response functions for different energy gamma-rays. Giving the different analytical approaches to the shapes of full-energy peaks and that of the response function outside the full-energy peaks, an

algorithm is given to generate spectra of monoenergetic gamma-rays by interpolation from measured standard spectra. Examples of the application and limitation of calculated spectra are shown.

Chapter 4 deals with computer peak recognition and peak location in complex gamma spectra. After the trivial maximum-finding method, the details of the more sophisticated smoothed first derivative and generalized second differences are also shown.

In quantitative gamma spectroscopy the most important task is to determine the intensities of the individual components of complex spectra. Chapters 5, 6 and 7 deal with this problem.

Chapter 5 explains the different methods of peak area calculation, how to select the boundaries and approximate the shape of the peaks in a spectrum from which the intensities are calculated as the number of counts in the peak region. Both curve fitting and base line construction are described in detail and the merits of relative and absolute intensity determinations are discussed.

In Chapter 6 the analysis of complex gamma spectra by the method of weighted least-squares is amply described. Because the availability of high speed digital computers has made the numerical calculations a relatively simple matter, and for a given set of data this method usually gives the solution with the smallest statistical error, least-squares techniques are used extensively for spectrum decomposition. After an explanation of the basic concepts, gain and threshold compensation by computer programs, the selection of weighting factors, the effect of a missing component and the validity of the results are described.

Chapter 7 explains spectrum stripping and other methods which can be applied for intensity determination without the use of a computer.

Chapter 8 shows such illustrative examples as decay curve analysis, optimization and activation analysis programs, sensitivity calculations and on-line application of computers in modern gamma spectroscopy.

Chapter 9 describes in brief some special measuring apparatus while Chapter 10 gives the most frequently occurring experimental errors for which correction must be made by proper programming.

Numerous figures and references and several tables supplement the text.

2. STATISTICAL FLUCTUATIONS AND SPECTRUM SMOOTHING

This chapter describes briefly for the experimental nuclear scientist, how statistical methods may be applied to get more information from the measured data, and how accuracy and precision is limited by statistical fluctuations. The treatment presented here is neither rigorous nor complete. Only those subjects which are most frequently encountered in applied gamma-ray spectroscopy are dealt with. For a more comprehensive summary and the details, we refer the reader to the numerous textbooks published in this field, e.g. refs. [13–16].

2.1 STATISTICAL FLUCTUATIONS OF THE MEASURED COUNTS

Both the decay of radioactive nuclei and the detection of the emitted gamma-rays are statistical processes. It can not be predicted exactly either when a certain nucleus disintegrates or how many nuclei will decay from a given specimen in a definite time interval. Even if we knew the exact number of disintegrations, this would not determine unambigously the number of counts measured by any type of radiation detector because the detection process itself is also statistical in nature. The laws of probability govern the whole phenomena, and the most we can do from a knowledge of all the essential parameters of the disintegration and detection processes, is to predict the expected number of measured counts and its scatter.

In actual experiments this situation is reversed. Nuclear parameters, most often intensities and half-lives, must be determined from the measured counts. Due to the ambiguity mentioned above this can not be performed exactly. Results obtained from nuclear measurements always have an inherent statistical error. Several authors have discussed the statistics of nuclear detection processes. This problem is amply discussed, and the special needs of the experimental nuclear scientist emphasized, e.g. in Jánossy's book *Theory and Practice of the Evaluation of Measurements* [13].

In gamma spectroscopy the most often occurring problems are (1) the measurement of gamma energy from the shape of the pulse-height distribution; (2) the determination of half-life from the time-dependence of the counts; and (3) the calculation of the (individual) gamma-ray intensities from the number of counts in a given region of the spectrum. The first problem will be answered in Section 3.2 and Chapter 4, the second in Section 8.1, and the third in Chapters 5 and 6. The influence of statistical fluctuations on energy and/or half-life measurement is lessened by proper smoothing or curve fitting. Therefore, in this section we restrict ourselves only to their effect on intensity determination.

The intensity of a radioactive source containing A_0 radioactive nuclei at $t = 0$, is a step function which oscillates around its expected value

$$I(t) = I_0 e^{-\lambda t} = \lambda A_0 e^{-\lambda t}. \tag{2.1}$$

where I_0 and $I(t)$ are the intensity of the source at $t = 0$ and t, respectively and λ is the decay constant related to the half-life ($T_{1/2}$) of the nucleus as $\lambda = \ln 2/T_{1/2}$.

In deriving Eq. (2.1), it has been assumed that the source contains only one type of radioactive nuclei. If there are nuclei with different decay constants (i.e. half-lives) present, and the decay of each individual component is independent of any other one, then the total intensity, I, is the sum of the intensities of the individual components, I_k,

$$I(t) = \sum_{k=\text{all comp.}} I_k(t) = \sum_k I_{k0} e^{-\lambda_k t} = \sum_k \lambda_k A_{k0} e^{-\lambda_k t}. \tag{2.2}$$

If we denote by p the probability that a gamma-ray will be detected after a decay (this detection can mean either the simple registration of the photon or the registration of a pulse caused by this particle falling into a predefined amplitude interval), then neglecting dead-time effects the expected counts collected by the detector during the period (t_1, t_2) are

$$N(t_1, t_2) = \int_{t_1}^{t_2} I(t)\, p(t) dt = p \int_{t_1}^{t_2} I(t) dt \tag{2.3}$$

as in most experiments p is time-independent.

Due to the finite dead-time of the detector, particles interacting with the material in its sensitive volume within this time will not be detected separately, but will be recorded as being only one event. This effect causes an apparently lower counting rate than the true one. The dead-time correction depends on the type of detector, but in most practical cases it can be approximated by

$$N_{\text{corr}} \approx \frac{N}{1 - N_r \tau_D}. \tag{2.4}$$

where N_{corr} and N are the dead-time corrected and the measured counts, respectively, N_r the (uncorrected) counting rate, and τ_D is the dead-time of the detector. The arguments t_1, t_2 have been omitted for brevity.

If N_{corr}, calculated from N, is substituted into $\langle N(t_1, t_2)\rangle$, I_0 can be determined from Eqs. (2.3) and (2.1). As there is only a certain probability that $N_{\text{corr}} = N_{\text{true}}$, the same applies to the I_0 intensity calculated from the result of this measurement; there is only a certain probability that it is equal to the true intensity, $I_{0,\,\text{true}}$. If there are different types of decaying nuclei, so that Eq. (2.2) should be used instead of Eq. (2.1), then the number of measurements should be equal to or larger than the number of the components (see Section 8.1).

It can be shown that not only the number of decayed nuclei but that of the detected gamma photons too follows Poisson's distribution. This means

that the scatter of the measured value is

$$\sigma^2(N) = \langle N \rangle \approx N_{\text{corr}} \approx N \tag{2.5}$$

and the relative scatter of the intensity is

$$\frac{\sigma(I_0)}{I_0} \approx \frac{\sigma(I_{0,\text{true}})}{I_{0,\text{true}}} \approx \frac{1}{\sqrt{N}}. \tag{2.6}$$

For the experimental physicist or chemist the meaning of this equation is that he knows that the relation

$$I_0 - \alpha(\varepsilon)\,\sigma(I_0) < I_{0,\text{true}} < I_0 + \alpha(\varepsilon)\,\sigma(I_0) \tag{2.7}$$

is true with a probability $1 - \varepsilon$, where ε is the confidence parameter. Provided that $N \gg 1$, $\alpha(\varepsilon) = 2$ gives a 0.95 and $\alpha(\varepsilon) = 3$ gives a 0.997 probability that (2.7) is valid.

As can be seen from Eqs. (2.5) or (2.6), the larger the number of collected counts the smaller is the error of the intensity calculated from them. In mathematics, $N \to \infty$ needs only good imagination and can be achieved without any difficulties, but in real physical experiments this never comes true as either the equipment or the patience of the researcher breaks down. For these, and also for some other reasons, the measuring time and the accumulated counts are always finite. What we can do is to distribute the time between the different types of measurement so that we should obtain maximum statistical accuracy, and to repeat the measurement several times not only to obtain better statistical accuracy from the larger numbers but also to check the stability of the equipment.

If a measurement is repeated k times, then the best approximation of the true value of its result obtainable from these data is

$$\overline{m} = \frac{\sum_{i=1}^{k} m_i/\sigma_i^2}{\sum_{i=1}^{k} 1/\sigma_i^2},$$

where the m_i's are the results of the individual measurements and the σ_i's their standard deviations. In the special case when all σ_i's are equal $\overline{m}$ is the arithmetical mean

$$\overline{m} = \frac{1}{k} \sum_{i=1}^{k} m_i$$

and

$$\sigma(\overline{m}) \approx \frac{1}{\sqrt{k}}\,\sigma_i.$$

The small difference between $\sigma(\overline{m})$ and σ_{exp} is due to the fact that $\overline{m}$ is not known *a priori:* it is substituted from the measured $\overline{m}_i$'s. Therefore the individual components of σ_{exp} are not completely independent and their standard deviation is somewhat smaller than that of independent components. However, the difference is negligible in practice, where usually $k \gg 1$.

In this frequently occurring case the experimentally observed variance is defined as

$$\sigma^2_{\text{exp}} = \frac{1}{k-1} \sum_{i=1}^{k} (\overline{m} - m_i)^2 .$$

If $\sigma_{\text{exp}} \approx \sigma_i$ is not valid, then the different results of the individual measurements are caused not only by statistical fluctuations but also by other factors. In this case a thorough investigation must be made which can sometimes lead to new physical discoveries, but usually shows up some instrumental instability or other experimental error.

In practice, intensities are always determined as the difference and/or the ratio of two activities. Without going into the details, which can be found in Chapter IX of ref. [13], we quote only the results for optimum time scheduling for measuring approximately constant intensities:

(1) When a difference, $I_1 - I_2$, is to be determined, the best result is obtained when more time is spent on the measurement of the larger intensity, I_1, than on the measurement of the smaller one, I_2. The total measuring time should be divided between the two measurements in proportion to the square roots of the intensities.

(2) When the ratio I_1/I_2, or I_2/I_1, of two intensities is to be determined, the best result is obtained when more time is spent on the measurement of the smaller intensity, I_2, than on the measurement of the larger one, I_1. The total measuring time should be divided between the two in inverse proportion to the square roots of the intensities. The explanation of these 'contradictions' in optimal time distribution is that to obtain the variance of the result in the first case the absolute variances are added, so even a relatively large error in the smaller component does not give a large contribution to the total variance, while in the second one the relative variances are summed, so the smaller component has to be determined with higher absolute precision. As the precision is not very sensitive to the actual time division near the optimum, in practice a short preliminary measurement or calculation must be made to determine the time schedule of the actual measurement.

If the measuring time can be much larger than the half-life of the decaying radioisotope the initial activity of which is smaller than the background, then in practice the best precision is obtained by integrating the counts over a period approximately twice as long as the corresponding half-life [17].

2.2 SPECTRUM SMOOTHING

Due to the statistical nature of nuclear disintegrations and detection processes, counts in the individual energy intervals (channels) of observed gamma-ray spectra can differ considerably from their expected values. Such channel-to-channel scattering results in small changes in the shapes of spectra being overlooked. As there is a definite correlation between the counts of adjacent channels, by a properly performed procedure, using counts of neighbouring channels, most of the statistical fluctuations can be removed while retaining virtually all the significant features of the original

data. This mathematical procedure is called spectrum smoothing. Although the production of smooth spectra is usually an intermediate step only, followed by other data reduction procedures, we discuss spectrum smoothing separately because it is so often used (sometimes even unnecessarily).

The channel-by-channel statistical fluctuations can be regarded as noise on the expected shape of the spectrum; therefore, they can be filtered out partly from the Fourier spectrum of the measured spectrum in the same way that a suitable filter circuit removes most of the noise differing in frequency from a desired electrical signal, and the high frequency part of the Fourier transform is cut off. Another solution for lessening statistical fluctuations is to perform a convolution integral with a suitable filter response curve between the measured data, assuming some distribution function for the counts in the individual channels of the entire spectrum [18].

Instead of highly sophisticated methods, a much simpler smoothing procedure can be applied in nearly every practical case. A small portion of the measured spectrum can be well approximated by a polynomial. This polynomial can be determined by a least-squares fitting to the measured data. It can be shown that the values and the derivatives of this polynomial can be expressed as functions of the measured counts as follows:

$$Y_{n,m}(i) = \frac{1}{K_{n,m}} \sum_{k=-m}^{m} c_{k,n,m} y(i+k). \tag{2.8}$$

where $Y_{n,m}(i)$ is the nth derivative of the smoothed spectrum in channel i ($n = 0$ denotes the smoothed spectrum), $y(i + k)$ is the measured count in channel $(i + k)$, $c_{k,n,m}$ and $K_{n,m}$ are constants independent of the spectra, and $m' = 2m + 1$ data points were used for fitting the polynomial, i.e. for smoothing [19]. In practice, fitting with a second or third degree polynomial is sufficient, and for intensity determination and peak location, in addition to the smoothed spectrum, only a knowledge of the first two derivatives is necessary. Numerical values of the smoothing constants, $K_{n,m}$ and $c_{k,n,m}$ are listed in Table I for second and third degree polynomial fitting.

The optimum number of points used for smoothing depends upon the shape of the fitted region. If m' is too large, the smoothing flattens peaks and fills in valleys, and the original features of the spectrum become distorted. On the other hand, if m' is too small, scatters in the individual channels of the smoothed spectrum do not decrease sufficiently, so the significant features of the spectrum will not come out. Assuming that the spectrum does not vary rapidly in the region used for calculating the smoothed value, and that the scatter of the counts is caused only by statistical fluctuations (not by electronic or other experimental instabilities), the error of the smoothed data is:

$$\Delta Y_{n,m}(i) \approx \Delta_{n,m} \sqrt{y(i)}\,,$$

where the $\Delta_{n,m}$ values are listed in Table II for fitting by second and third degree polynomials. As a general guide, it is reasonable to use 1–2 channels less in the smoothing than the energy resolution of the detector (FWHM) in the region in question [20].

Table I. Numerical Values of the

Degree of fitting polynomial	Order of derivative, n	$m' = 2m + 1$	$K_{n,m}$			
				0	1	2
2 or 3	0	5	35	17	12	−3
		7	21	7	6	3
		9	231	59	54	39
		11	429	89	84	69
		13	143	25	24	21
		15	1105	167	162	147
2	1	5	10	0	1	2
		7	28	0	1	2
		9	60	0	1	2
		11	110	0	1	2
		13	182	0	1	2
		15	280	0	1	2
3	1	5	12	0	8	−1
		7	252	0	58	67
		9	1188	0	126	193
		11	5148	0	296	503
		13	24024	0	832	1489
		15	334152	0	7506	13843
2 or 3	2	5	7	−2	−1	2
		7	42	−4	−3	0
		9	462	−20	−17	−8
		11	429	−10	−9	−6
		13	1001	−14	−13	−10
		15	6188	−56	−53	−44

Sometimes, the statistical fluctuation is considerable even in the smoothed spectrum. In this case it is often advantageous to repeat the smoothing, i.e. smoothing the smoothed data. It can be shown that a smoothing repeated l times, each time from $2m + 1$ points, is equivalent to a modified smoothing using $2ml + 1$ points [19]. The repeatedly smoothed values can also be expressed as linear combinations of the measured data, but the coefficients differ from that of Eq. (2.8), giving larger weight to the counts near the centre of the smoothing. The effect of five-point smoothing on a small peak to find

Table II. Ratio of the Statistical Scatter of the Smoothed Data to that of the Measured One, $\Delta_{n,m}$

Order of derivative, n	Degree of fitting polynomial	Number of points used in smoothing, m'					
		5	7	9	11	13	15
0	2 or 3	0.698	0.577	0.505	0.455	0.418	0.389
1	2	0.316	0.189	0.129	0.095	0.074	0.060
1	3	0.950	0.513	0.338	0.246	0.189	0.152
2	2 or 3	0.534	0.218	0.114	0.068	0.044	0.031

Smoothing Constants $K_{n,m}$ and $c_{k,n,m}$

k					
3	4	5	6	7	$c_{-k,n,m}$
−2					$c_{k,n,m}$
14	−21				
44	9	−36			
16	9	0	−11		
122	87	42	−13	−78	
3					$-c_{k,n,m}$
3	4				
3	4	5			
3	4	5	6		
3	4	5	6	7	
−22					$-c_{k,n,m}$
142	−86				
532	294	−300			
1796	1578	660	−1133		
17842	18334	14150	4121	−12922	
5					$c_{k,n,m}$
7	28				
−1	6	15			
−5	2	11	22		
−29	−8	19	52	91	

its maximum for energy determination and boundary values for a peak area calculation is shown in Fig. 1.

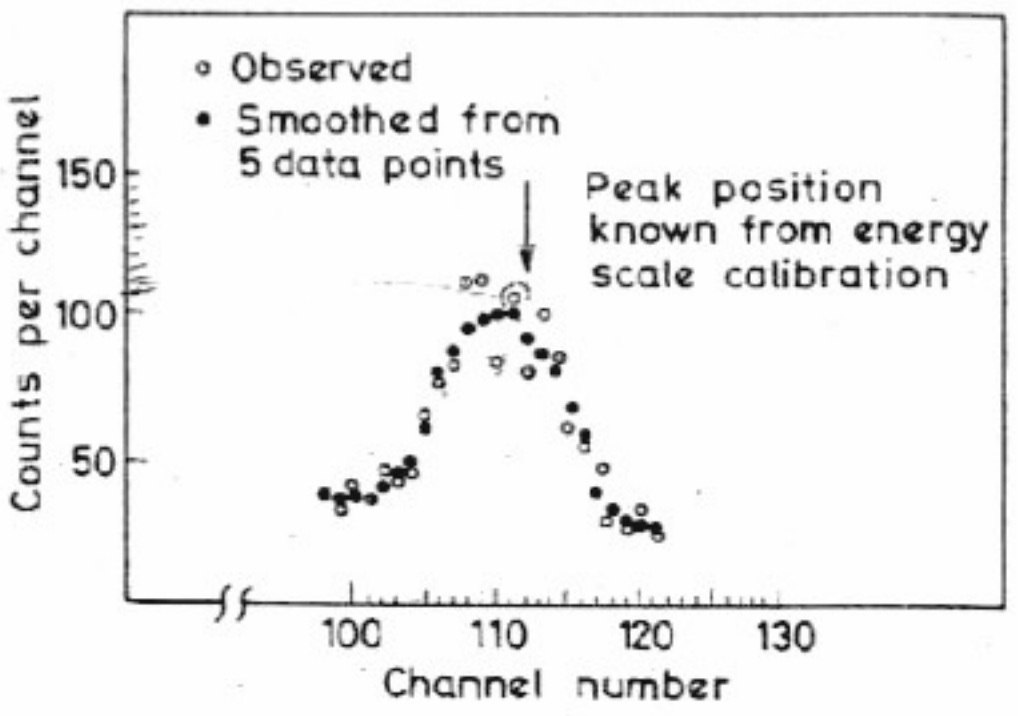

Fig. 1. Effect of smoothing from five points on a small peak. The centre of the peak known from energy calibration, is in channel 111

3. DETERMINATION OF DETECTOR RESPONSE FUNCTION

3.1 GENERAL DESCRIPTION

Gamma-rays interact with matter in three principal processes: photoelectric effect, Compton scattering and pair production. These processes are discussed at length in all basic nuclear physics texts (e.g. refs. [21–23]). The possibility for different interactions under identical circumstances causes even the theoretical detector response function for monoenergetic gamma-rays to be very complicated. In practice, other effects, such as bremsstrahlung, annihilation, escape, backscattering, multiple internal scattering, pulse pile-up, statistical fluctuations in the gamma-ray energy to pulse-height conversion, inhomogeneity in the detector, etc., contribute to the pulse-height spectrum; therefore, response functions calculated by the Monte Carlo method from the physical processes either for NaI(Tl) [24, 25] or for Ge(Li) detectors [26, 27] are usually inadequate for quantitative analysis.

The usual procedure for constructing a pulse-height distribution caused by monoenergetic gamma-rays of a desired energy is to measure the spectra of a number of suitable monochromatic gamma-rays and to carry out an interpolation between these experimental spectra. The disadvantage of this method is that the calculated spectra are correct only for the particular experimental arrangement in which the calibrating spectra were measured. Change of the detector or any variation in the source positioning or in the surrounding affects the response function and can cause erroneous results, as will be discussed in Chapter 10.

A list of isotopes used to calibrate the measuring apparatus and calculate the detector response to monoenergetic gamma-rays is given in Table III along with their most widely used production method, decay mode, half-life, the energy of the gamma-ray, the percentage of decays which result in the desired photons and other disturbing radiations, excluding low energy X-rays, emitted by the same source for which correction must be considered.

Detailed descriptions of the different physical processes contributing to the pulse-height spectrum, and their influence on the shape of the detector response function are described in the literature [22, 29–31]. To generate pulse-height spectra from calibrating pulse distributions, it is sufficient to realize the main features in the spectra of monoenergetic gamma-rays. These are the following: full-energy peak, Compton edge, Compton continuum, annihilation escape peaks, annihilation peak, backscatter peak, bremsstrahlung and X-ray escape peak (Fig. 2). There is a full-energy peak, backscatter peak, Compton continuum and Compton edge in every experimentally measured gamma-ray spectrum. Bremsstrahlung is present significantly only if the source emits β-rays as well. Escape peaks occur only

Table III. Sources Used for Calibrating the Detector Response to Monoenergetic Gamma-Radiation

Source	Production	Decay	Half-life[a]	$E\gamma$[a] (keV)	Rel. Intensity[a] (% of decays)	Accompanying radiation[a,b]		
						$E\gamma$ (keV)	(%)	$E\beta_{max}$
^{125m}Te	n, γ	IT	58 d	110	0.3	35	7	
^{134m}Cs	n, γ	IT, β^-	2.9 h	128	14			550
^{141}Ce	n, γ	β^-	33 d	145	48			580
^{47}Sc	n, p	β^-	3.4 d	160	73			600
^{139}Ce	n, γ	EC	140 d	165	80			
^{97}Ru	n, γ	EC	2.8 d	215	91	324	8	
^{203}Hg	n, γ	β^-	47 d	279	77			214
^{51}Cr	n, γ	EC	28 d	320	9			
^{115m}In	n, γ	IT, β^-	4.5 h	335	50			830
^{113m}In	^{113}Sn decay,	IT	1.7 h	393	64			
^{7}Be	d, n; p, α	EC	53 d	477	10			
^{85}Sr	n, α	EC	64 d	514	100			
^{91m}Y	fission[d]	IT	50 m	551	95			
^{137}Cs	fission	β^-	30 y	662	85			1176
^{95}Nb	fission	β^-	35 d	765	100			160
^{54}Mn	p, n	EC	303 d	835	100			
^{92m}Nb	α, n	EC	10 d	934	99			
^{65}Zn	n, γ	EC, β^+	245 d	1115	49	511[e]	34.	
^{22}Na	d, α	β^+, EC	2.6 y	1275	100	511[e]	181	545[f]
^{41}Ar	n, γ	β^-	1.8 h	1293	99			1198[f]
^{24}Na	n, γ	β^-	15 h	1369	100	2754	100	1389[f]
^{52}V	n, γ	β^-	3.8 m	1434	100			2470
^{42}K	n, γ	β^-	12 h	1524	18	310	0.2	3520
^{28}Al	n, γ	β^-	2.3 m	1780	100			2850
^{38}K	α, n; d, α	β^+	7.7 m	2170	100	511[e]	200	2680
^{24}Na	n, γ	β^-	15 h	2754	100	1369	100	1389[f]
^{12}C	n, n	β^-	—	4430				

[a] Data from ref. [28].
[b] X-rays not listed
[c] From the β^- decay of ^{114}Cd
[d] Some other weak γ rays are present in these nuclides or their daughters.
[e] From positron annihilation
[f] Higher energy β group exists with much weaker intensity.

if the gamma-energy exceeds ~1.2 MeV. Annihilation peaks are found only if the gamma transition is preceded by a β^+-decay or $E\gamma \gtrsim 1.2$ MeV. X-ray escape peaks in scintillation detectors can be resolved from the full-energy peaks only for low energy photons, and the X-rays following the photo-electric absorptions can leave the detector without being absorbed if the interactions took place near the surface, i.e. for low-energy gamma-rays. For very high energy gamma-rays, $E\gamma \gtrsim 5$ MeV, the escape of the brems-strahlung produced by the recoil electrons must also be taken into account, especially for Ge(Li) detectors.

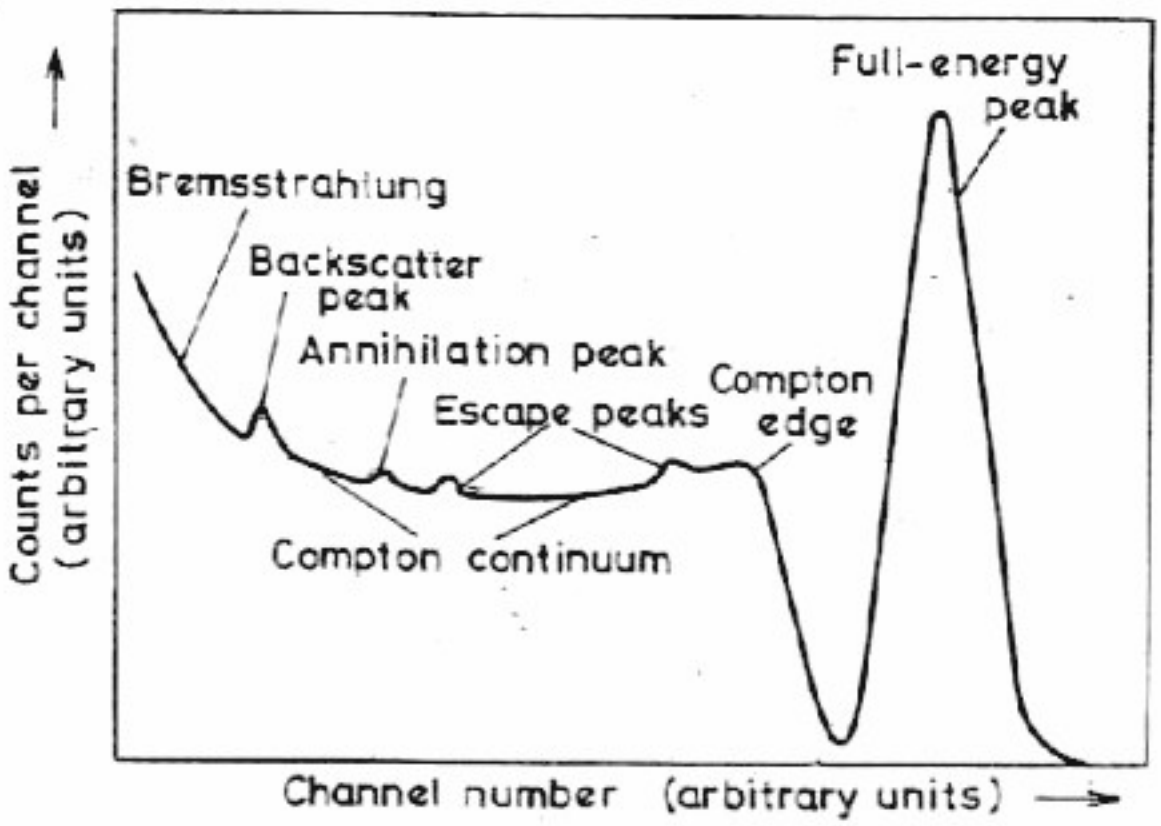

Fig. 2. Main features of detector response function for monoenergetic gamma-rays. Full-energy peak, backscatter peak, Compton edge and continuum are in every spectrum

3.2 SHAPE OF THE FULL-ENERGY PEAK

The full-energy peak is produced by events in which the total energy of the incident photon is absorbed in the detector. Therefore, its position contributes to the energy measurement of the radiation and, through this, often to the identification of the emitting nuclei. For low energy gamma-rays and small detectors it corresponds to the total energy transfer to a single electron in a photoelectric process; therefore, it is often termed 'photopeak'. However, at medium and high energies and in large detectors, many signals in the full-energy peak are produced by single or multiple Compton scatterings, followed by the photoelectric absorption of the scattered photon or by pair production when both of the annihilation gammas are absorbed in the detector. Since the total photon energy is absorbed in the detector for a signal falling into the full energy peak, it is often referred to as 'total absorption peak'.

The statistical processes in the detector, following the energy transfer to the electrons, broaden the line corresponding to total energy loss; the calculated shape of the full-energy peak, $\bar{y}(x)$, can be approximated as a Gaussian:

$$\bar{y}(x) = A e^{-\frac{(x-p)^2}{2\sigma^2}}, \tag{3.1}$$

where x is the pulse-height, A is the amplitude, and p is the centre of the peak. The scatter of the Gaussian is related to the resolution of the detector, Γ, (full width at half maximum, FWHM) as $\Gamma = 2.355\,\sigma$, and the area under the peak is $N = 1.064\ A\ \Gamma$.

Multiple Compton scattering, non-linearity in the electron energy to pulse-height conversion, and wall effects in the detector distort the low-energy side of the Gaussian. (Besides these 'statistical', intensity-independent distortions, pulse pile-up also alters shapes of the spectra. This activity-dependent distortion will be discussed in Section 10.3.)

For this reason, the parameters A, p and Γ are calculated from an iterative least-squares fitting to the measured data, $y(x)$, only between $p - \sigma$ and $p + 3\sigma$. From the approximate starting values, A_0, p_0 and σ_0, $Z(i) = y(i) - \bar{y}(i)$ is calculated for each point, and a linear least-squares fitting is performed to calculate ΔA, Δp, and $\Delta\sigma$ by minimizing the expression

$$\sum_{i=p_0-\sigma_0}^{p_0+3\sigma_0} w(i)\left[Z(i) - \frac{\partial\bar{y}}{\partial A}\Delta A - \frac{\partial\bar{y}}{\partial p}\Delta p - \frac{\partial\bar{y}}{\partial\sigma}\Delta\sigma\right]^2 \qquad (3.2)$$

where $w(i)$'s are the weighting factors, usually 1, $y(i)^{-1}$ or $\exp[-(i-p_0)/2\sigma_0^2]$. A_0, and the response function is regarded as a discrete function of the channel number i. (The derivatives are taken in the point $\bar{y}(A_0, p_0, \sigma_0)$.) Then the whole calculation is repeated with the new $A_1 = A_0 + \Delta A_0$, $p_1 = p_0 + \Delta p$, $\sigma_1 = \sigma_1 + \Delta\sigma$ values calculating the next approximation. The iteration is finished when the new parameter values do not differ substantially from the previous ones or the number of iterations exceeds a given number. In practice, the method is not very sensitive to the starting values and sufficient convergence is nearly always achieved after 3–5 iterations.

A desire for more precise calculations led Kowalski and Isenhour to use a hyperbolic secant [32], while Heath and his co-workers proposed a modified Gaussian of the form:

$$y(x) = A\,(1 + \alpha_1(x - p)^4 + \alpha_2(x - p)^{12}) \times \exp[-(x - p)^2 / 2\sigma^2], \qquad (3.3)$$

where the parameters A, p, σ, α_1, and α_2 must be determined for each peak. Using NaI(Tl) spectra, the powers 4 and 12 were found to be the best combination over the energy range of interest, and the measured data could be well fitted with Eq. (3.3) [29, 33]. For Ge(Li) data, a simple Gaussian, i.e. $\alpha_1 = \alpha_2 = 0$, was found to give better fitting, but even in this case there were differences between the measured and calculated full-energy peaks [34].

3.3 RELATIONS BETWEEN THE PEAK PARAMETERS

To calculate the shapes of full-energy peaks, Eqs. (3.1) or (3.3) can be used. When a peak is fitted, the parameters obtained can give information for several purposes. The peak-height (A) and the peak area usually serve for absolute or relative intensity determinations because for a given detector system and gamma-ray energy they are proportional to the intensity of the corresponding radiation. This problem will be discussed in detail in Section 4.1.

The peak position can be used either to calibrate the spectrometer by obtaining the pulse height vs. gamma-ray energy relationship from known

gamma energies, or, knowing this calibration curve, for calibrating the energies of gamma-rays and for the identification of the radiation source by its energy.

The peak position, p, is to a first approximation a linear function of the gamma-ray energy, E_γ. However, for very precise energy determination or pulse height vs. energy calibration, small deviations from linearity and proportionality must be taken into account. For Ge(Li) detectors these deviations are very small, and are mainly due not to the detector itself but to the electronics, amplifiers and pulse-height measuring devices [35, 36].

For scintillation detectors the deviations are more pronounced because the phosphors themselves have a slightly non-linear and a somewhat more pronounced non-proportional response to gamma-rays [37, 38]. From a least-squares fit to the peak positions of gamma-rays having well-known energies, Heath *et al.* [33, 34] found that for their NaI(Tl) spectrometer:

$$E_\gamma = k_1(-1.105 + h - 5.18\times10^{-4}h^2 + 8.11\times10^{-6}h^3 - 3.59\times10^{-8}h^4 + 5.04\times10^{-11}h^5) \quad (3.4)$$

and for their Ge(Li) detector

$$E_\gamma = k_2(0.455 + h + 2.63\times10^{-7}h^2) \quad (3.5)$$

where h is the pulse amplitude and k_1 and k_2 are constants. Although the actual numerical coefficients would be different for other detectors, their orders of magnitude can be regarded as representative. From the coefficient ratios in the different powers of h, the superior linearity and proportionality of the Ge(Li) detector is apparent. For the same NaI(Tl) detector the relative pulse-height vs. gamma-ray energy normalized to the 661 keV ^{137}Cs line can be seen in Fig. 3.

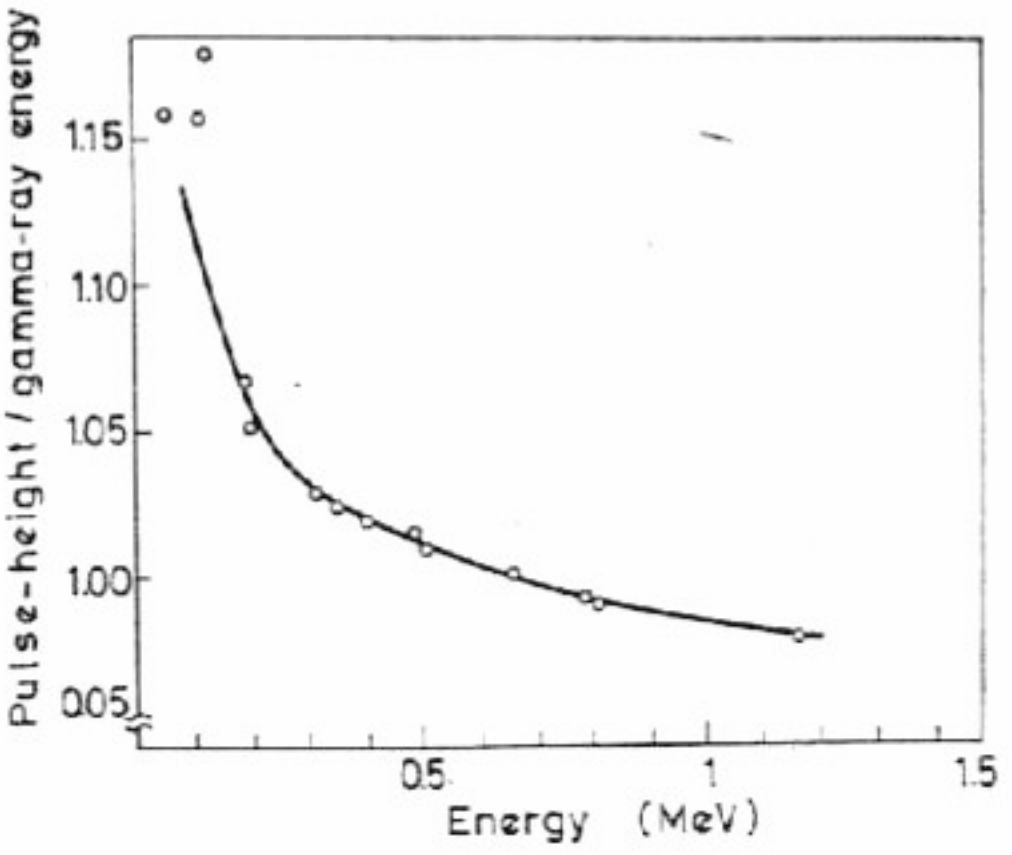

Fig. 3. Variation of the (pulse-height) / (gamma energy) ratio for a NaI(Tl) detector. The data are normalized to the 661 keV ^{137}Cs gamma-ray

The number of terms used in expressions of type (3.4) or (3.5) for energy vs. pulse-height calibration depends on the accuracy needed in the energy determination. However, there is a practical limit due to the instability and the finite resolution of the system. There is usually no reason to consider terms whose contribution is less than 0.05 FWHW or 0.25 times the shift which may occur through instabilities.

For most of the practical applications, (3.4) can generally be restricted for any scintillation detector to the first two terms. From this

$$h = k(E_\gamma + b) \quad \text{for} \quad E_\gamma > 100\,\text{keV} \quad \text{and} \quad b > 0\,.$$

For NaI(Tl) detectors this straight line intersects the energy axis between -15 and -30 keV depending somewhat on the crystal. Below 50 keV the $h(E_\gamma)$ curve is definitely not linear. Due to this non-linearity a sum peak will have an apparently higher energy than a monoenergetic one.

The resolution of the detector (full width at half maximum, FWHM), $\Gamma = 2.355\sigma$, depends on the statistical fluctuation in the number of electrons produced by the gamma-rays, on intrinsic noise effects in the detection system and on the channel width of the spectrometer. Due to the statistical effects $\Gamma^2 \sim E_\gamma$, while the contribution of the intrinsic effects is approximately constant for scintillation detectors. Therefore, a good agreement can be obtained by fitting

$$\Gamma \approx \sqrt{\Gamma_0^2 + aE_\gamma}, \tag{3.6}$$

where Γ_0 and a are constants and the second term usually dominates.

For semiconductor detectors Γ_0^2 depends on the detector capacity and is comparable with aE_γ, since the energy required for the production of an electron-hole pair is about two orders of magnitude less than that of producing a photoelectron reaching the first dynode of the photomultiplier. For this reason the (number of electrons and/or holes)/(unit gamma-ray energy) is larger by the same magnitude, and the higher number of statistical processes leads to a smaller relative statistical fluctuation.

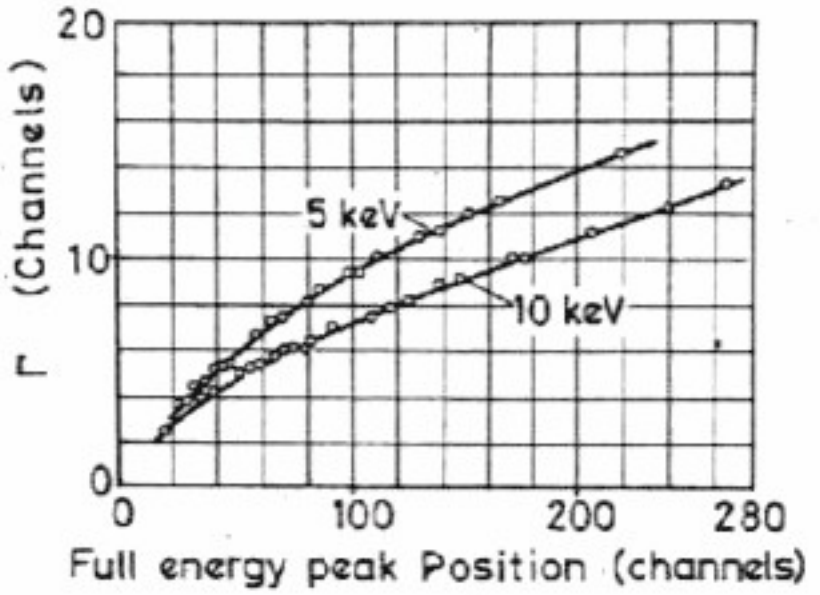

Fig. 4. Full-energy peak width (Γ) as a function of peak position, for 5 and 10 keV channel gain scales for a particular NaI(Tl) scintillation spectrometer

Experimentally measured resolution vs. energy curves for a particular NaI(Tl) detector for different channel widths are shown in Fig. 4 taken from ref. [34].

In spite of the $E_\gamma(\Gamma$ or $p(\sigma))$ relation, in the determination of the peak parameters σ and p are regarded as independent parameters and, after calculating them, Eq. (3.6) serves as control. If the Γ value obtained from the fit deviates substantially from that calculated from Eq. (3.6), this indicates that two or more peaks were unresolved and the fit must be repeated including not one but two or more Gaussians for fitting the measured data.

3.4 RESPONSE FUNCTION OUTSIDE THE FULL-ENERGY PEAK

Several analytical functions have been proposed to describe the shape of the spectrum outside the full-energy peak. Except for the Monte Carlo calculations [24–27] which are usually not accurate enough for quantitative analysis, all these functions are empirical or at least semi-empirical, i.e. there is no real physical basis for their selection. These response functions contain several adjustable parameters. The latter are chosen in the same way as in Eq. (3.2), i.e. by the criterion that the parameters should give the best fit of the measured data in the calibrating spectrum to the calculated pulse-height distribution. After the fitting of each calibration spectrum, the energy dependence of all parameters is established and from this the parameters of photons of any energy can be interpolated or extrapolated. If these parameter values are substituted into the analytical form of the response function, the shape of the spectrum of the desired photon energy can be obtained.

Salmon proposed a response function for the complete spectrum [39]

$$\bar{y}(x) = a_1 \left(\frac{1 + a_2^2 \exp\left[(x - a_3)/a_4\right]}{\exp\left[(x - a_3)/a_4\right] + \left\{1 - a_2 \exp\left[(x - a_3)/a_4\right]\right\}^2} \right)^{\frac{1}{2}} + a_5 \exp\left[-\left(\frac{x - a_6}{a_7} \right)^2 \right] + a_8 \exp\left[\left(\frac{x - a_9}{a_{10}} \right)^2 \right], \tag{3.7}$$

where the last term represents the contribution of the full-energy peak. The influence of the individual parameters on the calculated response function can be seen in Fig. 5a.

This expression does not take into account bremsstrahlung, and additional terms must be added for the annihilation and escape peaks if $E_\gamma \gtrsim 1.2$ MeV.

Another possible approximation of the complete response function is the following [32]:

$$\bar{y}(x) = (ax^2 + bx + c)\left[1 - \tanh(Ax + B) - \exp(Cx + D)\right] + y_5 \exp(-qx) + y_0 \operatorname{sech}^r\left[x(x - p)\right] + \sum_j y_j \exp\left[-\frac{(x - x_j)^2}{\beta_j} \right]. \tag{3.8}$$

Here the first term describes the Compton edge and continuum; the second, the bremsstrahlung; the third, the full-energy peak; and the summation extends to the backscatter, annihilation and escape peaks.

Several approaches similar to those mentioned above have been described in various papers, but none of them (including Eqs. (3.7) and (3.8)) has come to be used either regularly by any author or generally by several research groups.

A more accurate response function can be obtained by the method proposed by Heath [29, 33], but its proper application requires a lot of calibration spectra.

All the calibration spectra measured strictly under the same conditions are normalized to have the full-energy peak in the same channel and to the same number of emitted photons. The contributions of the full-energy peaks calculated by Eq. (3.3) are subtracted. If the energy of the gamma-ray is less than 1.2 MeV, the remaining part of each normalized spectrum is divided into three segments according to the conditions

$$1 \leq z \leq z_b + 4; \quad z_b - 4 \leq z \leq z_c + 4; \quad z_c - 4 \leq z \leq z_\gamma, \tag{3.9}$$

where z_b, z_c and z_γ are the channels of the normalized pulse-height scale (z) corresponding to the backscatter peak, $E_b = E_\gamma/(1 + 3.91E_\gamma)$ (MeV), the Compton edge, $E_c = E_\gamma - E_b$ and the full-energy peak, E_γ, respectively. If $E_\gamma > 1.2$ MeV, two additional segments are created with the dividing points at z_1 and z_2, where z_1 and z_2 are the channels of the single and double-escape peaks having energies $E_1 = E_\gamma - 0.511$ and $E_2 = E_\gamma - 1.02$ MeV. The new borders of the former segments will then be $z_1 \pm 4$ and $z_2 \pm 4$ respectively. Each segment of each spectrum is fitted separately with the function

$$g(z) = a_0 + b_0 z + \sum_{k=1}^{n} b_k \sin\left[k\pi(z - z_L)/(z_L - z_R)\right], \tag{3.10}$$

where z_L and z_R are the left and right borders of the fitting sections and the number of terms in the summation is $n \approx (z_R - z_L)/2$. The overlapping of the fitting sections assures smooth joints between the different portions of the same spectrum. To fix z, a polynomial is fitted to the calibration spectra represented by Eq. (3.10). This polynomial describes the dependence of $g(z)$ on E_γ for any given z. As z_b and z_c depend on E_γ, this fit includes only the same types of sections of the spectra. From these polynomials the $g(z)$ values can be obtained for every z value and for any E_γ by interpolation. The normalized $g(z)$ response function can be retransformed to the original pulse-height scale.

Similar pulse shape distribution can be calculated by fitting $g(z)$ with a polynomial instead of trigonometric functions. The degree of the polynomial is increased till $\chi^2_{k-1}/\chi^2_k < 1.2$ for each calibration spectrum, where χ^2_k is

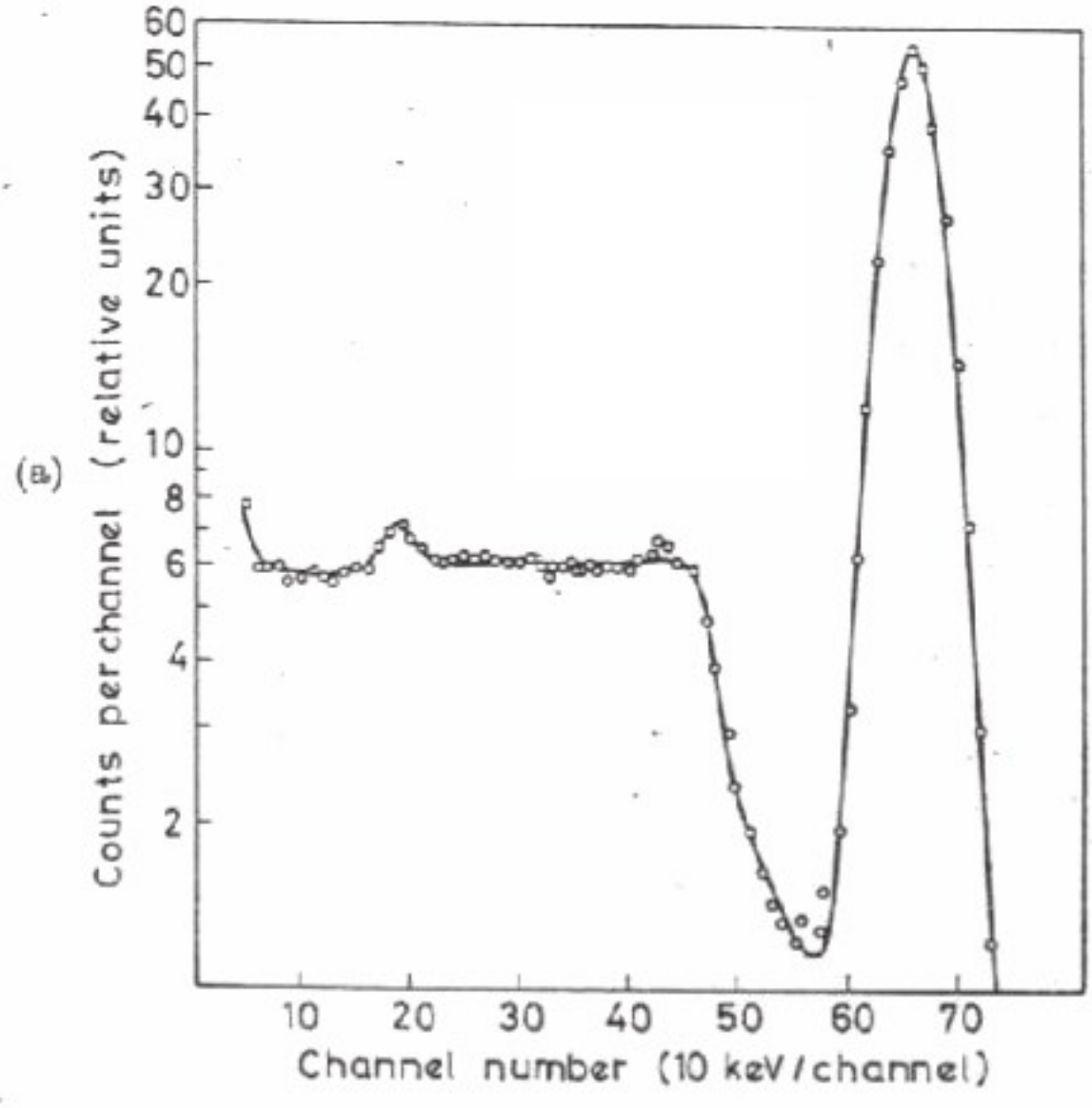
(a)
Counts per channel (relative units)
60
50
40
30
20
10
8
6
4
2
10
20
30
40
50
60
70
Channel number (10 keV / channel)

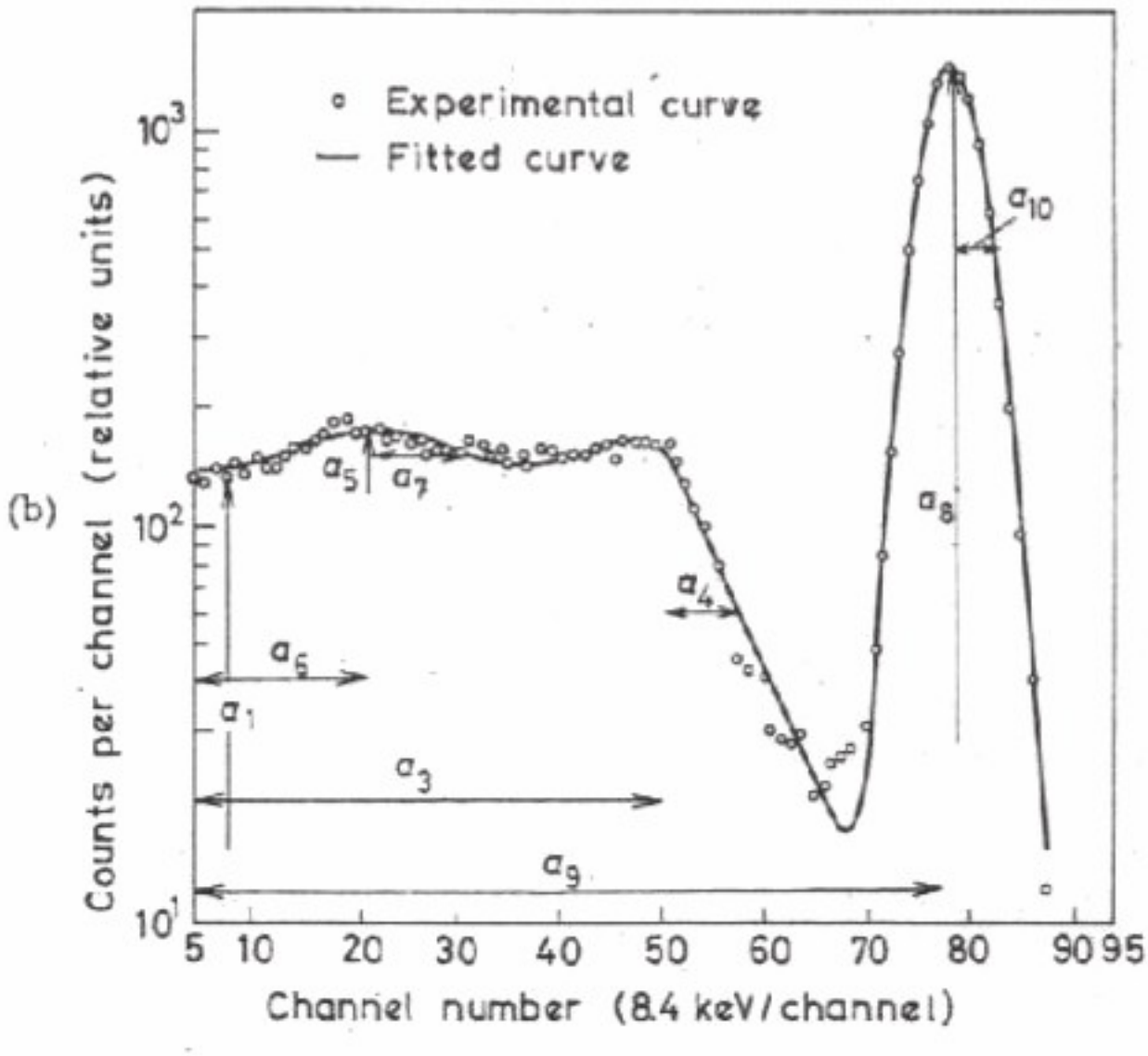
(b)
Experimental curve
Fitted curve
Counts per channel (relative units)
10^3
10^2
10^1
a_1
a_2
a_3
a_4
a_5
a_6
a_7
a_8
a_9
a_{10}
5 10 20 30 40 50 60 70 80 90 95
Channel number (8.4 keV / channel)

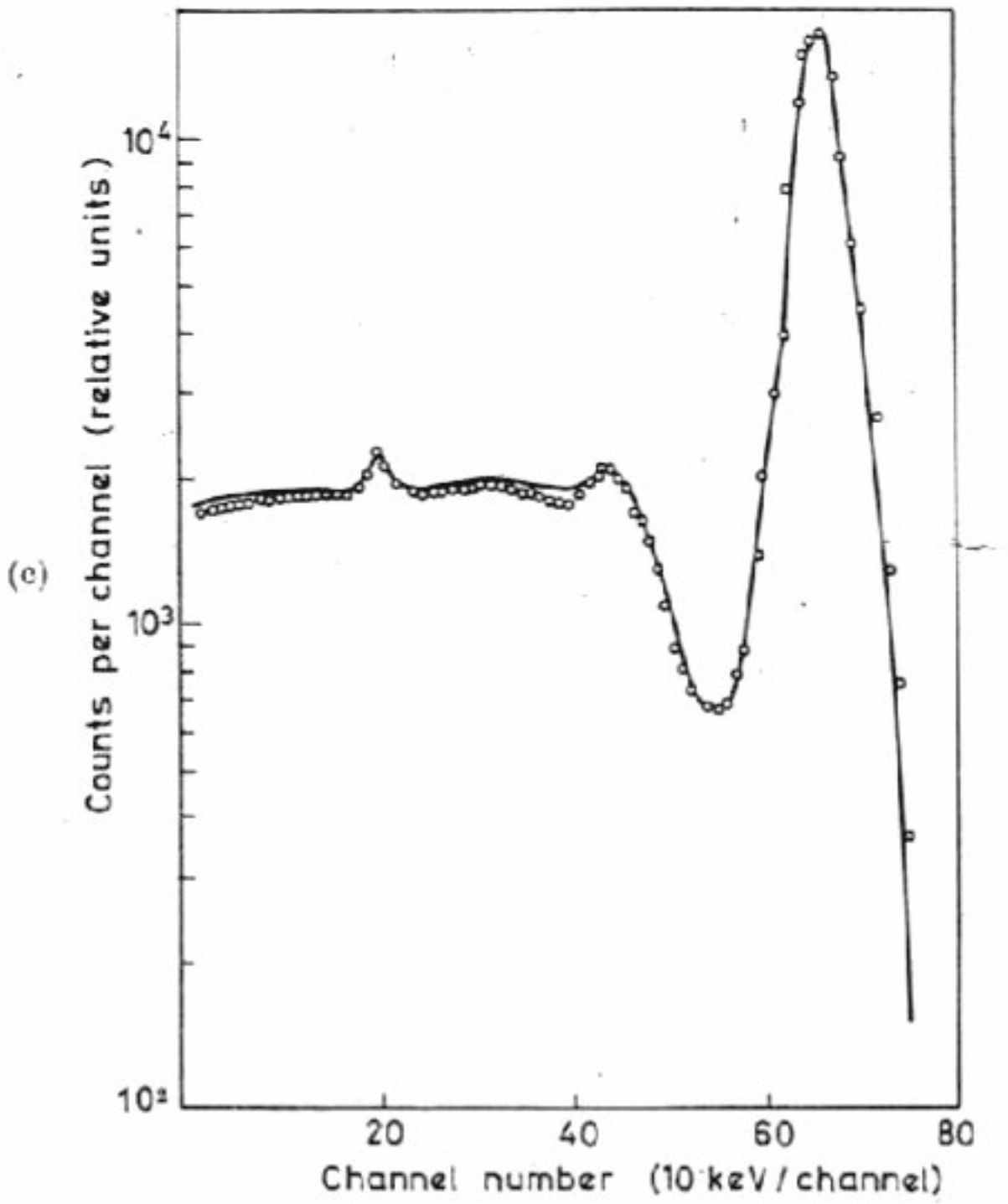

Fig. 5. Calculated and measured spectrum of ^{137}Cs for NaI(Tl) detectors. The calculated spectrum (solid line) was fitted with (a) Eq. (3.7) (from ref. [39]), (b) Eq. (3.5) (from ref. [32]) and (c) Eqs. (3.3) and (3.10) (after ref. 33])

the (weighted) sum of the squares of the differences between the measured and calculated spectra when the kth degree polynomial was fitted (see Section 6.2). The coefficients of the polynomials are the gamma energy-dependent parameters by which any response function can be generated.

In Fig. 5 experimentally measured ^{137}Cs spectra are compared with calculated ones. The first two calculations mentioned above (Eqs. (3.7) and (3.8)) were performed and checked on data measured by NaI(Tl) detectors. However, since gamma-ray energy transfer to electrons and the disturbing effects of the surrounding are the same for semiconductor spectrometers, these principles for response function generation can be applied for Si or Ge(Li) detectors as well [40–43]. In Fig. 6 are shown the measured spectra of 511 keV photons for a 1 cc Ge(Li) detector and those calculated from Eqs. (3.1) and (3.10).

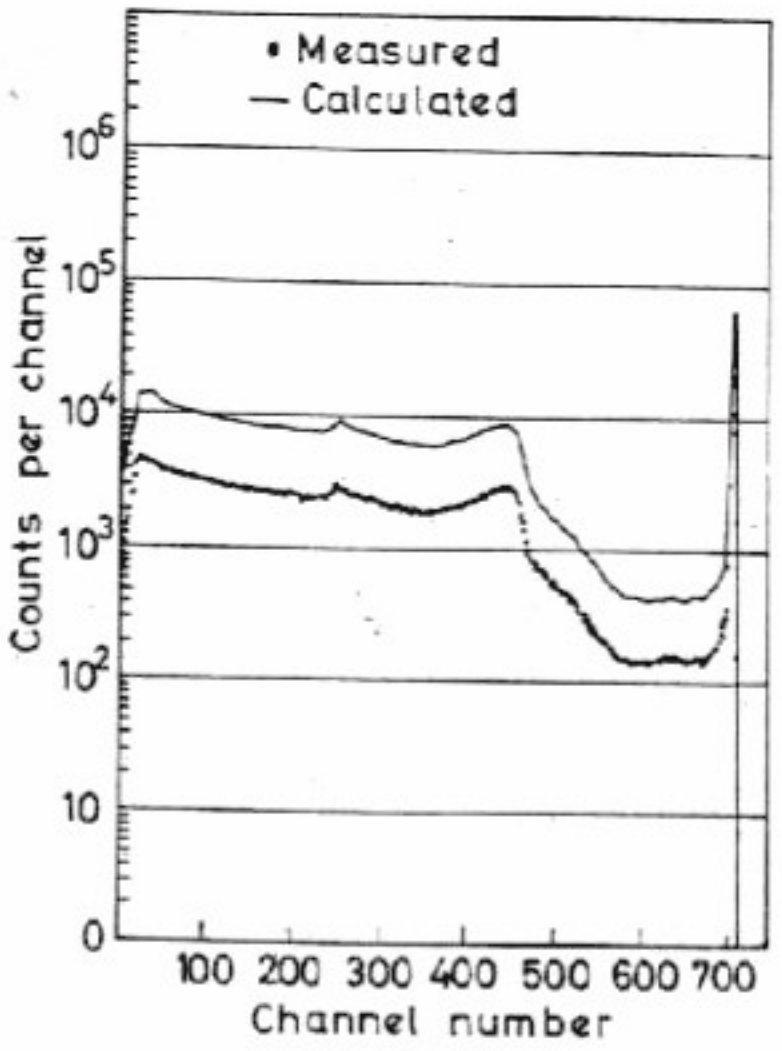

Fig. 6. Measured and calculated (from Eqs. (3.1) and (3.10)) spectra of 511 keV photon for a 1 cc Ge(Li) detector

3.5 APPLICATIONS AND LIMITATIONS OF THE CALCULATED SPECTRA

The use of calculated spectra for determining intensities by peak area methods (Chapter 5), or for generating a library of standards to resolve complex spectra to their constituents by either least-squares resolution or by stripping (Chapters 6 and 7), can save a lot of measuring time if the detector is once calibrated appropriately, and the reproducibility is high. The results obtained by evaluating measurements with calculated spectra are satisfactory provided that, in the region of calculation, the contribution of the component to be determined to the total counts is comparable to that of the other components of the complex spectra. However, if the area of a small peak superimposed on a large Compton continuum, or a small component of a complex spectrum must be determined, the uncertainties in the calculated spectra, especially outside the full-energy peak, can lead to serious errors.

For instance, if a single full-energy peak of a Ge(Li) detector could really be described by a pure or a modified Gaussian such as Eq. (3.1) or (3.3), then the expected value of

$$\chi^2 = \frac{1}{n-3} \sum_{i=1}^{n} [y(i) - \bar{y}(i)]^2 / \sigma^2(i)$$

should be

$$\langle \chi^2 \rangle = 1 \pm \sqrt{\frac{2}{n-3}} ,$$

where $y(i)$ is the measured and $\bar{y}(i)$ the calculated count in channel i, $\sigma(i)$ is the scatter of their difference, and n is the number of channels in the peak region which were included in the fit.

The frequency distribution of χ^2 for 81 peaks measured by a 2.5 $cm^2 \times 0.8$ cm Ge(Li) detector having 0.9 keV resolution at 100 keV is shown in Fig. 7. The large number of high χ^2 values indicates that the analytical function used for the fitting procedure does not describe the phenomena sufficiently.

Although such χ^2 distribution patterns vary considerably from detector to detector, Fig. 7 can be regarded as characteristic from the point of view that, due to the relatively large discrepancy between the measured and calculated spectra, the intensity of a small peak near a larger one can be determined only with large error when the peaks are fitted not by actually measured but by calculated response functions.

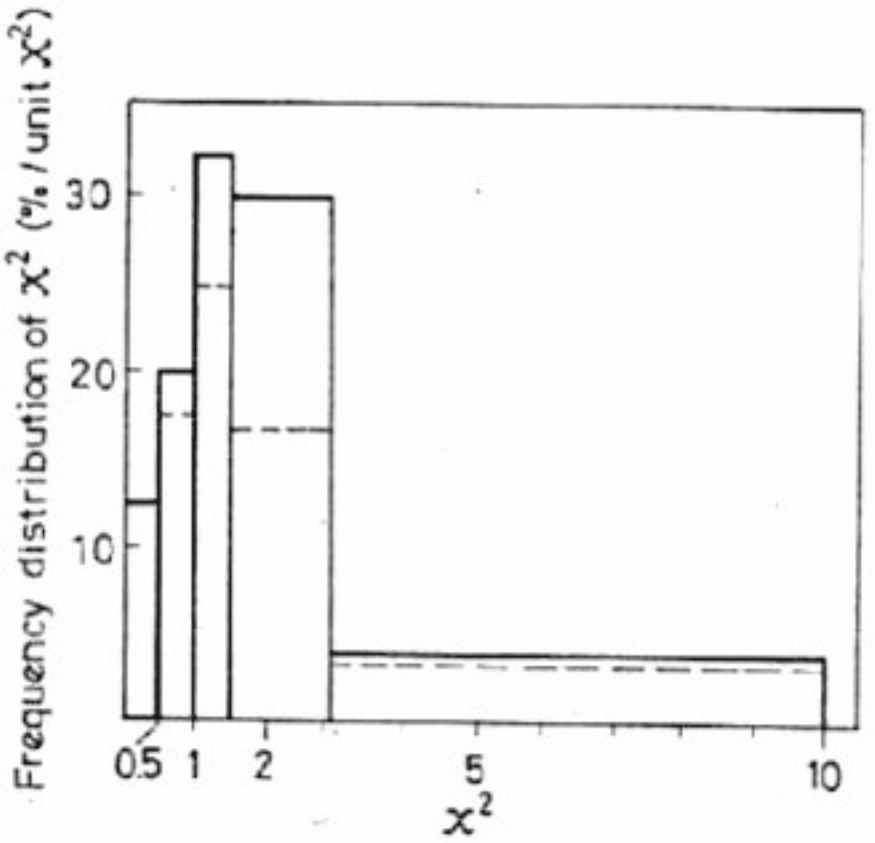

Fig. 7. Frequency distribution of χ^2 values obtained by fitting 81 full-energy peaks measured by a Ge(Li) detector by a Gaussian. In the histogram drawn by the solid line the resolution vs. pulse-height function obtained by calibration was used, while in the dotted histogram σ was regarded as an independent parameter

4. PEAK-LOCATION

4.1 PRINCIPLES OF PEAK-LOCATING METHODS

In scintillation and semiconductor gamma-ray spectrometry the full-energy peaks contain the most valuable information. Energies of gamma-rays are determined by locating the peaks in the spectra, and the areas under them are often used for intensity determination. Large peaks can easily be located visually, but to search spectra measured by 1,000–4,000 channel analyzers for all the possible peaks which could be interesting for some reason would be very time-consuming. In an examination of the raw data, small peaks could be overlooked due to statistical fluctuations, while smoothing the spectra needs a computer anyway. Therefore, it is economical and useful to instruct the computer how to find peaks in a complex spectrum.

Several computer programs have been written for this purpose. Some of them not only locate peaks, but also determine whether they are real single full-energy peaks, Compton edges, backscatter peaks, or multiplets, composed of two or more overlapping peaks.

There are three different methods which can be used routinely for finding peaks by computer in a complex spectra. These methods are general and can be applied not only for gamma-ray, but also for alpha-ray, neutron time of flight, and other spectra, although in the general case some slight modifications might be necessary depending on the symmetry of the peak.

The first peak-locating method is the fastest and simplest one. It searches the measured data channel by channel for a region where there are significantly more counts than in the adjacent channels on either side. This technique is described in Section 4.2.

The second method uses the first or the second derivative of the measured data instead of the original data itself. It exploits the fact that the first derivative changes sign and the second derivative has a pronounced minimum at a peak as can be seen in Fig. 8. To lessen statistical fluctuations, some type of smoothing (or averaging) is applied. Some other expressions which take into account the number of counts in several neighbouring channels can be constructed, by means of which some characteristics such as peaks or discontinuities in composite pulse-height spectra can more easily be determined. These peak-locating methods are explained in Sections 4.3 and 4.4.

Suggestions have been made to use third or higher order derivatives to find small peaks or to resolve very complex ones [44, 45], but due to the large statistical fluctuations in the higher order derivatives the behaviour of the third and higher derivatives does not seem to give any more information than that obtainable from the first two derivatives.

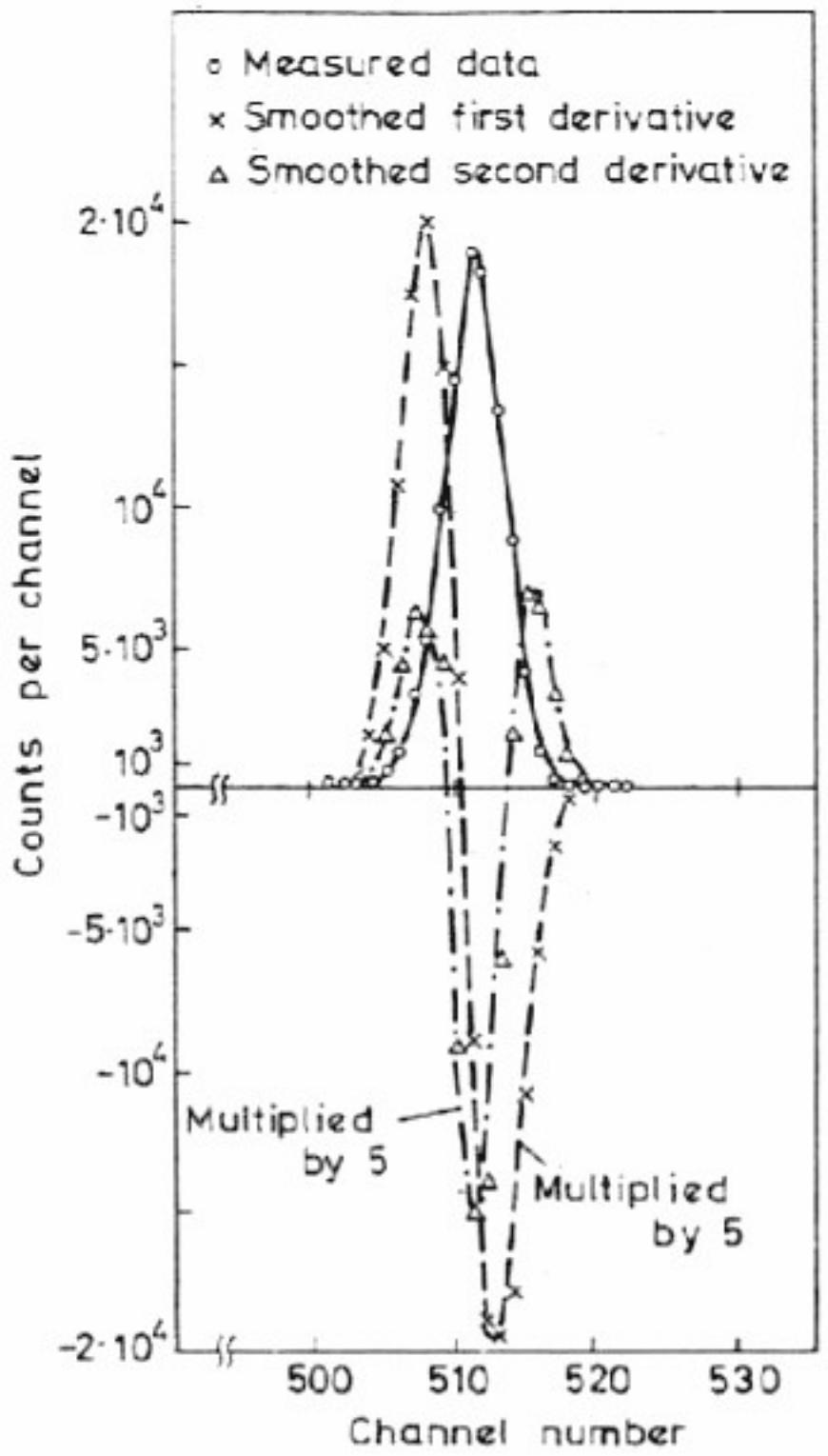

Fig. 8. Behaviour of the smoothed first and second derivatives in the vicinity of a full-energy peak

The third method fits one or more Gaussians to the experimental points by least-squares techniques. The centroid of this curve is the peak position. This method was discussed in detail in Section 3.2 where the determination of detector response function in the full-energy peak region was described.

4.2 PEAK-LOCATION BY FINDING MAXIMA

The simplest peak-locating program first scans the entire spectrum and then selects the possible peaks by finding those channels where the counts fulfil the conditions

$$y(p-2) < y(p) - K\sqrt{y(p)}$$

and

$$y(p+2) < y(p) - K\sqrt{y(p)}\,, \tag{4.1}$$

where K is a constant chosen experimentally. Analyzing different spectra,

$K = 1$ gavé satisfactory results. The border channels of the peak, $p - l$ and $p - r$, are determined on both sides of the possible peak channel, p, by the criterion that the decrease in the channel contents should no longer be statistically significant. This is equivalent to finding the nearest channels on both side of p for which

$$y(p - l - 1) \geq y(p - l) - K\sqrt{y(p - l)}$$

and (4.2)

$$y(p + r + 1) \geq y(p + r) - K\sqrt{y(p + r)}$$

The area, N, of the peak and its standard deviation, ΔN, are then calculated by Eqs. (5.4) and (5.5) as described in Section 5.3 and the peak is retained as true peak if $N > 2\Delta N$. Its final location is determined by calculating the symmetry axis of the background corrected peak.

This method is fast and can be programmed easily [46–48] but often overlooks peaks, especially small ones, and cannot separate double peaks.

4.3 METHOD OF SMOOTHED FIRST DERIVATIVE

If the number of counts is regarded as a continuous function of the channel number, then the first derivative of the spectrum changes sign at the top of peaks. Before a peak it is positive and after it it is negative in a few adjacent channels. The first derivative attains a maximum positive value at about half maximum height on the left side of a peak, continuously decreases as the channel number increases, becomes approximately zero at the peak centre and reaches a minimum negative value at about half height on the right side of the peak (see Fig. 8). This fact can also be used for locating peaks. The computer looks for groups of neighbouring channels such that the smoothed first derivative, Y_1, fulfils the following criteria:

$$Y_1(p) \leq 0$$

$$Y_1(p + i) < 0 \qquad \text{for } i = 1, 2, \ldots, r$$

and

$$Y_1(p - i) > 0 \qquad \text{for } i = 1, 2, \ldots, l$$

To be able to recognize significant peaks but disregard statistical fluctuations, r and l must be chosen in accordance with the energy resolution. For NaI(Tl) spectra having 15 keV/channel calibration, satisfactory results were found with $r = 4$, $l = 2$, using the first derivative of second degree polynomials fitted to five points [49]. To be able to detect small peaks in Ge(Li) spectra, the peak area is calculated whenever the smoothed first derivative changes from positive to negative and the peak is regarded as a true one if $N > 2\Delta N$ [50].

A monoenergetic gamma-ray, having energy E_γ, produces a Compton edge and a backscatter peak in the spectrum at energies $E_B = \dfrac{E_\gamma}{1 + 3.91 \times E_\gamma}$ and $E_C = E_\gamma - E_B$, respectively (see Chapter 3). These can be distinguished from full-energy peaks by finding a peak with the appropriate energy and sufficient intensity to produce such peaks. However, back-

scatter peaks cannot usually, be resolved from each other and often not from low energy photopeaks either, especially in scintillation spectra.

The resolution of the detector increases monotonically as a function of the gamma-ray energy, and the constants of Eq. (3.6) are usually known from calibration. By calculating the widths of the measured peaks, the unresolved multiple peaks can often be distinguished from single ones by giving larger Γ than that predicted from Eq. (3.6).

4.4 GENERALIZED SECOND DIFFERENCES

By a procedure proposed by Mariscotti, it is possible not only to find and locate peaks with high precision in the presence of a large background, but also to distinguish single full-energy peaks from Compton shoulders and double peaks by their shape [51].

In a small interval the number of counts as a function of the channel number i can be approximated as

$$y(i) = Ag_p(p - i) + B + Ci, \tag{4.3}$$

where $g_p(p - i)$ is a Gaussian function centred in channel p with unit amplitude, A is the height of the peak and B and C are constants describing the background. The scatter of the Gaussian is $\sigma = \Gamma/2.355$, where Γ is the full width at half maximum of the peak, i.e. for a single full-energy peak the energy resolution of the detector at channel p.

Assuming again that $y(i)$ is a continuous function, its second derivative $y''(i) = A\ g_p''(p - i)$ becomes independent of the background. As $g_p''(p - i) \approx 0$ everywhere except in the vicinity of the peak channel p, a peak will be located whenever $y''(i) \neq 0$.

Because of the discrete nature of the data, the second derivative must be replaced by the second difference

$$S(i) = [y(i + 1) - y(i)] - [y(i) - y(i - 1)] = y(i + 1) - 2y(i) + y(i - 1) \tag{4.4}$$

which, like $y''(i)$, should be different from zero only around a peak. Unfortunately, $\Delta S(i)$, the statistical fluctuation of the second difference is so large that the expected value of $S(i)$ in a peak with $\sigma = 4$ exceeds its variance, even if there is no background under the peak, only if $A > 1600$.

To detect much weaker peaks, $S(i)$ is replaced by a 'smoothed' second difference; neglecting the presently unimportant normalizing constant, this is the average of the $S(i)$'s over $w = 2m + 1$ neighbouring channels around i

$$S_w(i) = \sum_{j=i-m}^{i+m} S(j). \tag{4.5}$$

The relative statistical fluctuation of $S_w(i)$ is smaller than that of $S(i)$.

$$\frac{\Delta S_w(i)}{S_w(i)} \approx \frac{\Delta S(i)}{S(i)}\, w^{-1/2},$$

if $S(j)$ does not vary rapidly in the interval used for the averaging.) To

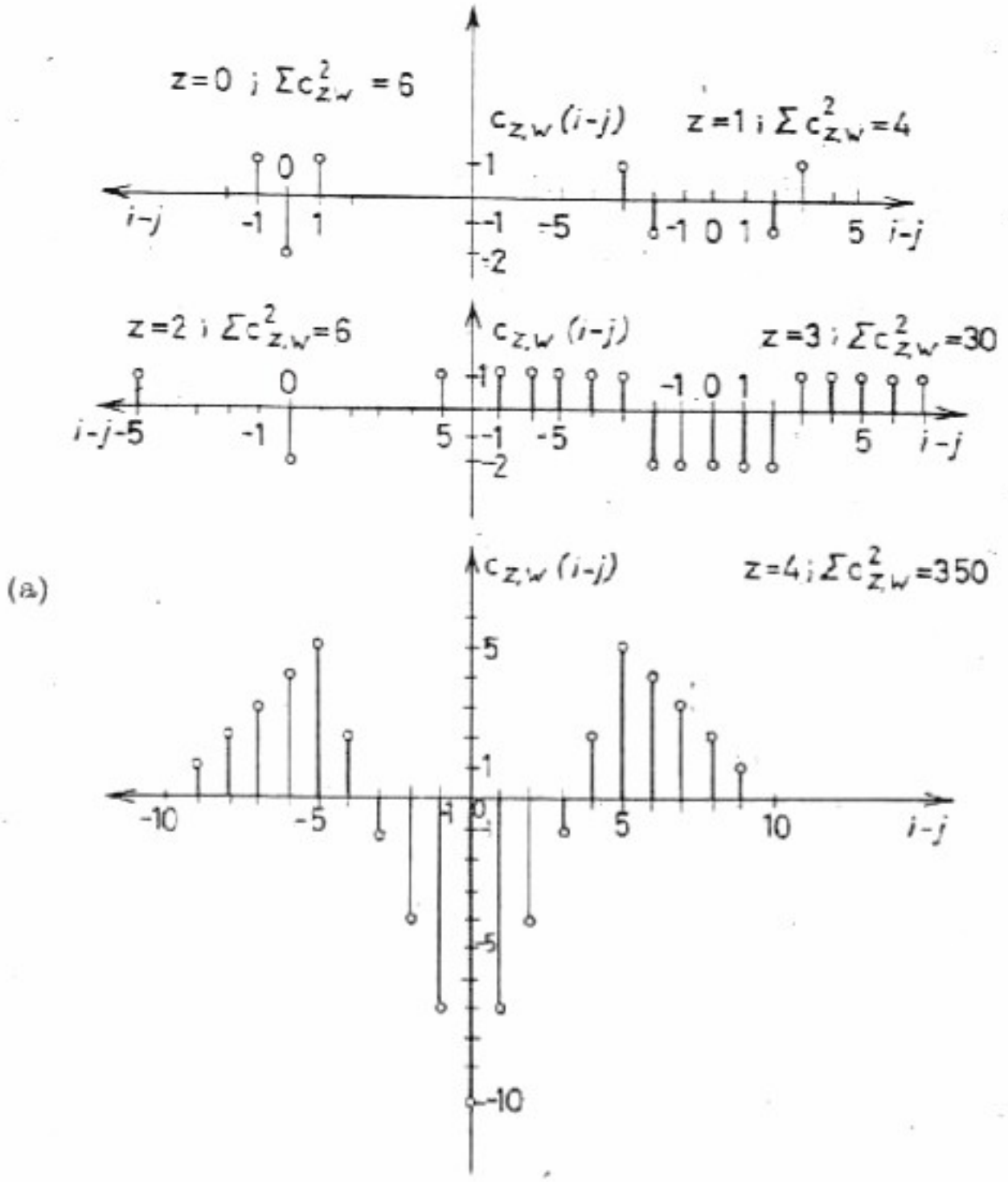

Fig. 9. (a) Coefficients $c_{z,w}\ (i-j)$ of the generalized second difference for $w = 5$ (after ref. [51])

lessen the influence of statistics even more, this process is repeated. The averages are averaged (again without normalizing) and the generalized second difference is defined as

$$S_{z,w}(i) = \sum_{j=i-m}^{i+m} S_{z-1,w}(j). \tag{4.6}$$

In obtaining $S_{z,w}(i)$, the averages of the second difference were averaged z times over w channels around i. Equations (4.4) and (4.5) are the definitions of the special cases $S_{0,w}(i)$ (in this case w has no practical meaning) and $S_{1,w}(i)$, respectively. For numerical calculations $S_{z,w}(i)$ and its error can be expressed as

$$S_{z,w}(i) = \sum_{j=i-zm-1}^{i+zm+1} c_{z,w}(i-j)y(j) \tag{4.7}$$

and for small peaks

$$\Delta S_{z,w}(i) \approx \sqrt{y(i)} \left[\sum_{j=i-zm-1}^{i+zm+1} \left(c_{z,w}(i-j)\right)^2 \right]^{\frac{1}{2}}. \tag{4.8}$$

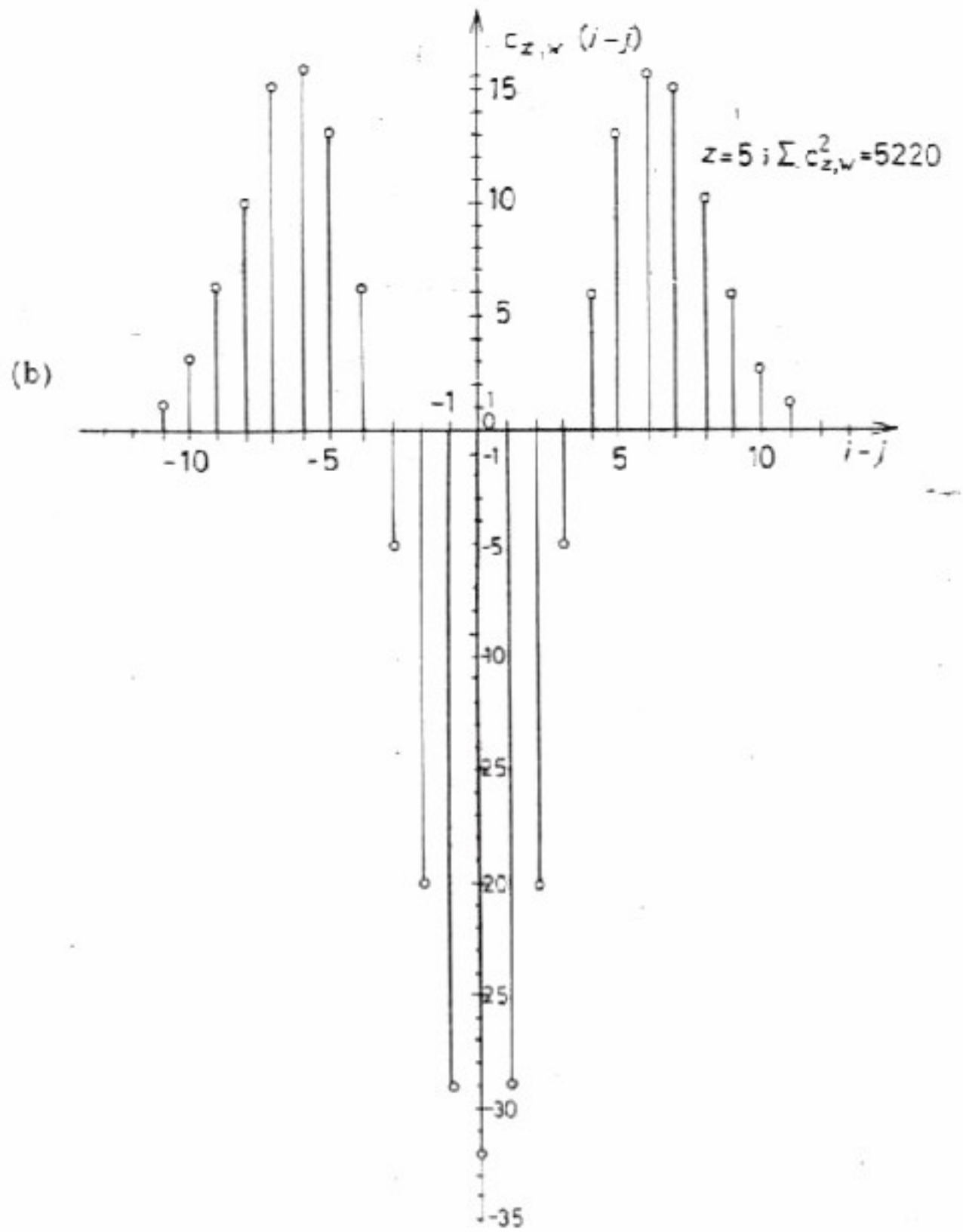

Fig. 9. (b) Coefficients $c_{z,w}$ $(i-j)$ of the generalized second difference for $z \leq 5$ (after ref. [51])

In obtaining Eq. (4.8) it was assumed that the error is due only to statistics, gain and threshold shifts, and other experimental error sources can be neglected. For big peaks Eq. (4.8) overestimates $\Delta S_{z,w}(i)$, but in this case $S_{z,w}(i)$ is much larger even than this overestimated error. The coefficients $c_{z,w}$ and $\Delta S^2_{z,w}(i)/y(i) = \Sigma c^2_{z,w}$ are shown in Fig. 9 for $w = 5$ and $z < 5$.

Constructing the generalized second differences defined in Eqs. (4.4)–(4.6) or in (4.7) as a linear combination of the measured counts, one obtains a function which is proportional to the second derivative of the spectrum and has small statistical fluctuation if z and w are chosen correctly. Thus, $S_{z,w}(i) \approx 0$ at the background and Compton continuum, differs significantly from zero around a peak, and is proportional to the second derivative of a Gaussian if the peak is a full-energy peak superimposed on a linear background. It can be seen from Fig. 9 that the effect of this iterative

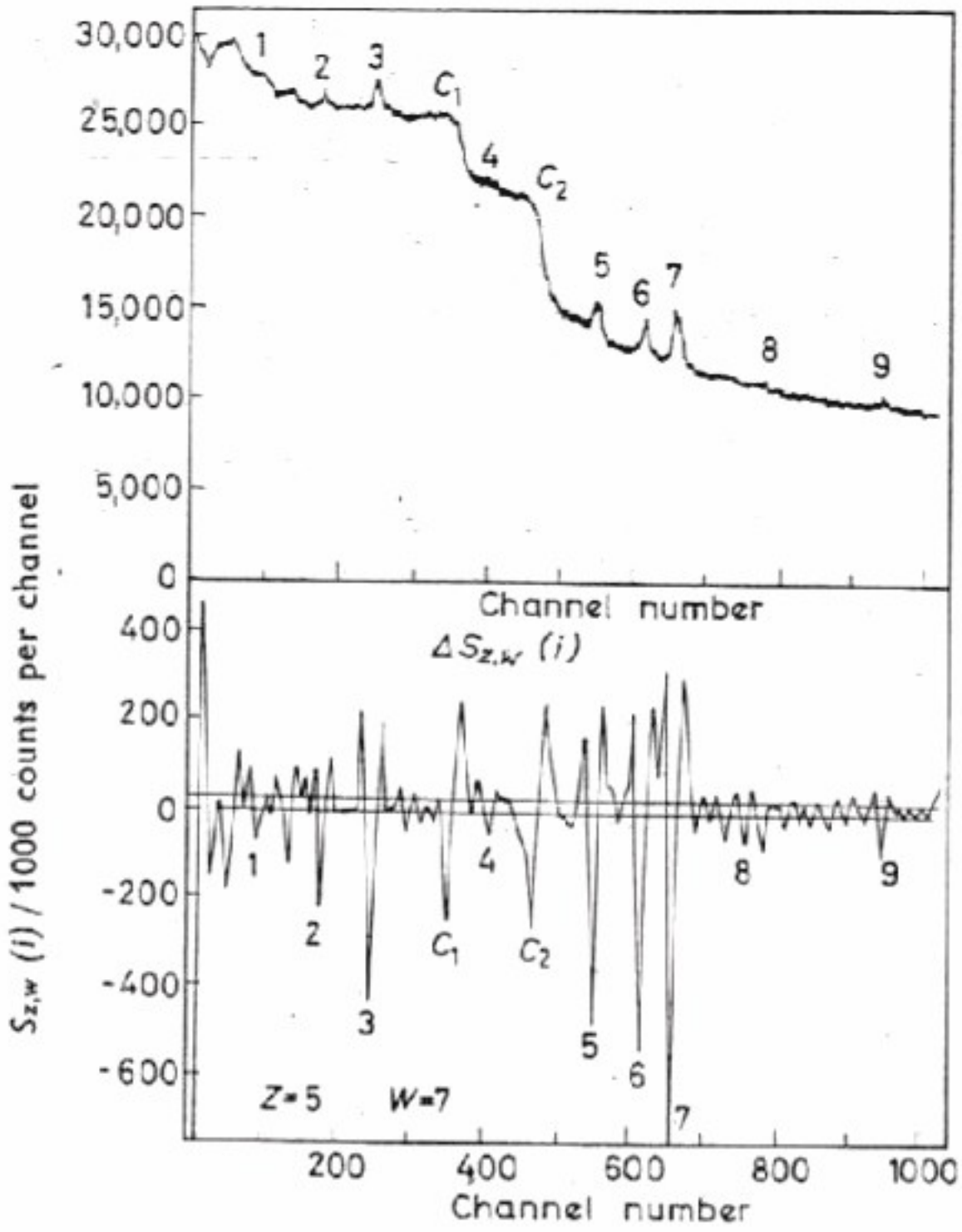

Fig. 10. Peak location by the generalized second difference. The generalized second difference, $S_{z,w}$, corresponding to the experimental spectrum at the top, is plotted with its standard deviation. The nine peaks numbered are those identified by the computer as full-energy peaks (after ref. [51])

procedure gives a weighted difference between the counts in, and just out of, the peak region. Therefore, by this method weaker peaks can be detected than by the second difference or by the methods described in Sections 4.2 and 4.3. Mariscotti made a detailed study of the optimum selection of the averaging parameters, w and z [51]. The results of his calculations were that from the practical point of view the best results are achieved when $w \approx 0.6\,\Gamma$ and $z = 5$ are selected. With these averaging parameters it is possible to identify not only peaks having amplitude $A \approx 50$ and width $\Gamma \approx 9$ on a background $B \sim 5000$ ($C \sim 0$), but also to resolve double peaks. Using a larger w (more points for averaging) would increase the probability of detection of small peaks but would considerably reduce the possibility of recognizing and resolving overlapping ones. The increase in z would

lead to the same reduction without any considerable improvement in the peak detection.

A peak is identified in channel p if $-S_{z,w}(p) > 2\Delta S_{z,w}(p)$ ($S_{z,w}$ is negative around the peak !). Then it is tested whether it is a real full-energy peak or a Compton shoulder. For a real full-energy peak which has a Gaussian shape, the number of channels around p, n_1, where $S_{5,0.6\Gamma}(i) < 0$, is $n_1 \approx [1.22\Gamma + 1/2] \pm 2$, where the $[a]$ symbol denotes the integer part of a. The number of channels where $S_{z,w}(i) > \Delta S_{z,w}(i)$, must be between certain limits for a real single full-energy peak, so these can serve as further tests to discriminate between full-energy peaks and Compton edges. A Gaussian plus a linear term is fitted to the data around p by iterative weighted least-squares techniques (see Section 3.2), and the exact position of the peak is identified as the centre of the Gaussian.

Figure 10, taken from ref. [51], shows the application of the method with $z = 5$ and $w = 5$ to a complex spectrum. $S_{5,5}$ and $\Delta S_{5,5}$ are also plotted. The nine peaks numbered are those defined by the computer. It can be seen for example that the Compton edges C_1 and C_2, in spite of giving a large significant minimum in $S_{z,w}$, can be identified unambiguously by the lack or the smallness of the positive peak in $S_{5,5}$ before the significant negative values.

Ádám, Quittner and Zentai [52] presented a method which uses instead of the generalized second differences other expressions, obtained from the counts in successive adjacent channels, by which some characteristic such as peaks or discontinuities in composite pulse-height spectra can be identified even when the statistical fluctuation does not allow their visual observation either in the original or in the smoothed data. They used this method successfully in fast neutron spectroscopy, but it can be applied without any variation in gamma-ray spectroscopy.

Studying the following expressions

$$A_k = \sum_{l=0}^{L} \left[y(k+l) - \frac{1}{2L+1} \sum_{j=-L}^{L} y(k+l+j) \right] \times \left[y(k-l) - \frac{1}{2L+1} \sum_{j=-L}^{L} y(k-l+j) \right]$$

$$B_k = \sum_{l=0}^{L} \left[y(k+l) - \frac{1}{2L+1} \sum_{j=-L}^{L} y(k+j) \right] \times \left[y(k-l) - \frac{1}{2L+1} \sum_{j=-L}^{L} y(k+j) \right]$$

and

$$C_k = \sum_{l=0}^{L} [y(k+l) - y(k-l)]^2$$

they found that for suitably selected (not too small and not too large) L, the quantity C_k was the most sensitive to the change in the shape of the spectra around channel k.

5. PEAK AREA DETERMINATION

5.1 ABSOLUTE AND RELATIVE INTENSITY DETERMINATION

Intensities can be determined from the number of counts either in the entire spectrum of the gamma-ray or in a part of it. Besides the desired gamma-ray, the detector measures other radiations too; therefore, it is necessary to determine how many counts in the spectrum are due to the selected one. In Chapter 6 and Section 7.1 we discuss how to resolve a complex spectrum into its individual constituents by weighted least-squares resolution and stripping techniques. In the methods explained in this chapter, a part of the complex spectrum is selected where the activity due to the photons to be determined is well distinguishable from the background and other radiations. This part is a peak in the spectrum of the photons in question. The higher the probability that a detected photon gives a signal in this peak region, the better is the detector for gamma-ray spectroscopy, provided that other factors, e.g. total efficiency, energy resolution, linearity, are approximately equal. Germanium has a higher atomic number than silicon. Therefore, for photon energies above $\sim$100 keV the photoelectric process/Compton scattering ratio is significantly higher in Ge than in Si. This is the reason why Ge(Li) detectors, in spite of being more difficult to handle, are preferred to Si detectors in gamma spectroscopy except for very low energy radiation measurement.

The gamma-ray intensity is calculated from the number of counts in the peak region, often called peak area. For peak area calculations the full-energy peaks are most often used. For energies above a few MeV the double-escape peak becomes more intense than the full-energy peak. In this energy region the escape peak is preferred for intensity calculations. The gamma energy where this change occurs depends on the type and the size of the detector and is higher for large NaI(Tl) scintillators, used for detecting high-energy gamma-rays, than for Ge(Li) detectors. Figure 11 shows the experimental intensity ratios of the full-energy and escape peaks for different detectors as a function of the gamma-ray energy [35, 41, 53]. In the subsequent part of this chapter when we refer without any adjective to a peak, the most intense peak is meant in the spectrum of the gamma-ray to be measured.

Intensities can be calculated from the peak area either by absolute or by relative methods. In the first case the intensity, I, is obtained from the measured peak area, N, as

$$I(t) = 4\pi N(t)/\Omega\varepsilon_p, \tag{5.1}$$

where Ω is the solid angle subtended by the detector from the source and ε_p is the intrinsic peak efficiency of the detector, i.e. the fraction of the

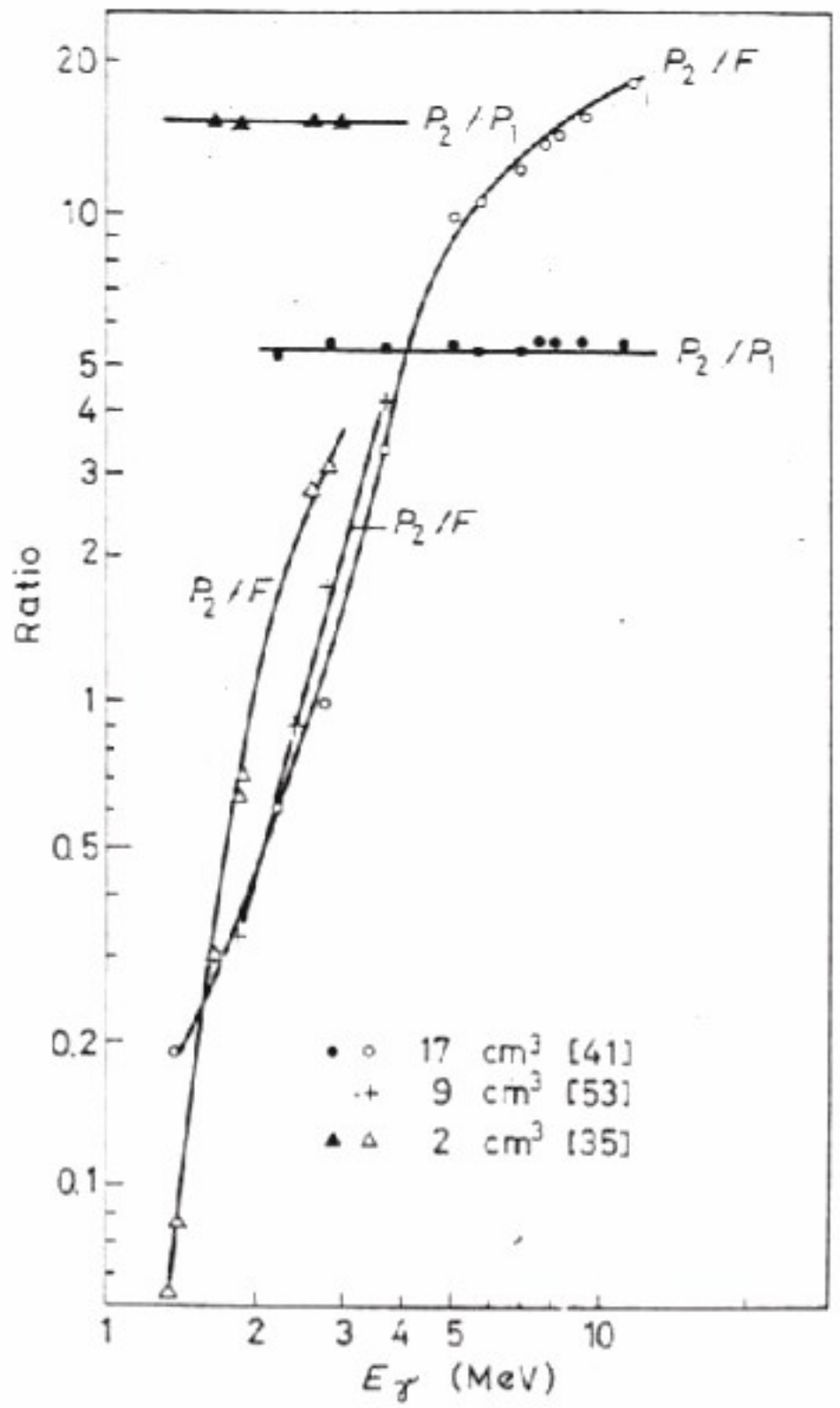

Fig. 11. Experimental ratios of double-escape peak to single-escape peak (P_2/P_1) and double-escape peak to full-energy peak (P_2/F) probabilities for different Ge(Li) detectors • ○ 17 cm³ [41]; + 9 cm³ [53]; ▲ △ 2 cm³ [35]

gamma-rays impinging the detector which give a signal into the peak. In Eq. (5.1) $N(t)$ is expressed in counts per second, and the total accumulated counts are $N = \int N(t)\mathrm{d}t$. In practice, the total counts, N, are usually used and time corrections are performed if necessary to calculate $N(t)$. The expression $\varepsilon = \Omega\varepsilon_p/4\pi$, which we call total peak efficiency, is known either by calculation or by calibration with standard sources for the photon energies where the intensities are to be obtained.

In the relative method the peak areas of the same energy gamma-rays are compared and their ratio gives the ratio of the intensities. In this case it is obligatory that all areas should be calculated by the same method as there are several methods for computing peak areas (Sections 5.3 and 5.4).

In activation analysis, where comparative sources can easily be produced,

relative intensity measurements are nearly always performed (see Section 8.3). In other types of experiments both relative and absolute determinations are used, depending on the problem.

5.2 DETECTOR EFFICIENCY CALIBRATION

By measuring peak areas of sources of known intensity, the energy dependence of the total efficiency can be determined by Eq. (5.1) [34]. For NaI(Tl) crystals where the sensitive volume is well defined it can also be calculated with sufficient precision [29, 54–56], but for semiconductor detectors (except for some true coaxial detectors), for the present calculated absolute efficiencies are far from being accurate. Unfortunately, the number of calibrated sources is usually not sufficient to cover the entire energy range, and their activities are not known very accurately. Efficiency measurements for gamma-ray energies up to 2.76 MeV (^{24}Na) are usually made by calibrated radioactive sources, and above this by using capture gamma-rays. The high energy calibration is usually more complicated because capture gamma-rays are emitted virtually immediately after a target nucleus captures a neutron. Therefore the detector must be calibrated by an open channel of a thermal reactor.

For calculating the total peak efficiency, both ε_p and Ω must be determined. Several attempts have been made to calculate ε_p. The best results were obtained by calculating from the well-known cross-sections the total intrinsic efficiency ε_T, which is the probability that a gamma-ray striking the detector will interact with at least one electron in the sensitive volume; this is multiplied by the experimentally measured peak to total ratio R. R is the probability that if a photon interacts with the detector the resulting signal will fall in the peak region.

As R is nearly independent of the detector-source distance and can be measured with good accuracy, $\varepsilon_p = \varepsilon_T R$ is also well known for different

Table IV. Energies in keV and Relative Intensities of Gamma-Rays Utilized in the Determination of the Detector Full-Energy Peak and Double-Escape Peak Efficiencies

	Radioactive decay										
	^{133}Ba		^{180m}Hf		^{108m}Ag	^{22}Na	^{228}Th	^{46}Sc	^{88}Y	^{60}Co	^{24}Na
E_1	81		215		432	511	583	889	898	1173	1368
E_2	356	332	443	618	727	1274	2614	1120	1836	1333	2753
I_1/I_2	0.52	0.86	0.98	0.994	0.993	1.82	0.852	1.00	0.94	1.00	1.001

	Capture gamma-ray						
	^{47}Ti			^{54}Cr			^{53}Cr
E_1	341	1497	835	1783	2239	3720	2319
E_2	6413	4876	8883	7100	6642	5999	5610
I_1/I_2	1.00	1.00	1.56	1.15	1.00	0.75	1.00

experimental arrangements. For NaI(Tl) detectors, Ω is well defined. The calculated total efficiencies for crystals having various forms and sizes are tabulated and compared with measured values obtained from calibrated sources by Eq. (5.1) in several books and papers, e.g. [29, 54, 55].

Numerous Monte Carlo calculations of both full-energy and double-escape peak efficiencies have been made for Ge(Li) detectors as well [26, 27, 42]. The former agree with the measurements, but the calculated double-escape peak efficiencies deviate considerably from the measured values. For this reason, and because efficiencies calculated for one Ge(Li) detector are not valid for another due to uncertainties and wide variations in the sensitive volumes, it is best to use a relative calibration method which avoids the calculation of ε_T and Ω [35, 53]. Naturally, this method can be applied for scintillation detectors as well [57].

For calibration, sources are used which emit two or more gamma-rays with accurately known relative intensities. The areas of the peaks are determined by any of the methods described later in this chapter. The ratio of the peak areas is equal to that of the peak efficiencies divided by the intensity ratio. Energies and relative intensities of gamma-rays utilized in the determination of detector efficiency are compiled in Table IV. In Fig. 12 is shown the energy interval covered by these sources. By fitting

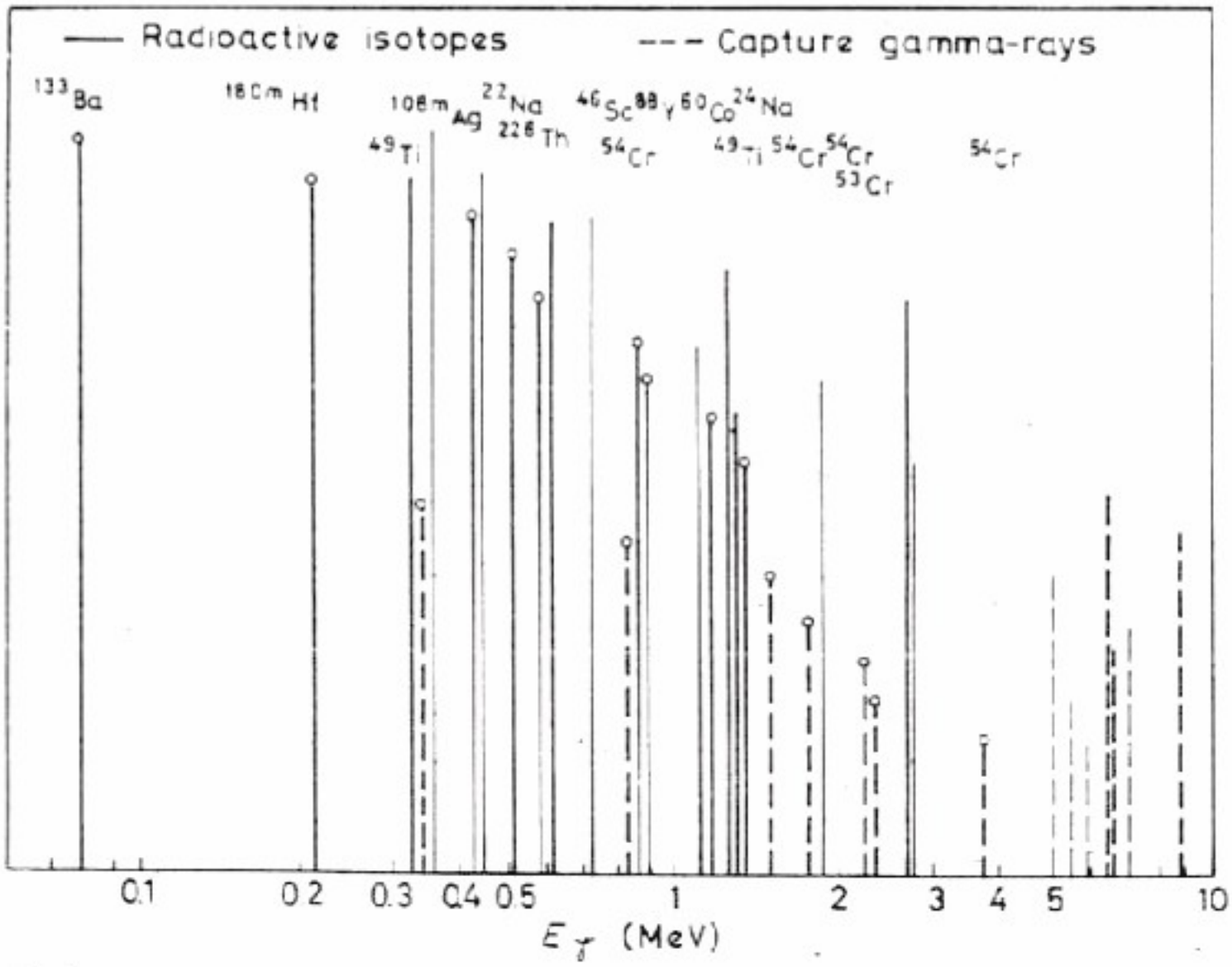

Fig. 12. Gamma-rays used for relative efficiency calibration. Gamma-rays emitted by the same isotope with accurately known relative intensities have the same lengths. The lowest energy gamma-ray of each isotope is marked by a full circle. Solid lines represent photons emitted by radioactive sources, the dotted ones are capture gamma-rays. The intensity ratios are listed in Table IV

pairs of such gamma-rays (having the same length in the figure) and interpolating between the measured points, a satisfactory relative efficiency calibration can be obtained. An arbitrary efficiency is adopted for one calibrating photon energy and the efficiencies relative to this are calculated for the gamma-rays of the same isotope (or level). This efficiency 'curve' is interpolated or extrapolated to the energy of another calibration point. For this energy the efficiency so obtained is adopted, and the relative efficiencies compared to this value are again calculated with the help of the other gamma energies of the second calibrating isotope. The efficiency curve is extended by the new points. This process is then continued for all the calibration sources.

A simple and rapid method to obtain an approximate relative calibration curve is to measure the spectrum of the ^{228}Th radioisotope and its daughters. The energy range of these radio isotopes covers nearly completely the energy region up to 2.7 MeV, and the relative intensities of the individual gamma energies can be fairly well determined.

As Ω is independent of E_γ, and in practical spectrometer arrangements the dependence of ε_p on Ω can be neglected, this relative calibration is good for a given detector in any geometry. The absolute efficiency can be obtained by measuring a source with accurately known intensity or for which the detector has a well-known (usually 100%) intrinsic peak efficiency, and then Ω is calculated.

The detector total peak efficiency is stored in the computer either as a set of corresponding $\varepsilon(E_\gamma)$ values from which the total peak efficiency can be calculated by interpolation for any energy, or as an analytical $\varepsilon(E_\gamma)$ function. For Ge(Li) detectors the full-energy peak efficiency $\varepsilon_p \sim E_\gamma^{-k}$ in a wide energy range, where the k constant depends on the size and shape of the detector. Significant deviation from this curve occurs only under 100 keV due to the self-absorption in the detector itself. A better fit was obtained by the approximation

$$\ln \varepsilon_p = b \ln \frac{E_0}{E_\gamma} + c \ln^2 \frac{E_0}{E_\gamma},$$

where b, c and E_0 were constants for a given detector and geometry [53]. Good agreement was also found [54] with the following formula:

$$\varepsilon_p \sim 1 - \exp(-\tau C) + A\sigma \exp(-BE_\gamma),$$

where A and B are empirical constants, C is the detector thickness and τ and σ are the photoelectric and Compton absorption coefficients, respectively.

Relative efficiencies of a 35 cm^3 planar, a 9 cm^3 coaxial, and a 4 cm$^2 \times 0.5$ cm Ge(Li) detector, measured by the above mentioned method, are shown in Fig. 13. The data were taken from refs. [58, 35] and [53] respectively. All relative efficiencies are normalized in the same way, to be 1.0 at $E_\gamma =$ 0.511 MeV.

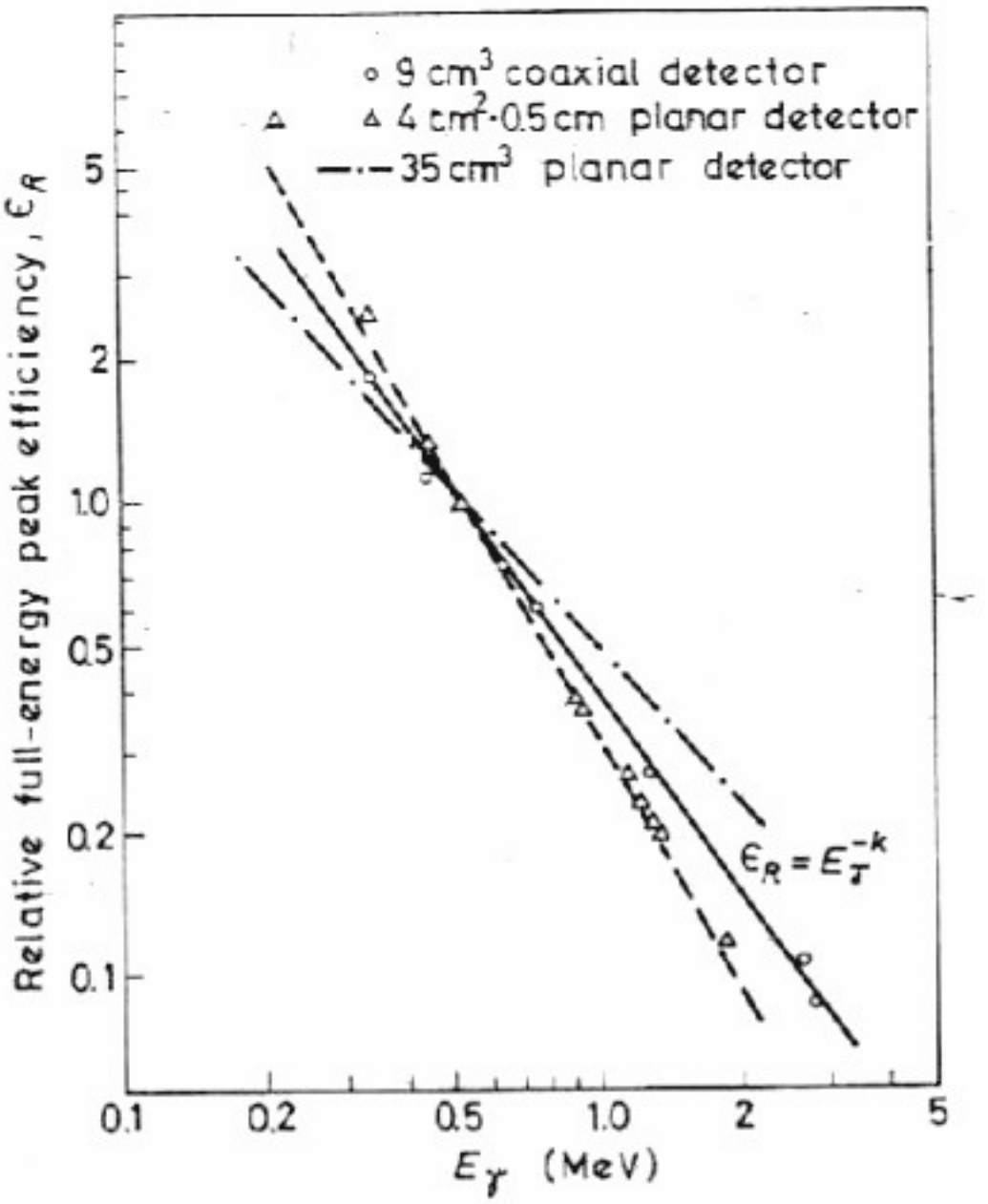

Fig. 13. Relative efficiencies of a 9 cm³ coaxial, a 4 cm² × 0.5 cm and a 35 cm³ planar Ge(Li) detector. The data are taken from refs. [53, 35] and [58], respectively. All relative efficiencies are normalized in the same way to be 1.0 at $E_\gamma = 0.511$ MeV

For very precise intensity determinations a correction for the summing effect (Section 10.2) is necessary. For every count under the sum peak, one count is removed from the peak of each coincident member. To obtain the correct peak area in the first approximation, the measured counts must be divided by $[1 - \varepsilon_{T2} \times f\,(1, 2)]$, where ε_{T2} is the total detection efficiency for the other coincident gamma-ray and $f(1, 2)$ is a factor describing the angular correlation between the simultaneously emitted photons. (If there is no angular correlation $f(1, 2) = 1$.) For large volume scintillation detectors this correction can be as large as 10–20%.

5.3 CURVE FITTING

As it was discussed in Section 3.2, full-energy peaks can be very closely approximated by a Gaussian in NaI(Tl) spectra and with less accuracy for peaks in Ge(Li) spectra. In most cases the peaks are superimposed on a background or a Compton continuum which is regarded as linear in the region of the peak. Therefore, the function which is to be fitted to the measured data by iterative weighted least-squares techniques has the

form [54]

$$\bar{y}(i) = A \exp\left[-\frac{(i - p)^2}{2\sigma^2}\right] + Bi + C. \tag{5.2}$$

The area of the peak is

$$N = 2.5A\,\sigma = 1.064\,A \times \Gamma. \tag{5.3}$$

For more precise calculations, either the background is regarded as quadratic or the Gaussian in Eq. (5.2) may be replaced by the modified Gaussian of Eq. (3.3). In this latter case Eq. (5.3) is modified slightly [34].

If the shape of the spectrum or the Γ values obtained from the first fitting indicate that there is more than one peak in the fitting region, a fitting can be performed by the function:

$$\bar{y}(i) = \sum_{j=1}^{\text{all peaks}} A_j \exp\left[-\frac{(i - p_j)^2}{2\sigma_j^2}\right] + Bi + C$$

and the intensity of each component is $N_j = 2.5A_j\sigma_j$. To reduce the number of parameters, σ can be regarded as constant for overlapping peaks.

The advantage of using peak areas instead of peak heights for intensity determination is that changes in detector resolution, mainly due to counting rate variations and overloading, do not effect the results. High count rates can significantly broaden full-energy peaks, especially when no pole-zero cancellation and/or baseline restoration (Section 10.1) is used. According to the author's own experiments, without pole-zero cancellation the resolution of a 3 cc Ge(Li) detector increased by a factor of two for the ^{60}Co peaks when the count rate was increased from 10^3 count/sec to 3×10^4 count/sec. Using the pole-zero cancellation circuitry, the deterioration of the peaks was much less pronounced and the increase in resolution was about 20% for the same counting rate variation. At any rate, one must remember that if the full width at half maximum cannot be estimated precisely (which is usually the case in graphical evaluation) more precise intensity results can be obtained by comparing the peak heights rather than the areas, if the latter are calculated by Eq. (5.3).

5.4 BASELINE CONSTRUCTION

There are several procedures by which peak areas can be calculated without any assumption for the shape of the peak. The disadvantage of these methods is that areas of overlapping peaks cannot be calculated individually.

The background under the peak is estimated from the spectrum outside the peak and a baseline is interpolated to distinguish the activity due to background and Compton scattering from the counts in the peak. The (net) peak area is given by $N = T - B$, where T is the total measured count under the peak and B is the area, measured in counts, under the

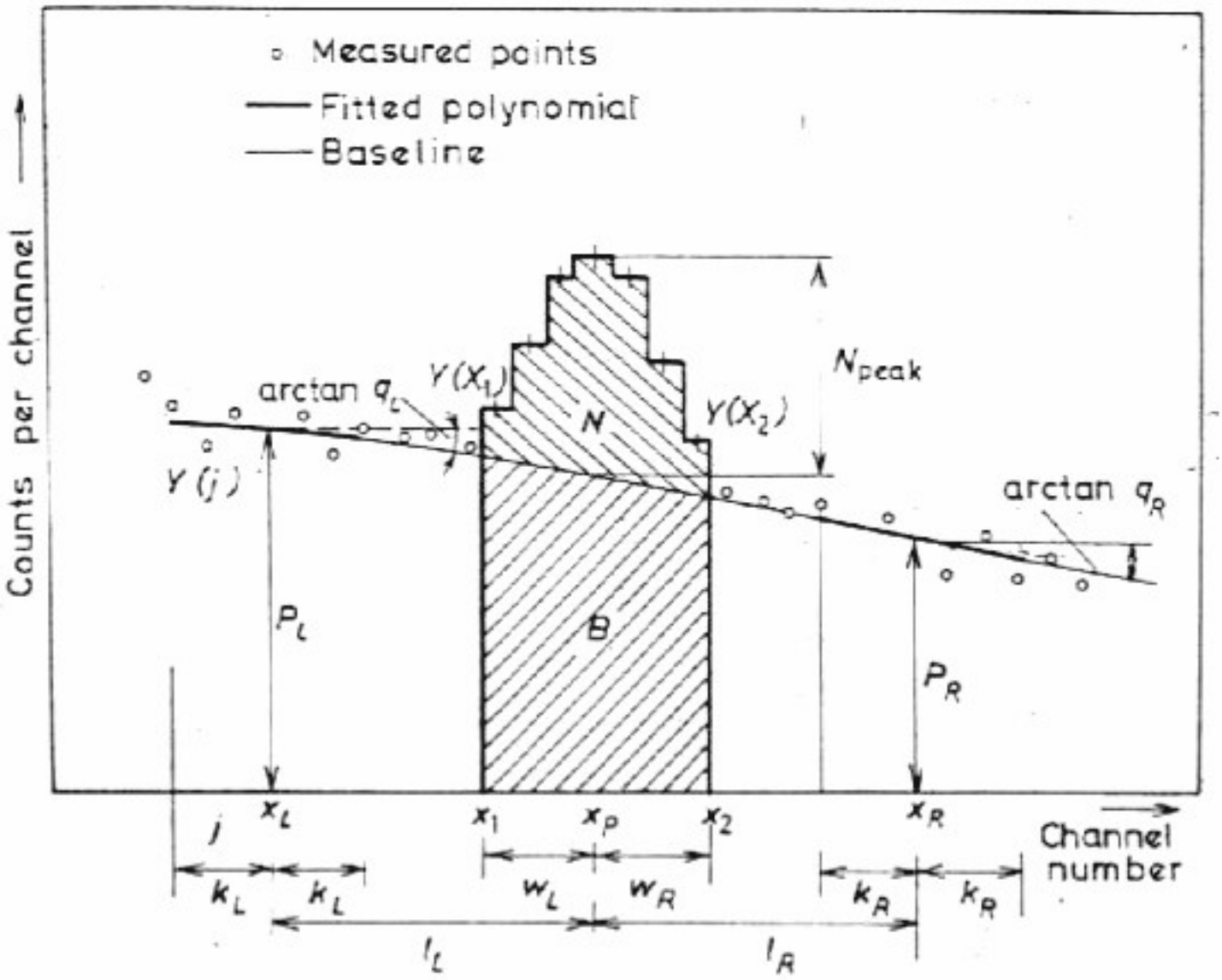

Fig. 14. Peak area determination. x_1 and x_2 are the boundaries of the peak region used for peak area calculation, $T = N + B = \Sigma Y(i)$ = total peak area, B = base area, N = (net) peak area

baseline in the peak region (Fig. 14). The selection of the peak boundary channels, between which the channel contents are to be summed to obtain the peak area, must be consistent for a given gamma energy in all spectra for which intensities are compared. The optimum selection of the boundary channels, i.e. the optimum portion of the peak region which should be included into the peak area calculation, will be discussed in the next section. In this section we restrict ourselves only to baseline construction.

The simplest method for constructing the baseline is to connect the data of the selected boundary points, x_1, x_2, by a straight line [59]. The base area is then a trapezoid. The peak area and its error are

$$N = \sum_{i=x_1}^{x_2} Y(i) - \frac{x_2 - x_1 + 1}{2} [Y(x_1) + Y(x_2)] \tag{5.4}$$

and

$$(\Delta N)^2 = \sum_{i=x_1}^{x_2} Y(i) + \frac{(x_2 - x_1 + 1)(x_2 - x_1 - 3)}{4} [Y(x_1) + Y(x_2)]$$

$$\approx T + \frac{x_2 - x_1 - 3}{2} B. \tag{5.5}$$

As the baseline is influenced strongly by the statistical fluctuations in the chosen boundary channels, better results can be obtained by using for the determination of the baseline the smoothed values at the boundaries instead of the raw data. A five-point smoothing (Section 2.2) reduces the error approximately to

$$(\Delta N)^2 \approx T + \frac{x_2 - x_1 - 3}{4} B \tag{5.6}$$

To lessen further the effect of the statistical fluctuations more points ought to be used in the smoothing. But for good precision the boundaries, where the baseline constructed in this way starts, have to be in or very near the peak region where only a small portion of the spectrum can be approximated by the second or third degree smoothing polynomials.

Other methods fit the straight baseline either to the smoothed first derivative on the left of the peak [49, 60], or to functions fitted to the raw data on each side of the peak [61, 62].

If the base area is much smaller than the peak area, there is no significant difference between the various methods mentioned above. However, if B is comparable to T, as is the case when measuring low intensity radiations or gamma-rays in the presence of intense higher energy gamma-rays, the method of baseline construction can influence the peak area very strongly. Even small deviations of the actual baseline from linearity can cause large errors in the intensity determination. To overcome this, higher degree polynomials constructed as explained below can be used as baseline [63, 64].

Due to the excellent energy resolution of Ge(Li) detectors, there are several channels on each side of the peaks of interest which in most practical cases do not contain any other peaks. In these regions a second degree polynomial is fitted to the measured values with least-squares techniques, using $2k_L + 1$ and $2k_R + 1$ points around the centres $x_L = x_p - l_L$ and $x_R = x_p + l_R$, respectively, where x_p is the location of the peak (see Fig. 14). The baseline is then constructed in such a way that at x_L and x_R it has the same magnitudes (p_L, p_R) and slopes (q_L, q_R) as the fitted polynomials. The simplest polynomial satisfying these conditions is the following cubic:

$$b(x) = p_L + q_L(x - x_L) + \left[\frac{-q_R - 2q_L}{l_L + l_R} + \frac{3(p_R - p_L)}{(l_L + l_R)^2}\right](x - x_L)^2 + \left[\frac{q_L - q_R}{(l_L + l_R)^2} + \frac{2(p_L - p_R)}{(l_L + l_R)^3}\right](x - x_L)^3. \tag{5.7}$$

The net count in the peak is:

$$N = \sum_{i=x_1}^{x_2} [Y(i) - b(i)]. \tag{5.8}$$

The values (p_L, p_R) and the derivatives (q_L, q_R) of the fitting polynomials can be expressed as function of the measured counts using the smoothing

constants of Table I (pp. 16–17), or for $K > 7$ the Tables of ref. [19] (corrected for misprints!).

For an often occurring practical case, when $x_p - x_1 = x_2 - x_p = 4$, Eq. (5.8) can be written in the form:

$$N = \sum_{i=x_1}^{x_2} Y(i) - 4.5(p_L + p_R) - F(l_L, l_R)\,(q_L - q_R)\,, \qquad (5.9)$$

where $F(15, 15) = 32.75$ and $F(18, 18) = 39.667$.*

The first two terms on the right side of Eq. (5.9) give the net peak area calculated with a linear baseline, while the third term gives the correction for the non-linearity. For a large number of experimental spectra this correction ranged from 10–20 counts to 160–250 counts for a base composed of Compton scattering and with B varying from 1,400 to 30,000 [64].

It has been experimentally demonstrated [64] that peak areas are nearly independent of the fitting regions, provided that sufficient points are used to reduce the statistical fluctuation (k_L, $k_R \geq 5$), and that fitting regions are outside the peak to be determined (l_L, $l_R > 3\Gamma$) and do not contain any other peak.

If too few points were used for fitting the polynomials (i.e. k_L, $k_R < 5$), then the baseline and the area under the baseline were influenced strongly by the statistical fluctuations in the individual channels. The effect is shown in Fig. 15(a), where baselines are constructed for the same spectrum with $l_L = l_R = 18$, fitting second degree polynomials to $7(k_L = k_R = 3)$ and $23(k_L = k_R = 11)$ points, respectively, for the determination of the boundary values of the baseline. Unsatisfactory results were obtained when too many points were included from the peak region into the fitting interval. In this case the influence of the peak distorted the baseline. This can be seen from Fig. 15(b), where baselines were constructed by fitting with second degree polynomials in the regions specified by $k_L = k_R = 7$ and $l_L = l_R = 13$ and 18, respectively.

* The slopes and the magnitudes of the second degree fitting polynomials are ($M = L, R$)

$$q_M = 3/[k_M(k_M + 1)(2k_M + 1)] \sum_{i=-k_M}^{k_M} i\, Y(x_M + i),$$

$$p_M = \frac{1}{1105}\left(\frac{167}{2} y_0 + 162y_1 + 147y_2 + 122y_3 + 87y_4 + 42y_5 - 13y_6 - 78y_7\right)$$

for $k_M = 7$,

$$p_M = \frac{1}{805}\left(\frac{70}{2} y_0 + 78y_1 + 75y_2 + 70y_3 + 63y_4 + 54y_5 - 43y_6 + 30y_7 + 15y_8 - 2y_9 - 21y_{10} - 42y_{11}\right)$$

for $k_M = 11$, where $y_i = Y(x_M + i) + Y(x_M - i)$, $(i = 0, 1, 2, \ldots, 11)$.

It can be shown that when the same data are fitted with a second or a third degree polynomial the errors in the magnitudes of the functions are

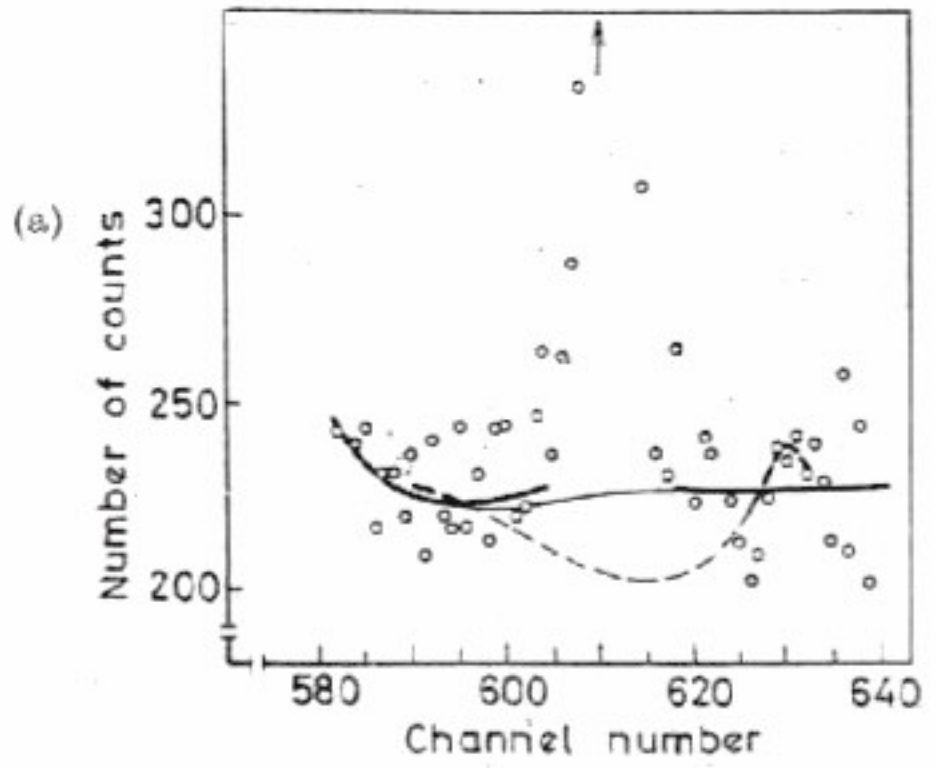

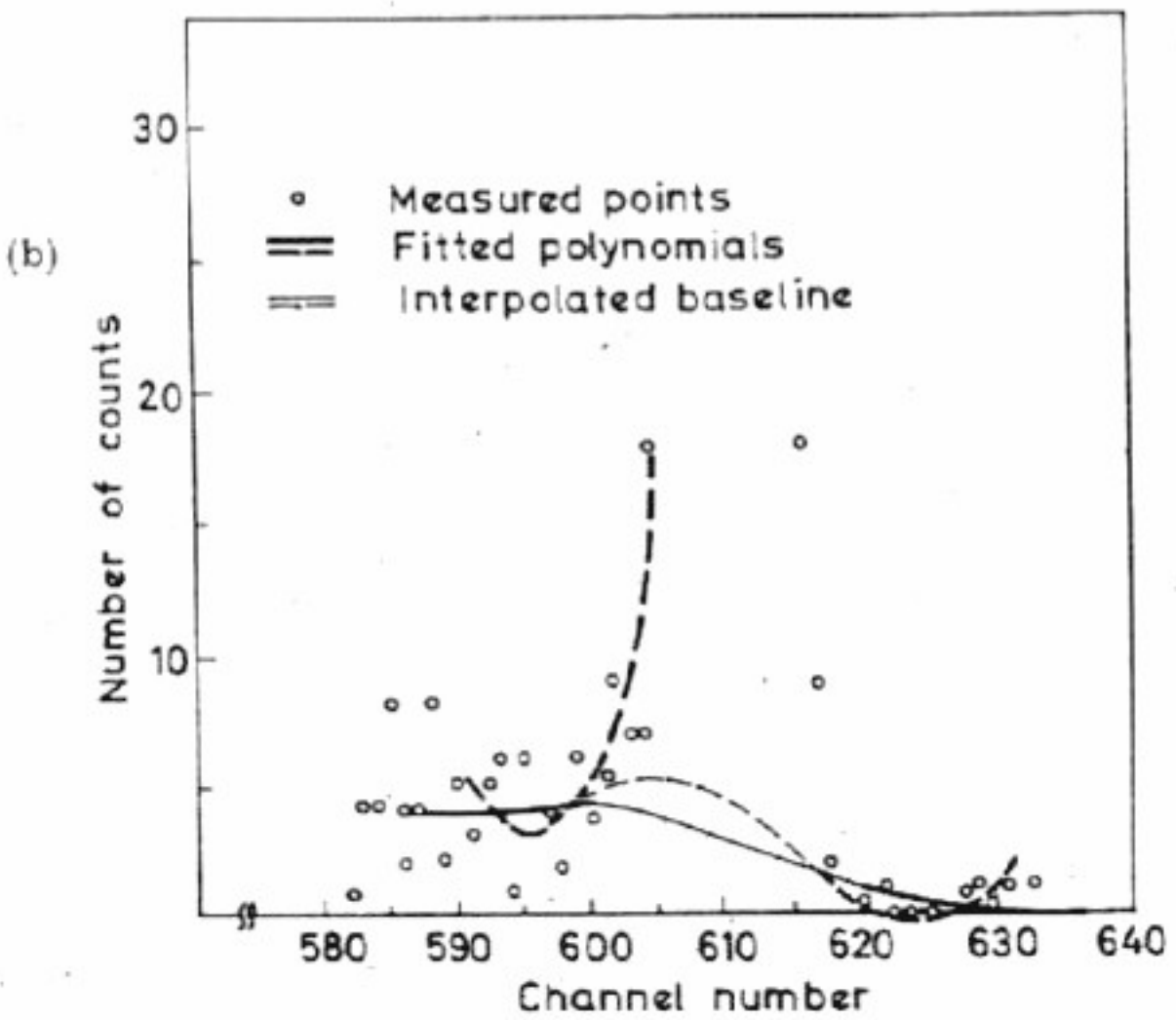

Fig. 15. Baselines interpolated by using different fitting polynomials. The solid curves were obtained from suitably fitting polynomials while the dotted ones were from unsatisfactory fittings.

(a) Using too few points for fitting, the statistical fluctuations in the individual channels influences the baseline.

(b) If the fitting interval contains too many points from the peak region, the peak distorts the baseline

the same, while the error of the first derivative is $\sim$ 2–3 times smaller in the first case. χ^2 tests showed that both the background and the Compton continuum could be well approximated by second degree polynomials in intervals containing about 20 or 30 channels (20–30 keV). Therefore, it can be expected that baselines constructed from fitting by second degree polynomials would lead to higher precision than those interpolated from third degree polynomial fitting.

Indeed, for a 1 keV/channel calibrated Ge(Li) spectrometer the results of the repeated measurements showed that best results were obtained for peak areas when 15–23 measured points were fitted with second degree polynomials ($k_L = k_R = 7$–11) centred about 15–21 channels away from the peak ($l_L = l_R = 15$–21). The optimum width of the peak area (w_L, w_R) depended on the ratio of baseline to total peak height and was in agreement with the calculations [65].

It can be shown [63] that for $k_L = k_R = 11$ and $l_L = l_R = 15$, the error of the peak area calculated by Eq. (5.9) is $\Delta N \approx \sqrt{T + 1.3\,B}$, which for large B is considerably less than the errors of other peak area methods.

In Fig. 16 the precisions of different peak area determinations are shown as functions of the baseline height-to-total peak height ratio for a peak

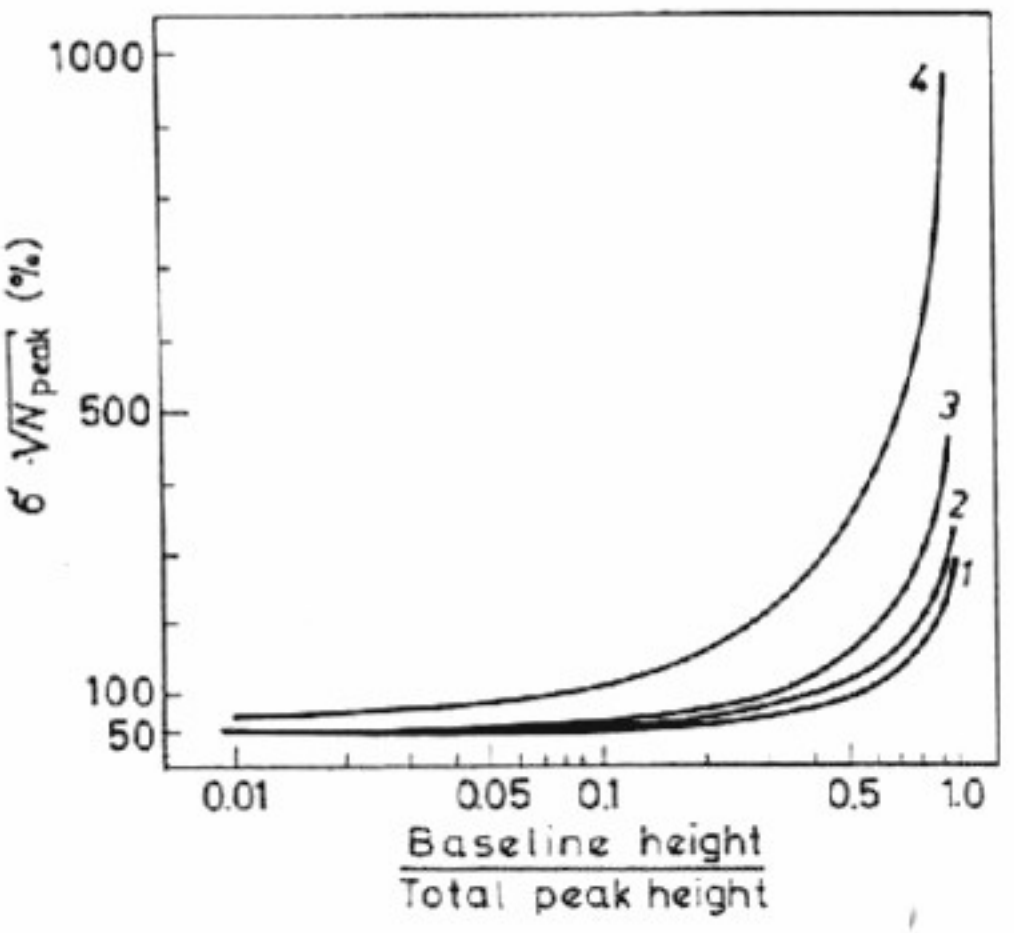

Fig. 16. Calculated statistical errors of different methods used for peak area determination as a function of the (baseline height)/(total peak height) ratio for a peak with $\Gamma = 5$ channels. To obtain the standard deviation (1σ) in percentage for a given ratio, the ordinate must be divided by $\sqrt{N_{peak}}$, where N_{peak} is the net peak height, the number of counts above the baseline in the peak channel.

1 — Non-linear baseline [63], [64] constructed by Eq. (5.7) with $k_L = k_R = 11$; $l_L = l_R = 15$; *2* — trapezoid method [59] using the raw data according to Eqs. (5.4) and (5.5); *3* — trapezoid method using data smoothed from five points in the second term of Eq. (5.4). Error calculated by Eq. (5.6); *4* — method of the smoothed first derivative [49, 60]

having $\Gamma = 5$ channels. In calculating the errors, it was assumed that there is no systematical error in the baseline, i.e. the statistical fluctuations are the only sources of errors. One can see from Fig. 16 that if the height of the baseline (or area) is small compared to the total peak height (or area), all methods have about the same scatter. But for peaks superimposed on a large background and/or Compton continuum, the precision obtained with the non-linear baseline is higher than that of the others. However, it has to be mentioned that this latter method is not applicable to scintillation detectors, because there are usually not sufficient 'peak-free' channels available to construct the fitting polynomials of the baseline.

5.5 SELECTION OF PEAK BOUNDARIES

Once a peak has been located, its boundary channels, between which the counts in the individual channels are to be summed to obtain the area of the corresponding peak, must be selected. For intensity calculations the boundary selection must be consistent in each spectrum for a given gamma-ray energy. Since the exact location of the boundaries is influenced by various experimental parameters, the best way is to determine them from the actually measured spectra.

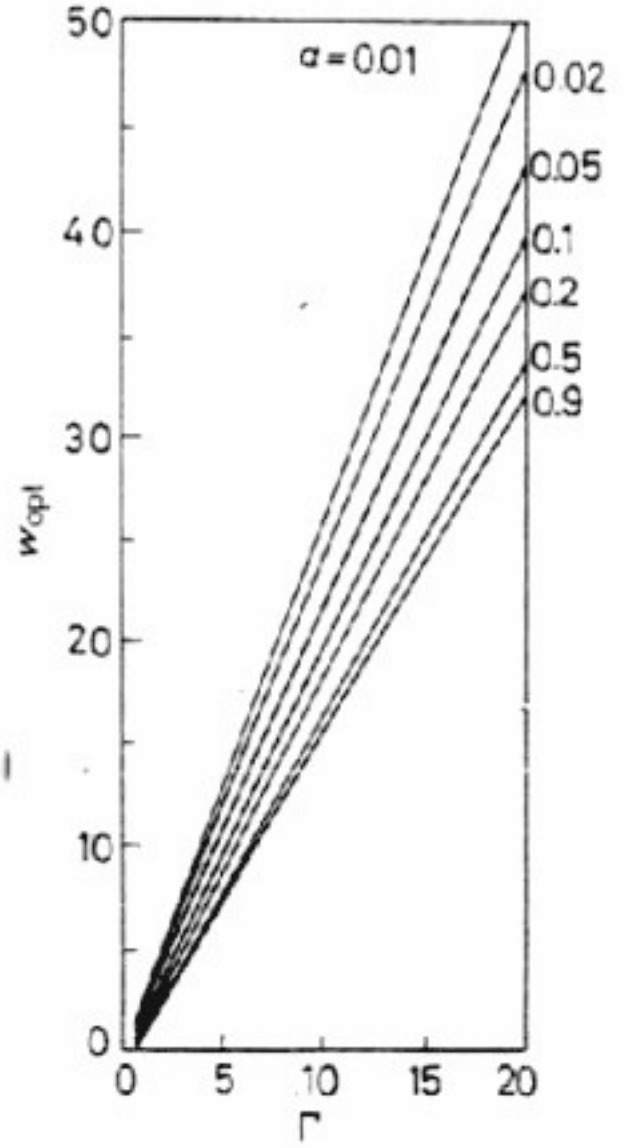

Fig. 17. Optimum portion of the peak region, w_{opt}, for minimizing the relative statistical error in the peak area calculation as a function of detector resolution Γ, for different baseline height-to-total peak height ratios, a. (from ref. [65]). In calculating w_{opt}, $N = \sqrt{T + B}$ was assumed

For NaI(Tl) spectra above a few hundred keV the left boundary is usually taken as the nearest minimum in the raw or the smoothed data below the peak channel. As was discussed in Section 4.2, Girardi *et al.* chose both boundaries such that from these channels the decreases in the channel contents were no more significant [46, 47].

The right side boundary channel is selected either symmetrical to the left one [59], or at the minimum on the right side of the peak, or where the smoothed first derivative drawn from the left side boundary intercepts the spectrum on the right side [20, 49, 60].

All these methods have the advantage that slight changes in detector resolution do not affect the peak area, but have the serious disadvantage that the positions of the boundaries themselves are influenced by statistical fluctuations and thus increase the variance of the peak area. This error can be eliminated by using a fixed number of channels (at least for a given gamma energy) when summing the counts. This can be seen in Fig. 16 where the precisions of different peak area methods are compared. The curves *1–3* relate to fixed boundary methods, while in curve *4* the boundary channels vary and are determined by the intersection of the spectrum and the smoothed first derivative drawn from the left side minimum. Since changes in resolution can be minimized by well-designed amplifying chain (built-in pole-zero cancellation, pile-up eliminator, baseline restorer, etc.), for well stabilized spectrometers the use of a fixed width peak region is preferred. It must be emphasized that the constant width must be valid only for a given energy, and the region for peak area calculation can increase with gamma energy in accordance with the increase in detector resolution.

The optimum portion of the peak region, w_{opt}, which should be included into the peak area calculation to minimize the relative statistical error in N depends on the baseline height-to-total peak height ratio, a, and on the detector resolution, Γ. Calculations for w_{opt} are shown in Fig. 17 taken from ref. [65]. However, these calculations can serve only as rough guidelines. First, they were performed with the assumption $\Delta N = \sqrt{T + B}$ which underestimates the error. The error of the base area, ΔB, is larger than the simple statistical error of B counts. Generally, $\Delta B \approx k\sqrt{B}$, where $k > 1$ depends on the method used for the baseline construction. In the second place, in practice the resolution for a given energy may vary with counting rate, especially for Ge(Li) detectors. Therefore, the width of the region used for peak area calculations must be wide enough that the change in resolution should not affect the peak area.

In Table V are the experimentally measured standard deviations of repeated peak area determinations. The same peaks were evaluated by the non-linear baseline and the trapezoid method (Eqs (5.9) and (5.4), respectively) using different numbers of channels for the peak area calculation. It can be seen that when the baseline-to-total peak height ratio is near 1, areas obtained from wider peak regions are less accurate than those obtained from relatively narrower ones. For low baseline-to-total peak height ratios the situation is reversed.

Table V. Precision of Peak Area Determination Using Different

Total peak height (counts)	Baseline / Total peak height*	Experimental standard							
		w/FWHM ≈ 0.5				w/FWHM ≈ 0.7			
		A	*B*	*C*	*D*	*A*	*B*	*C*	*D*
205	0.01	3.3	3.2	7.5	7.3	3.3	3.5	5.3	4.3
153	0.67	17	17	41	36	16	16	28	16
277	0.71	15	15	43	41	14	14	39	30
1567	0.85	12	14	39	28	14	16	39	16
4763	0.94	22	28	57	40	27	36	62	27

* Calculated in the channel which contained the maximum number of counts.
+ $w = w_R = w_L$ = number of channels on each side of the peak used for peak area determination
FWHM = measured full width at half maximum of the peak.

5.6 AUTOMATIC PEAK LOCATION AND PEAK AREA CALCULATION

The following computer program combining the smoothed first derivative and non-linear baseline methods has been routinely used in the author's laboratory for peak location and sensitive and precise peak area calculation in Ge(Li) spectra.

In the first step, possible peak positions (p_i) were chosen at the channels where the sign of the smoothed first derivative changed from positive to negative. The corresponding approximate peak areas (A_i) were calculated by the trapezoid method, Eq. (5.4). The number of channels used for the area calculations increased with gamma energy and was approximately equal to 0.6 × 'FWHM' on both sides of the peak.

If $A_e > 2\sigma(A_e)$ was fulfilled, the peak was regarded as definitely existing, if $0.2\ \sigma(A_p) < A_p \leq 2\sigma(A_p)$ then as a possible one, while if $A_r \leq 0.2\sigma\ (A_r)$ it was rejected. ($\sigma(A_i)$ was the standard deviation of A_i.) Then the channel differences were calculated between each possible peak and its nearest neighbouring definitely existing peaks. These distances and the A_e/A_p ratios determined the limiting factors for the k and l fitting parameters. If these values were larger than the optimum ones (see Section 5.4), the optimum values were used for non-linear baseline construction and peak area calculation. If they were smaller than the optimum, but larger than the minimum permitted k and l values, they were used.

However, in very complex spectra it occurred that peaks were not widely enough separated. If there were less than 6–8 points between the tails of adjacent peaks, the slope of the baseline could be determined only with large error. When this occurred, then on the corresponding side of the peak only the value of the fitting polynomial was calculated. The baseline was approximated by a second degree polynomial having the same values as the fitting polynomials on each side of the peak, and the same

Numbers of Channels for the Peak Calculation

deviation in percentages+

$w/FWHM \approx 1$				$w/FWHM \approx 1.2$			
A	*B*	*C*	*D*	*A*	*B*	*C*	*D*
3.2	3.2	3.7	4.1	3.1	3.0	3.0	3.0
18	15	29	19	18	18	40	31
15	23	45	29	16	22	34	21
12	15	19	27	15	17	33	29
33	37	38	33	32	33	50	44

A — non-linear baseline with second degree polynomial fitting, $k = 11$, $l = 15$;
B — same as *A*, but $k = 11$, $l = 18$;
C — trapezoid method (Eqs (5.4) and (5.5));
D — same as *C*, but using the smoothed data for determining the counts at the boundaries.
All deviations are the experimental values obtained from 10–15 measurements.

first derivative on the corresponding side where the polynomial was fitted to sufficient data points to give an accurate shape. It was shown that the (net) peak area did not depend on k and l provided both were in the allowed interval, and was the same even when the derivative was fitted only on one side of the peak. Therefore this method did not give uncorrect results except for unresolved or very close peaks.

For each possible peak the exact peak areas (N_p) were calculated by the non-linear baseline method, the parameters of which had been determined as described above, and all peaks were finally definitely identified for which $N_e > 2\sigma(N_e)$.

The N_e's could be used for both absolute and relative intensity calculations.

When neighbouring peaks were resolved but were so near that the non-linear baseline could not be fitted, then the area was calculated only by the trapezoidal method.

The peak widths were controlled and for too wide ones no areas were calculated, only warning messages were given.

The block-diagram of this program is shown in Fig. 18.

To have the program run faster when more information was available from visual examination of the data, an option was built in to jump through the peak locating part and calculate by non-linear baseline peak areas only in the peak positions and with k and l parameters given by the programmer.

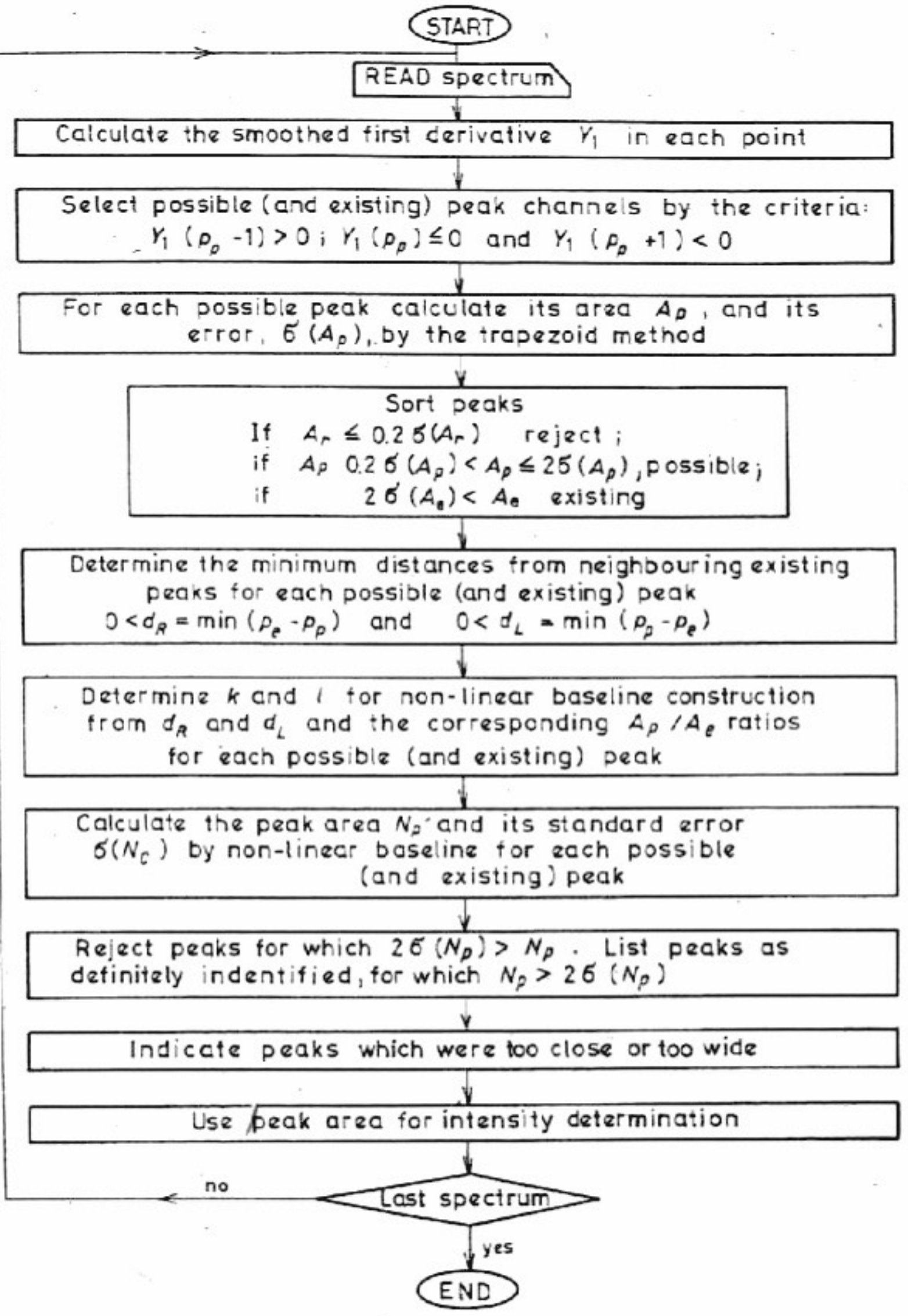

Fig. 18. Automatic peak-locating and area-calculating program

6. WEIGHTED LEAST-SQUARES RESOLUTION

The analysis of complex gamma-ray spectra by the method of weighted least-squares is now used extensively, because the availability of high-speed digital computers has made the numerical calculations a relatively simple matter and for a given set of data this method usually gives the solution which has the smallest statistical error. In this section, only the fundamental assumptions and the basic mathematical concepts of least-squares analysis are considered. More detailed information on the general problem can be found, e.g. in the book written by Hildebrand [66], and numerous authors have discussed its application to gamma spectrometry, e.g. refs. [12, 67–79].

6.1 BASIC ASSUMPTIONS

In the practical applications of weighted least-squares techniques to gamma-ray spectrometry, the following basic assumptions are made:

(*a*) The spectrum to be analysed results from a mixture of known nuclides and the exact shape of all of the standard spectra of these nuclides (often called spectrum library) are available either by direct measurements or by calculations described in Chapter 3.

(*b*) The activities of the individual components are added linearly and the response function of the detector system is not activity-dependent.

(*c*) Each component of the complex spectrum has a different spectrum, all of these being linearly independent. In practice, due to statistical fluctuations and electronic instabilities this condition must be strengthened so that the spectra are substantially different.

In principle, (*a*) could always be fulfilled by including the spectrum of each radioisotope into the standard spectra. But this has no practical reason because the more the number of standards included in the fit, the less the accuracy of the results. If the components are not known *a priori* then the possible components are selected by a preliminary calculation, usually based on the peaks in the spectrum. After completing the calculations, the residuals and the χ^2 test (see later) can prove the validity or invalidity of (*a*), i.e. whether all components of the mixture are among the standards or not.

If the counting rate is low, (*b*) can always be regarded as valid. For high counting rates, corrections must be made for pulse pile-up and dead-time losses. Some of these problems are discussed in Section 10.3.

Several radioisotopes emit gamma-rays differing in energy by less than the detector energy resolution. This is especially true for scintillation

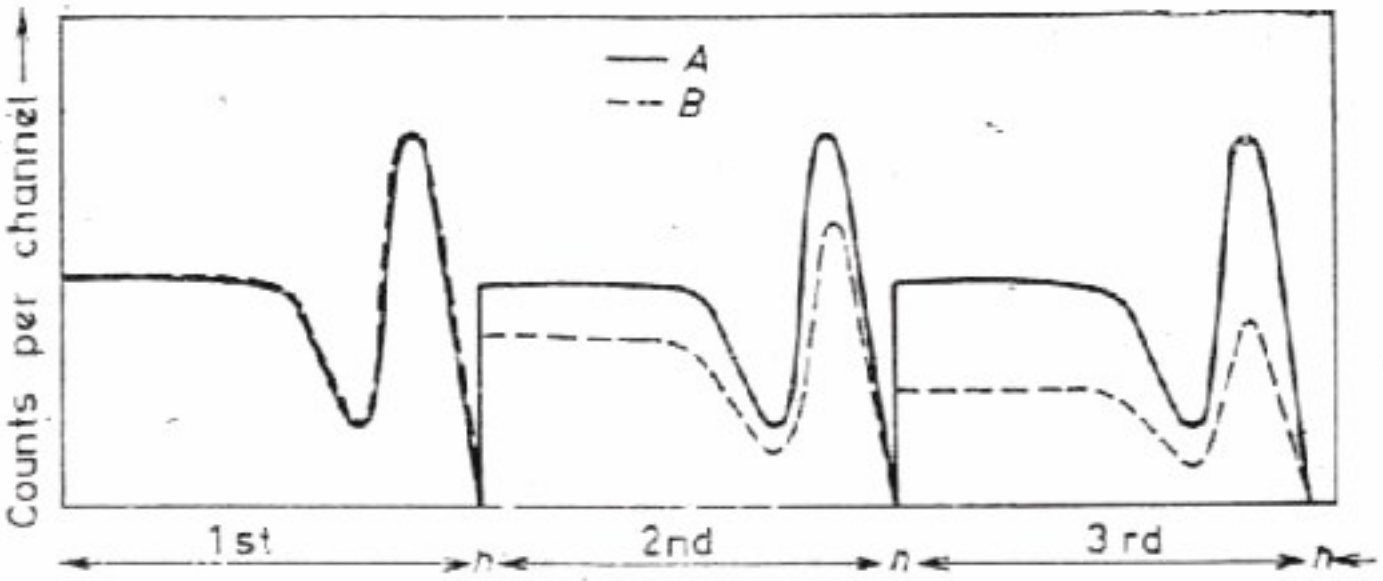

Fig. 19. The principle of spectrum combination. Radioisotopes A and B emit the same energy gamma-rays. The shapes of their spectra are identical at any time. Due to their different half-lives the shapes of their combined spectra differ substantially

detectors where least-squares techniques are most often applied. Due to the relatively poor energy resolution, full-energy peaks and Compton-edges of gamma-rays close in energy nearly coincide. The shapes of spectra of different radioisotopes become nearly identical, and the slight differences may be concealed by statistical fluctuations. For this reason assumption (*c*) may often be violated. The problem is further complicated when not the product radioisotope but the parent nucleus from which it was produced is to be determined. For example, in neutron activation analysis a radioisotope ${}^{A}_{Z}X$ can be produced from the isotopes ${}^{A-1}_{Z}X$, ${}^{A+1}_{Z}X$, ${}^{A}_{Z+1}Y$, ${}^{A+3}_{Z-2}W$ (if these isotopes exist in nature) via the reactions

$${}^{A-1}_{Z}X\ (n,\gamma)\,{}^{A}_{Z}X, \quad {}^{A+1}_{Z}X(n,2n)\,{}^{A}_{Z}X, \quad {}^{A}_{Z+1}Y(n,p)\,{}^{A}_{Z}X, \quad \text{and} \quad {}^{A+3}_{Z+2}W(n,\alpha)\,{}^{A}_{Z}X.$$

The measurement of the activity of X, without further consideration, cannot be used for the determination of one of the elements X, Y or W, if any of the other elements are present in comparable amounts.

To satisfy condition (*c*) for these unfavourable cases, the n channel spectra measured after j different decay times for each standard and sample (and for the background) are combined without any decay correction into one spectrum consisting of $n \times j$ channels [67]. The $1^{st}, 2^{nd}, \ldots, j^{th}$ spectra need not be measured under the same experimental conditions provided all the k^{th} spectra ($k = 1, 2, \ldots, j$) are measured in the same way. For example, the first measurement for each standard and sample can be performed using a large source-detector distance to reduce pulse pile-up and dead-time, while the later ones can be performed using a larger detector, improved counting geometry and longer measuring time to improve statistics. Following neutron activation, no different radioisotopes are produced having precisely the same half-lives and gamma-ray energies [80]. The combined spectrum can, therefore, be considered unique and substantially different for each pure radioisotope (Fig. 19).

Besides the desired radioisotope ${}^{A}_{Z}X$, other radioisotopes are produced from the elements X, Y, W by the (n, p), $(n, 2n)$ and (n, α) reactions. The

activity ratios of these isotopes to each other and to that of ${}^{A}_{Z}X$ are different. For this reason the combined spectra of each element are substantially different, even if they contain the same radioisotope, and in spite of the fact that when the activity of this isotope dominates their simple spectra are essentially the same.

Since the standard spectra measured and combined in the way described above fulfil all the given requirements, the usual weighted least-squares resolution of the combined spectrum of the sample is possible.

6.2 DERIVATION OF THE 'LEAST-SQUARES EQUATIONS'

If a complex spectrum measured in n channels has to be decomposed to l known components (one of them may be the background), the intensity x_k of each component relative to that of its standard is determined by the requirement that the value of the normalized χ^2, defined as

$$\chi^2 = \frac{1}{n-l} \sum_{i=1}^{n} w_i \left(Y_i - \sum_{k=1}^{l} x_k A_{ki} \right)^2 . \tag{6.1}$$

should be minimum. Y_i and A_{ki} are here the counts recorded under the same experimental conditions in the ith channel of the analyzer for the complex and for the known kth component spectrum, respectively, and w_i is a suitably selected weighting factor, usually the reciprocal of the variance of the difference between measured and calculated counts in the ith channel.

The relative intensities minimize χ^2 if

$$\frac{\partial \chi^2}{\partial x_k} = 0 \qquad \text{(for all } k\text{)}. \tag{6.2}$$

Equation (6.2) leads to the following set of equations for the unknown relative intensities

$$\sum_{m=1}^{l} x_m \sum_{i=1}^{n} w_i A_{ki} A_{mi} = \sum_{i=1}^{n} w_i A_{ki} Y_i \qquad (k = 1, 2, \ldots, l). \tag{6.3}$$

Naturally, a similar result is obtained when Eq. (6.2) is solved by the matrix techniques (see Section 8.1), the intermediate steps then being shorter, but their understanding needs somewhat more mathematics. It can be shown that for this problem the maximum likelihood method leads to the same set of equations [71].

If all the conditions mentioned in Section 6.1 are fulfilled then the expected value of χ^2 is $\langle \chi^2 \rangle = 1$ with the scatter $\sqrt{2/(n-l)}$ while the scatter of x_k is $\Delta x_k = \sqrt{M^{-1}_{kk}}$, where M^{-1} is the inverse matrix of the set of Eq. (6.3) [13, 72].

If χ^2 deviates significantly from its expected value, this indicates either a missing component from the standard spectra or alterations between the experimental conditions in which the standards and the composite spectra were measured, usually gain and/or threshold shift. A channel-by-channel plot of the residuals,

$$Y_i - \sum_{k=1} x_k A_{ki}, \quad \text{or the weighted residuals,} \quad w_i \left(Y_i - \sum_{k=1} x_k A_{ki} \right)$$

often gives a clue to the source of error. In this plot, missing components are characterized by a peak at the position of the peak in their own spectrum, while a valley and a peak in addition to a true peak in the spectrum suggest electronic instabilities.

To plot and examine the difference visually between the measured and calculated spectra is a lengthy time-consuming procedure, and anyway, a decision as to whether the fit is good, acceptable or poor, remains rather subjective. An increase in χ^2 — when the spectrum library is complete — is due mainly to the electronic instabilities of the measuring equipment. Several authors have investigated the relationship between the results of least-squares resolution and gain and threshold shifts.

Dudley and Ben Haim studied the influence of multiplier and amplifier gain variation on the values, computed by least-squares techniques, of the different contributions to complex spectra [81]. According to an earlier paper of the present author [82], the increase in χ^2, $\Delta\chi^2$, due to electronic instabilities can be fairly well approximated by

$$\Delta\chi^2 \approx \frac{1}{n-l} \sum_{r=1}^{s} F_r G_r I_r (d_r/F_r; C_r/G_r), \tag{6.4}$$

where C_r is the height of the baseline and G_r is the amplitude, both in counts,

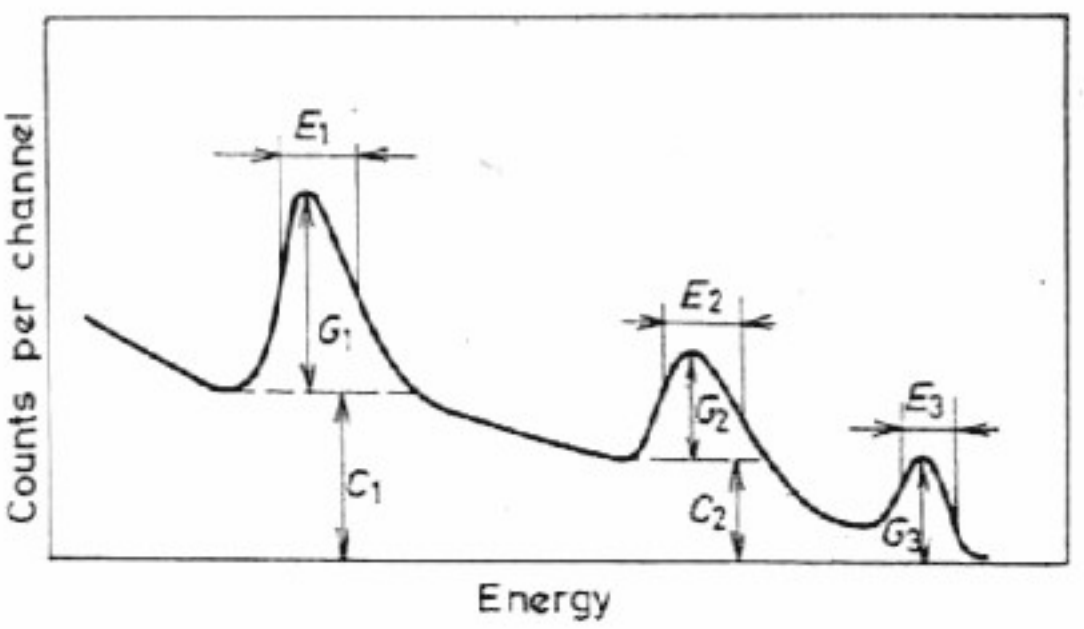

Fig. 20. The estimation of the increase in χ^2 due to electronic instabilities

and F_r the width and d_r the absolute value of the total shift, both in channel, for the rth peak (see Fig. 20). The summation is extended to all peaks present in the complex spectrum. The values of I_r $(d_r/F_r; C_r/G_r)$ as functions of d_r/F_r and C_r/G_r are shown in Fig. 21.
For the extreme cases

$$C_r \ll G_r;\ I_r \approx 5.85 d_r^2/F_r^2. \tag{6.5}$$

$$C_r \gg G_r;\ I_r \approx 2.25 d_r^2/F_r^2. \tag{6.6}$$

The instability of any detector system can be determined by repeating measurements on the same standard spectra over a reasonably long time. Knowing this, the maxima of the d_r's and from these the maximum permissible value of χ^2 can be determined by Eq. (6.4) and by means of Fig. 21 or Eqs. (6.5) or (6.6). The weighted least-squares decomposition of a complex spectrum for which χ^2 remains below this maximum can be accepted, while for higher values of χ^2 the decomposition is sure to be inadequate. If this happens, then in most cases one or more components have not been included in the standards. If the missing components can be figured out from the plot of residuals and their standard spectra are available, a new fit can be performed with the extended set of standards.

A priori known information can be used to improve the accuracy and validity of the results [83]. The most trivial case is where there are no 'negative intensities', $x_k \geq 0$ for all components. If $x_k < 0$ for any k, the least-

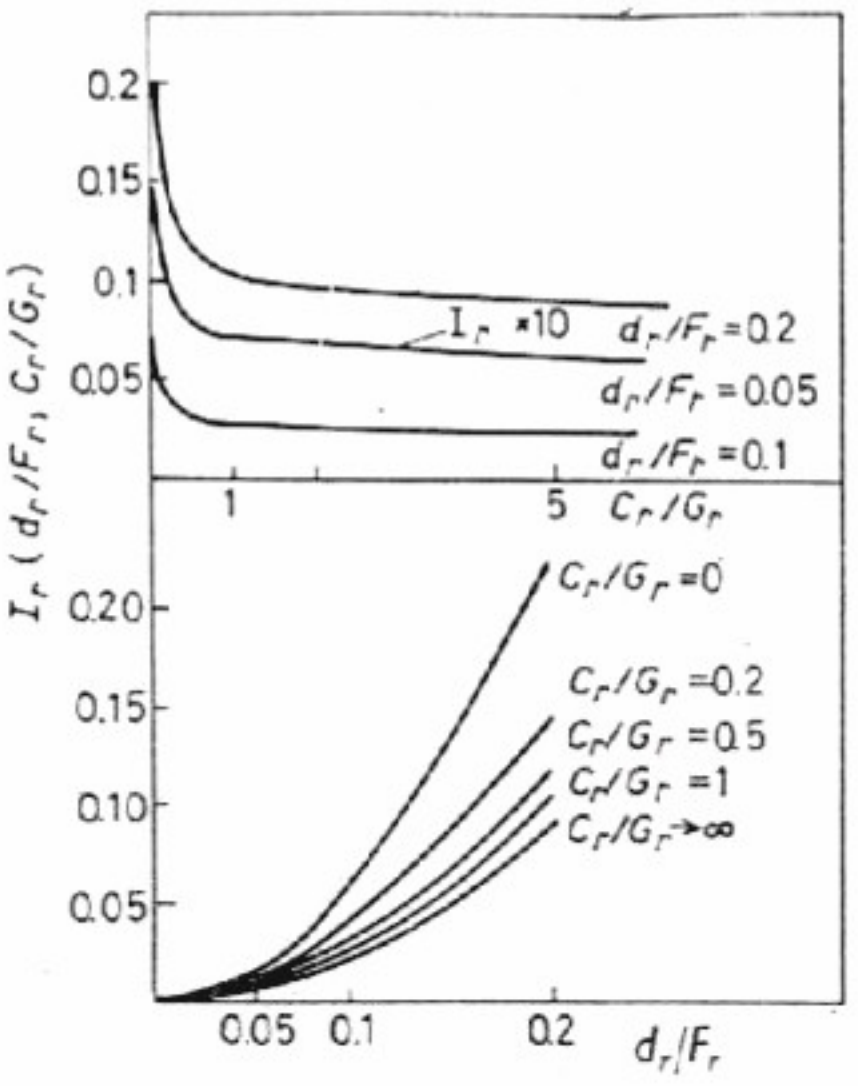

Fig. 21. The factor I_r of Eq. (6.4) as a function of C_r/G_r and d_r/F_r

squares procedure is repeated, excluding from the standards the spectra of these components. A more severe condition can be applied from the fact that the measured activity is the sum of the individual activities in each channel,

$$\sum_{k=1} x_k A_{ki} = N_i \qquad (i = 1, 2, \ldots, n)$$

from which

$$x_k \leq N_i/A_{ki} \qquad (i = 1, 2, \ldots, n; \quad k = 1, 2, \ldots, l).$$

In practice this is substituted by

$$x_k \leq \text{minimum}\left[\frac{N_i}{A_{ki}} + 3\Delta\left(\frac{N_i}{A_{ki}}\right)\right] \quad (i = 1, 2, \ldots, n; \quad k = 1, 2, \ldots, l),$$

where $\Delta(N_i/A_{ki})$ is the statistical error of N_i/A_{ki}.

Even for ideal electronic stability and a complete library of standard spectra, the accuracy of the decomposition is still affected by the difference between the shapes of the component spectra. The diagonal elements of the inverted matrix give the accuracies of the results only after the measurement. To predict what accuracy can be achieved by the least-squares techniques Fig. 30 in Section 8.4 and Wohlberg's graphs can be used [84].

6.4 GAIN AND THRESHOLD COMPENSATION

Instrumental instabilities appear mainly as gain and/or threshold shifts. These can be inherent in the electronic system itself, but can also be caused by varying experimental conditions, e.g. count rate variation, or pulses which are much larger than those to be measured. Several digital spectrum-stabilizer and amplifier baseline restoring circuits have been developed to minimize electronically the gain and threshold shifts (see Section 10.1). Parallel with or instead of these sophisticated devices, computer programs can also correct electronical instabilities. For compensating small changes in gain and zero intercept, linear interpolation is the simplest way [85, 86]. After a change in zero intercept of z channels and a fractional change in gain g, the new channel boundaries correspond to energy intervals different from the original ones. The new boundaries of channel i are:

$$L_i = i + z + g(i - z_0)$$

and

$$R_i = i + 1 + z + g(i + 1 - z_0),$$

where z_0 is the original zero-energy intercept corresponding to the standard energy calibration of the spectrometer.

If Y_i denotes the number of counts (or the counting rate) in channel i of the shifted spectrum, then the shift corrected count is given by

$$\overline{Y}_i = (1 - L_F)Y_{L_I} + Y + R_F Y_{R_I}$$

In this equation L_F and R_F denote respectively the fractional, and L_I and R_I the integral parts of L_i and R_i, and Y is the sum of the channel content between L_I and R_I

$$Y = \sum_{j=L_I+1}^{R_I-1} Y_i \quad \text{and} \quad Y = 0 \quad \text{if} \quad L_I + 1 > R_I - 1.$$

Although this method is very simple in principle, in practice it is often preferable to other more sophisticated procedures, provided that the gain shifts are smaller than the widths of the peaks. A number of other types of gain changing programs have been proposed in the last few years. Some of them apply quadratic fitting to groups of channels to determine peak positions and determine the gain changed spectrum after appropriate rescaling using the coefficients of these fits, while others rely in some way on the channel counts conservation method [87, 88, 89].

Another method for estimating gain and threshold shift by least-squares techniques was proposed by Schonfeld [12]. For small shifts the corrected count in channel i is

$$\overline{Y}_i \approx Y_i + 1/2(Y_{i+1} - Y_{i-1})\left[(g-1)(i - z_0) + z_0 - z\right]. \qquad (6.7)$$

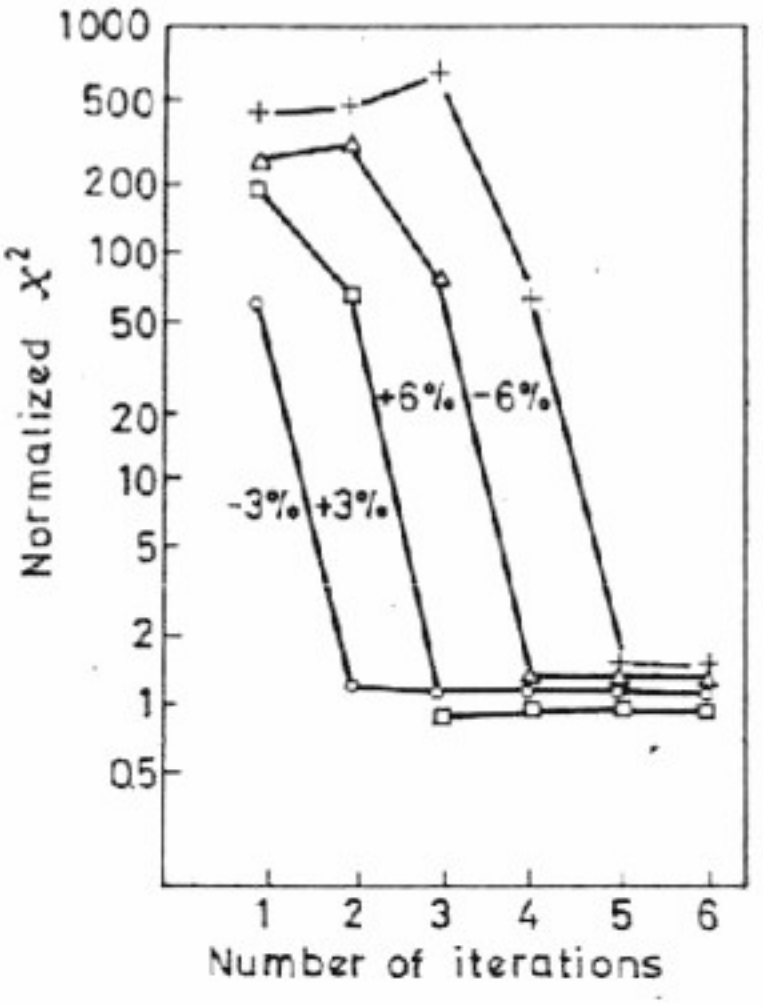

Fig. 22. Decrease in normalized χ^2 due to successive gain and threshold shift corrections. The eventual gain shifts are indicated on the curves. The threshold shift was less than 0.1 channel and the degree of freedom was 238

In this case instead of Eq. (6.1)

$$\chi^2 = \frac{1}{n-l-2} \sum_{i=1}^{n} w_i \left(\overline{Y}_i - \sum_{k=1} x_k A_{ki} \right)^2 \tag{6.8}$$

is to be minimized. Substituting Eq. (6.7) into Eq. (6.8) the minimizing condition leads to a similar set of equations to Eq. (6.2) with two more unknowns, g and z, and two more equations due to the conditions $\partial\chi^2/\partial g = 0$ and $\partial\chi^2/\partial z = 0$.

Since Eq (6.7) is only a first approximation to the corrected spectrum, it may be that several iterations are necessary to obtain the correct fit. From the first gain and threshold shifts a corrected spectrum is calculated, and a new gain and threshold corrected fit is performed with these corrected data. The dramatic decrease in the normalized χ^2 due to this gain and threshold compensation is shown in Fig. 22. The details of this procedure and its results are described in ref. [12].

6.5 SELECTION OF WEIGHTING FACTORS

The weighting factor for the data measured in channel i, w_i in Eqs. (6.1) and (6.2), is usually the reciprocal of the variance of the difference between the measured and calculated counts in the corresponding channel,

$$1/w_i = \left\langle Y_i + \sum_{k=1}^{l} x_k^2 \frac{t^2}{t_k^2} A_{ki} \right\rangle \tag{6.9}$$

if the background is regarded as an individual component, and

$$1/w_i = \left\langle Y_i + \frac{t^2}{t_B^2} B_i + \sum_{k=1}^{l} x_k^2 \left(\frac{t^2}{t_k^2} A_{ki} - \frac{t^2}{t_B^2} B_i \right) \right\rangle \tag{6.10}$$

if the background is substracted from each datum. Here B_i and A_{ki} are the counts accumulated from the background and the kth standard, respectively, during their corresponding measuring periods, t_B and t_k, t is the measuring time of the complex spectrum and experimental instabilities are neglected. The $\langle\ \rangle$ notation means the expected value.

In most cases Y_i or $Y_i + \frac{t^2}{t_B^2} B_i$ is much larger than the remaining parts between the brackets. The expected values can be approximated by the measured ones so

$$1/w_i = Y_i \quad \text{or} \quad 1/w_i = Y_i + \frac{t^2}{t_B^2} B_i. \tag{6.11}$$

If $1/w_i$ were zero according to Eq. (6.11), then $w_i = 1$ is usually taken arbitrarily. Using these weighting factors in Eq. (6.2), the equations are linear in the unknowns and can be solved directly.

If the statistical error of the standards is not negligible compared to that of the composite spectrum, then a weighted least-squares resolution is performed, first using Eq. (6.11) as weights, and from the x_k values so obtained the more precise weights are calculated according to Eqs. (6.9) or (6.10) and the fit is repeated [85].

Counts that are less than their expected values have a relatively larger weight than those that are larger than their expected values in the $\langle Y_i \rangle = Y_i$ approximation. This leads to a systematical underestimation of the x_k values, which can be significant when the numbers of counts are small in a lot of channels. In this case an iterative fit is necessary, and in the consecutive iterations $w_i = \sum_{k=1}^{I} x_k A_{kl}$ is used instead of Y_i [90]. For instance, for a complex Ge(Li) spectra the usual weighted least-squares resolution gave values of 0.85 and 0.86 for the ratio of the measured and true intensities with an experimental standard deviation of 0.05 around the measured mean value for spectra where the average counts per channel were ~ 10 and ~ 5, respectively [64].

If smoothed data are used in the fit, then the weighting factors must be multiplied by a corresponding factor, taken from Table I, due to the reduction of the statistical error of the smoothed data, or the expected value of the normalized χ^2 will be less than 1.

6.6 EFFECT OF MISSING COMPONENT

In gamma spectroscopy, especially in activation analysis, it can be always expected that appreciable activities are produced from the elements the spectra of which have not been included in the standard input spectra used for fitting. In this case the intensities of the standards determined by the method of weighted least-squares are usually higher than their actual values and the contribution of the unknown element is somewhat levelled off by the additional weight of the known components. The effect of a missing component is shown in Fig. 23. The curve of the residuals exhibits

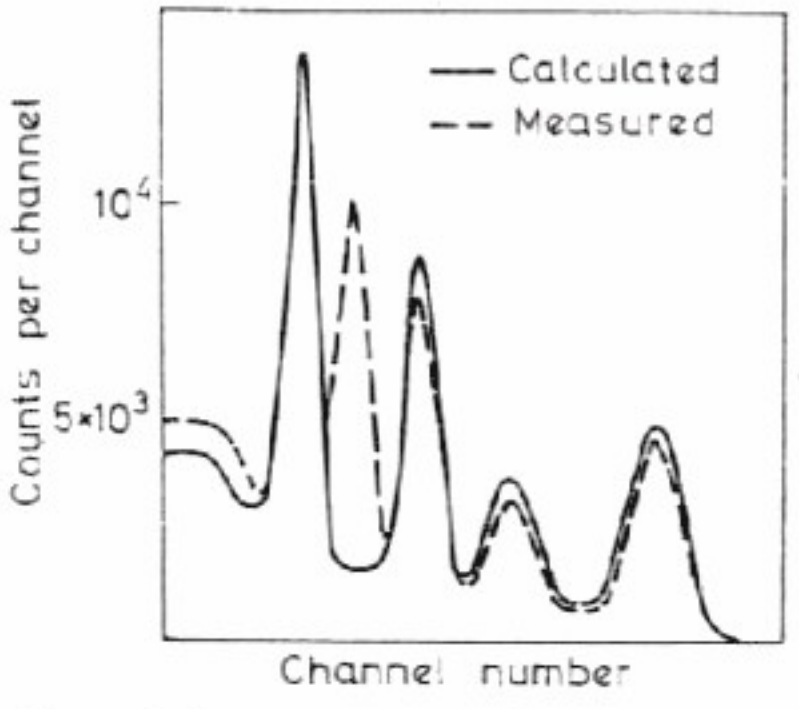

Fig. 23. Effect of a missing component in weighted least-squares resolution

(a)

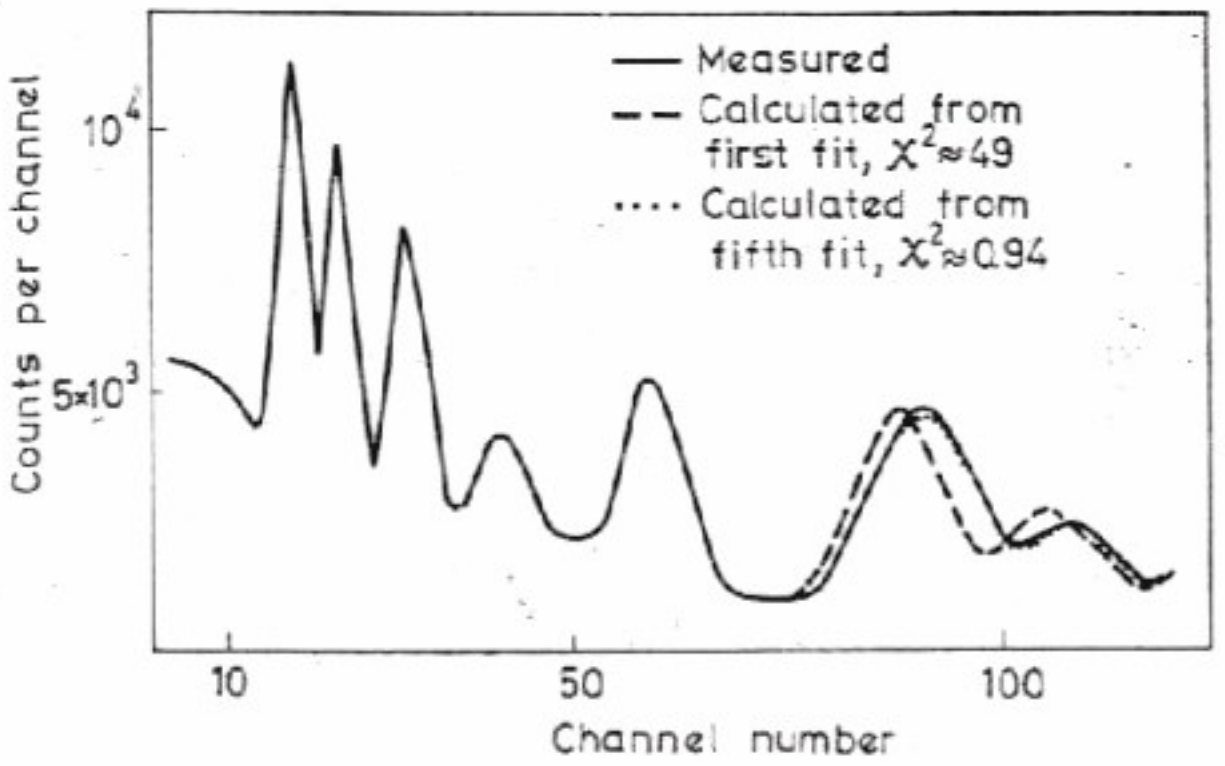

(b)

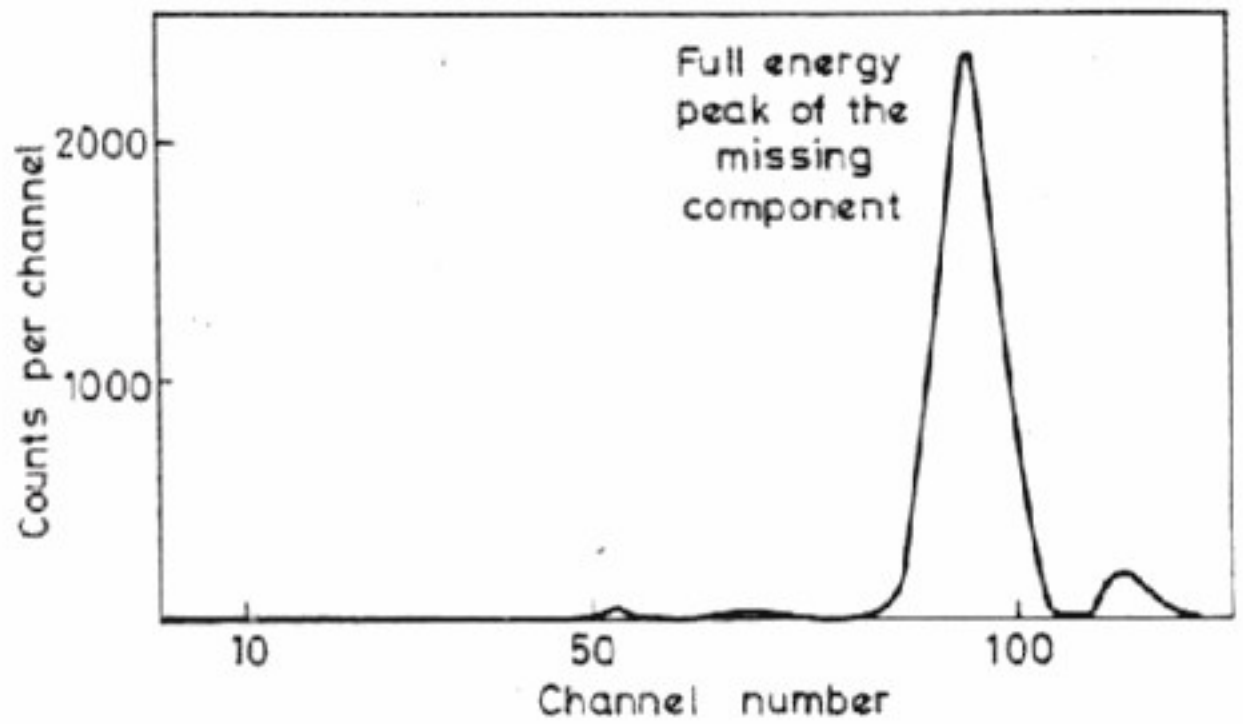

Fig. 24. Spectrum of the measured and calculated composite spectra after different numbers of iterations (a) and of the missing component (b)

Table VI. Relative Intensity Determination

Total counts in peak region	Net peak area[b]	Ratio of the measured and expected			
	Total counts in peak region	Non-linear baseline[a]	Trapezoid method	Trapezoid method (smoothed)	Smoothed 1st deriv.
522	0.95	0.97±0.06	0.98±0.06	0.98±0.10	0.97±0.05
1008	0.98	0.99±0.03	1.01±0.03	0.99±0.03	0.99±0.03
1165	0.23	1.02±0.15	0.91±0.45	0.91±0.16	1.23±0.50
1792	0.25	0.94±0.16	0.97±0.29	0.90±0.19	0.98±0.35
13463	0.072	1.08±0.12	1.02±0.19	1.06±0.16	1.12±0.50
30710	0.031	1.18±0.22	1.61±0.62	1.03±0.27	1.46±0.90

[a] Fitting with second degree polynomials, $k = 11$, $l = 15$

a peak close to the full-energy peak of the missing standard, and valleys appear in the vicinity of the peaks of the standards which are included. The nearer these peaks are to the peak of the omitted standard, the more pronounced are these features.

To eliminate erroneous results for the known components, due to activities of unidentified radioisotopes, an iterative procedure can be used [91]. The procedure yields not only the precise relative intensities of the known components but also the full-energy peak of the unknown component, from which its spectrum can be generated if necessary.

The procedure exploits the fact that for a good fit the residuals are significantly positive in the channels where the contribution of the unknown component is high. Consequently, the significantly positive counts give a very crude approximation to the contributions of the unknown constituents. This approximate shape is added to the known standards as a new standard, the fit is repeated, and the significantly positive residuals are added again to the shape of the unknown spectrum. It can be proved that the procedure is convergent and gives the shape of the missing component if this has the lowest energy among the standards, and gives the shape of its full-energy peak otherwise. The shape of the missing component and the measured and calculated spectra after different numbers of iterations are shown in Fig. 24.

6.7 PEAK AREA CALCULATION OR WEIGHTED LEAST-SQUARES RESOLUTION?

If the exact laws of mathematics could always be applied to experimental nuclear physics, this question could be answered without any hesitation in favour of least-squares techniques. The argument of the theoreticians would be: The more the counts used for evaluation, the less is the statistical error obtained from these data. Therefore the least-squares method is more preferable for semiconductor detectors, where the peak to total ratio is smaller, than for scintillation detectors.

by Different Methods

counts	Calculated relative error				
Weighted least-squares	Non-linear baseline[a]	Trapezoid method (smoothed)	Trapezoid method	Smoothed 1st deriv.	Weighted least-squares
0.94±0.07	0.06	0.06	0.06	0.10	0.04
0.99±0.03	0.04	0.04	0.04	0.05	0.02
0.86±0.18	0.17	0.35	0.20	0.45	0.11
0.98±0.11	0.12	0.26	0.15	0.32	0.10
0.99±0.04	0.18	0.24	0.19	0.80	0.10
0.98±0.17	0.26	0.55	0.28	1.00	0.20

Determined by non-linear baseline by fitting with second degree polynomials, $k = 11$, $l = 15$

Unfortunately, for those who actually perform experiments the answer is not so unambiguous.

Different peak area calculations and weighted least-squares resolutions were systematically compared for a two-component system measured by a 30 cc. Ge(Li) detector [64]. Peak areas were evaluated by the non-linear baseline method, by the trapezoid method, using the raw and smoothed data at the boundaries (Section 5.4), and by the method of the smoothed first derivative [49] (see Chapter 5). Relative intensities were also determined by weighted least-squares techniques using the iterative weighting process proposed by Schonfeld [90] and explained briefly in Section 6.5. The ratios of the measured and expected intensities obtained by different methods, together with their experimentally observed and calculated standard deviations, are listed in Table VI. For the non-linear baseline and the trapezoid methods, the optimum portion of the peak region was chosen for peak area calculation (Section 5.5). In calculating the errors, it was assumed that there was no systematic error in the baseline, i.e. statistical fluctuation was the only source of errors.

It can be seen from Table VI that the results of least-squares resolution are somewhat better than any peak area result. However, in spite of this, it is not so simple to answer the question in the title of this section. One has to consider that an ALGOL or FORTRAN computer program for weighted least-squares resolution of complex gamma spectra contains a few hundred instructions and needs thousands of memory spaces, depending on the number of components. On the other hand, peak area calculations could be performed even with a desk calculator. A computer program written in FORTRAN for this method usually requires less than 50 instructions and uses less than 100 extra memory locations (words) in addition to the space needed to store the contents of the channels read in from one spectrum.

The other big advantage is that for peak area determination one does not need the standard spectra of all of the components present in the complex spectrum but only the spectra of those elements whose relative intensities are to be calculated from their peak areas. In least-squares resolution, the standard spectra of each component must be measured with high statistical accuracy, and, furthermore, missing spectra can lead to systematic errors in the calculated intensities of any component. Using calculated spectra instead of measured ones can also lead to erroneous results, especially when gamma-rays giving very small peaks on a large Compton continuum are determined.

Taking all pros and cons into consideration, the personal opinion of the author of this book, based on his own experiences, is that for the determination of the intensities of individual components of a complex gamma spectrum measured by NaI(Tl) scintillation detectors, a weighted least-squares resolution is recommended whenever it is possible. For Ge(Li) detectors, however, the advantage of using much shorter measuring and calculating times more than compensates for the slightly better precision of the least-squares techniques over the non-linear baseline method.

7. SPECTRUM STRIPPING AND NON-COMPUTER METHODS

7.1 STRIPPING TECHNIQUES

Spectrum stripping or peeling has very often been used to decompose complex spectra by graphical or instrumental methods, e.g. [92–94]. Many modern multi-channel analysers have built-in hardware to perform spectrum stripping directly.

The essence of the method is the following: from the position of the highest energy peak the highest energy component is determined. The pulse-height distribution of this gamma-ray is multiplied in each channel by the same factor, Z, determined by the condition that after subtraction the mean difference between the composite and the multiplied spectra should be zero in the peak region. The intensity of this gamma-ray in the complex spectrum is Z times the intensity of the standard which has been used for the comparison, provided that both spectra were measured under identical circumstances. The spectrum shape needed is obtained either by measuring the pure spectrum of the corresponding radiation or from calculation (Chapter 3). The whole procedure is then repeated with the highest energy peak of the remaining composite spectrum and is continued for all observable peaks.

The principal disadvantage of this procedure is that the statistical and measurement errors accumulate at each stage of the stripping. After three or more spectra have been peeled off, the remaining data are usually very inaccurate. Intensity results for the highest energy gamma-rays of complex spectra have about the same precision and accuracy as those obtained from peak area calculation (Chapter 5), since the comparison is performed in the peak region. For lower energy gamma-rays the results are much poorer due to the errors accumulated in the successive strippings. The presence of bremsstrahlung further increases the uncertainties. It is very difficult to estimate the counts caused by this effect, if the complex spectra are resolved by peeling. Again, the errors are higher in the low energy part of the spectrum. For overlapping peaks there is ambiguity when the individual components are subtracted correctly. In this case it is advisable to substract the higher intensity peak even if its energy is lower.

Only when a peak is superimposed on a rapidly varying background is the stripping technique more advantageous than peak area calculation, but even in this case least-squares resolution gives better results than stripping. Because all problems and difficulties which arise in least-squares resolution exist in spectrum stripping as well, the peeling method is very scarcely used for computer data reduction nowadays, and is not recommended. However, for a rapid, but rough, estimation of the main components it may remain useful, because it can be performed with the more sophisti-

cated multi-channel analysers on the spot, while a prompt least-squares check would need an on-line coupled computer. But even this advantage is decreasing with the advance of small, direct-coupled computers substituting wired program multi-channel analysers.

When stripping is performed by the multi-channel analyser itself then the standard spectra are measured either immediately before or after the spectrum to be decomposed, or are stored on paper or magnetic tape. For rapid comparison one measures in -1 mode (subtracts) the standards individually after the complex spectrum till the corresponding peak is not visible on the oscilloscope screen of the analysers.

7.2 NON-COMPUTER METHODS

Complex gamma-ray spectra can be evaluated without computer by combining numerical calculations with graphical examination. In favourable cases, a trained person can determine intensities by spectrum stripping within a few percent accuracy, but a more realistic average value is about 8–12%. To speed up and simplify calculations the spectra are plotted on logarithmical or double logarithmical scales if changes in gain may occur. The intensity and gain ratios can then be easily obtained by shifting the logarithmically plotted response functions till they fit completely in the corresponding regions.

The other, more often used, faster and more simple method calculates gamma-ray intensities either from peak areas or from peak heights. The peak area can be determined either by planimeter (in which case the baseline is usually a straight line connecting two properly selected points on each side of the peak) or by the trapezoid method discussed in Section 5.4. The advantage of these methods over the procedure using only peak heights is that the area is not affected by changes in resolution.

Peak height is usually defined as the number of counts above the baseline in the channel containing the maximum number of counts in the peak region. This is sometimes substituted by the maximum in the 'graphically smoothed' spectrum, i.e. in the spectrum where a smooth curve is drawn by visual examination to approximate the measured data points 'as well as possible'. The baseline is a straight line either connecting the local minima on both sides of the peak or drawn as a tangent to the spectra on one (usually the left) side just outside the peak. If the resolution may vary, then the intensity is regarded as proportional to $A\Gamma$ where A is the height and Γ the width of the peak. For a true Gaussian the peak area is $1.064\ A\Gamma$. However, one must be very cautious, because intensities determined by peak area calculated in this way can be less accurate than those obtained only by peak height comparison, since a graphical determination of Γ gives a much higher weight to the measured points in the neighbourhood of the half maximum than to others. Therefore the error in Γ can cause a larger error in the intensity, when calculated as being proportional to $A\Gamma$, than the error due to change in resolution when intensity is calculated only from peak height.

8. MISCELLANEOUS APPLICATIONS

8.1 DECAY CURVE ANALYSIS

In Chapter 6, the resolution of complex, time-dependent gamma-ray spectra by weighted least-squares techniques was discussed. With this method the differences not only in the pulse-height spectra but also in the half-lives are taken into account and a decay-curve analysis is completed automatically.

There are experiments where a complete time-dependent least-squares resolution is either unnecessary or cannot be completed from the measured data. The former is the case when the intensity of interest is the only component or is determined from the complex spectra by peak area calculation (Chapter 5). The latter arises when the spectra of the different gamma-rays are experimentally identical or a single-channel analyser was used to measure the radiation. In the first case half-lives usually give only a check; while in the second, they do serve for the identification of the radioisotopes. For the identification of pure positron emitters by the measurement of the annihilation gamma-rays, only the decay of the radiation can be utilized. Rude decay-curve analyses are important also therefore, because from combined energy-half-life tables [80], the emitting radioisotope can be uniquely determined even if both data were measured with modest accuracy.

If N_j is the total count in the jth measurement over a period τ_j ($\tau_j = 1, 2, \ldots, m$) after a delay time t_j, then the decay-curve analysis requires a fit to the points

$$N_j = \sum_{k=1}^{n} x_k \exp(-\lambda_k t_j) \frac{1 - \exp(-\lambda_k \tau_j)}{\lambda_k} \quad (j = 1, 2, \ldots, m), \qquad (8.1)$$

where $n \leq m$ is the number of components contributing to the measured activity, x_k is the activity at $t = 0$, and λ_k the decay constant (ln 2/half-life) of the kth component. The x_k parameters (and sometimes some or all of the λ_k's) must be determined to give the best fit to the data.

In most experiments the measurement times are substantially shorter than the half-lives of the isotopes contributing significantly to the total activity. In this case Eq. (8.1) can be rewritten in the usual form:

$$A_j = \frac{N_j}{\tau_j} = \sum_{k=1}^{n} x_k \exp(-\lambda_k t_j) \quad (j = 1, 2, \ldots, m) \qquad (8.2)$$

or in matrix notation:

$$[A]_{m,1} = [A]_{m,n} \cdot [X]_{n,1}, \qquad (8.3)$$

where the A_j's are the measured total activities and the dimensions of the matrices are indicated for clarity. The elements of the $[\Lambda]$ matrix are $\lambda_{j,k} = \exp(-\lambda_k t_j)$ and for $[A]$ and $[X]$ $A_{j,1} = A_j$ and $X_{k,1} = x_k$, respectively.

The weighting factor of each datum is the reciprocal of its variance. The weighting matrix $[W]_{m,m}$ is diagonal, its elements are $W_{j,j} = \tau_j^2/N_j = \tau_j/A_j$, and $W_{j,k} = 0$ if $j \neq k$. In measurements where the statistical errors are smaller than the other experimental errors, Δ_i, it is advisable to use weights $W_{i,k} = 1/\Delta_i^2$.

If the half-life of each component is known, the problem is the same as that of Eq. (6.1) in Section 6.2, which has been solved by a linear least-squares fit. The same procedure could be repeated to find the best values of the x_k parameters. However, the matrix notation will be used by which the results can be expressed in a much condensed form. The initial activities obtained from the weighted least-squares fit are:

$$[X]_{n,1} = [B^{-1}]_{n,n} \cdot [\Lambda^t]_{n,m} \cdot [W]_{m,m} \cdot [A]_{m,1}$$

and the variances of the x_k parameters are:

$$\sigma^2(x_k) = B^{-1}_{k,k},$$

where $[B^{-1}]_{n,n}$ is the inverse of $[\Lambda^t]_{n,m} \cdot [W]_{m,m} \cdot [\Lambda]_{m,n}$ and t indicates the transpose matrix [95].

If any of the decay constants is unknown, then a direct linear least-squares solution is not possible. However, from a set of initial guesses, x_k^0 and λ_k^0

$$x_k \exp(-\lambda_k t_j) \approx x_k \exp[-(\lambda_k^0 + \delta\lambda_k)t_j] \approx x_k \exp(-\lambda_k t_j) - \delta\lambda_k x_k^0 t_j \exp(-\lambda_k^0 t_j)$$

and a solution for the $\delta\lambda$ terms is possible. An iterative procedure may then be used until sufficient convergence is attained — if convergence is attained at all. In the matrix notation, one extra column of the term $-x_k^0 t_j \exp(-\lambda_k t_j)$ is added to $[\Lambda]$ and one extra row, $\delta\lambda_k$, is added to $[X]$ for each unknown half-life [96].

It should be mentioned that the exponential functions characterizing the decay curves can be regarded as far 'less orthogonal' than the detector response functions for different gamma energies. Therefore, intensities obtained by decay-curve analysis are usually less precise than those obtained from the resolution of pulse-height spectra. This inaccuracy is more pronounced if some of the half-lives are also to be determined by the least-squares fit.

In the least-squares method the number of the decaying components and their exact or approximate half-lives must be known *a priori*. Using another approach this is not necessary [97, 98]. The Fourier-transform of Eq. (8.2) is a sum of delta functions. Expressed with the measured N_j's by numerical integration as a function of λ, the delta functions broaden into peaks at the decay constants of the components of the complex decay curve. The amplitude of each peak is related to the activity of the corre-

sponding component. Unfortunately, due to errors in the measured data and to the mathematical procedure, small 'false' peaks, not corresponding to any real decay constant, are also produced. Although they can be distinguished from 'real' peaks representing true components, they do mask weak activities.

The maximum likelihood method can also be used to perform decay-curve analysis. To find the best values of the x_k and λ_k unknown parameters of Eq. (8.1) by the maximum likelihood principle, the following equations must be solved numerically [13]:

$$\sum_{j=1}^{m} b_{kj} \left(1 - \frac{N_j}{a_j}\right) = 0 \quad (k = 1, 2, \ldots, n) \tag{8.4}$$

and

$$\sum_{j=1}^{m} B_{kj} \left(1 - \frac{N_j}{a_j}\right) = 0 \quad (k = 1, 2, \ldots, n) \tag{8.5}$$

where

$$a_j = \langle N_j \rangle = \sum_{k=1}^{n} x_k \int_{t_j}^{t_j+\tau_j} \exp(-\lambda_k t) dt$$

and the coefficients

$$b_{kj} = \int_{t_j}^{\tau_j} \exp(-\lambda_k t) dt \tag{8.6}$$

and

$$B_{kj} = x_k \int_{t_j}^{t_j+\tau_j} t \exp(-\lambda_k t) dt \tag{8.7}$$

are functions of the unknown intensities and decay constants.

In the favorable case when all decay constants (λ_k) are known, the x_k intensities can be estimated using only the set of equations (8.4), and equations (8.5) can serve as a check on whether the assumed λ_k values are really compatible with the measured data. However, these equations are very inconvenient for numerical calculations. Fortunately, they can be approximated by the following set of linear equations:

$$\sum_{k=1}^{n} x_k c_{ik} = b_i \quad (i = 1, 2, \ldots, m) \tag{8.8}$$

where

$$c_{ik} = \sum_{j=1}^{m} b_{ij} b_{kj} / (N_j + 1) \tag{8.9}$$

$$b_i = \sum_{j=1}^{m} b_{ij}$$

and b_{ij} is defined by Eq. (8.6).

Equation (8.8) can be solved without any serious difficulties and the relative differences between the solutions of Eqs. (8.8) and (8.4) are in practice smaller than the relative instrumental and statistical errors of the measurements. The scatters of the intensities are $\sigma^2(x_k) \approx c_{kk}^{-1}$, where c_{kk}^{-1} are the corresponding diagonal elements in the inverse matrix of Eq. (8.8).

A multi-channel analyser working as a multi-scaler records the total accumulated number of detected particles during the time period τ_f. With a precise timer and an on-line coupled computer, it is possible to store the exact decay time of each detected particle and to use these data for the maximum likelihood estimation of the intensities. Surprisingly, the results obtained from this extra information have scatters only a few percent smaller than the maximum likelihood estimates of the intensities measured by a multi-scaler whose time window (the time over which the counts are integrated to give the N_f values of Eqs. (8.4) and (8.9)) is small compared to the half-lives of the decaying radioisotopes.

Applications of the maximum likelihood method for decay-curve analysis are amply discussed in Chapter IX of ref. [13].

8.2 OPTIMIZATION PROGRAMS

In the production and measurement of radioisotopes, the flux of the irradiating particles and the sensitivity of the detector are usually given for a certain type of experiment and are in most cases maximized. But the irradiation, cooling and measuring times can be varied by the experimenter within wide limits. The results of experiments with optimum time schedule are often superior to one performed with a higher flux and a better detector but no proper time selection.

From the equation of growth and decay of radionuclides

$$N = n\sigma\varphi pG\left[1 - \exp(-\lambda T_I)\right]\exp(-\lambda\tau_D)\frac{1 - \exp(-\lambda T)}{\lambda},$$

where N is the total accumulated counts from the product radioisotope, n the number of target atoms, φ the constant flux of bombarding particles, σ the isotopic cross-section, p the isotopic abundance, λ the decay constant ($\ln 2/T_{1/2}$, $T_{1/2}$ the half life), T_I the irradiation time, T_D the cooling time, time elapsed between the end of irradiation and the beginning of measurement, T the measuring period, G the detection efficiency, the probability of detecting an emitted gamma-ray in the pulse-height interval determined by the energy selection of the detecting system.

If the irradiated sample is a mixture of different types of nuclei, then, according to the type of experiment, various expressions of N are to be maximized. The maximum condition usually leads to transcendent equations which are numerically solved for numerous nuclear parameters.

Isenhour and Morrison showed [99, 100] that the ratio of the activity of the jth component to the total activity is maximum if the irradiation and cooling times are chosen to fulfil the following equations:

$$\sum_k K_k(\lambda_k - \lambda_j)\,(1 - \exp(-\lambda_j T_I)]\exp(-\lambda_j T_D) = 0$$

and

$$\sum_k K_k\{\lambda_j \exp(-\lambda_j T_I)[1 - \exp(-\lambda_k T_I)] - \lambda_k \exp(-\lambda_k T_I)\,[1 - \exp(-\lambda_j T_I)]\}\exp(-\lambda_j T_D) = 0\,,$$

where $K_k = n_k \sigma_k p_k G_k$ and the summation is extended to all isotopes present in the irradiated sample.

To obtain maximum sensitivity for the isotope j in activation analysis, $N_j/\Delta N_j$ must be maximized. General equations for this problem together with numerical solutions for various parameters have been given by Quittner and Montvay [101]. The following can be regarded as general guidelines for optimum time scheduling in activation analysis:

(*a*) If $T_{1/2,j} < 2T_{1/2,\,k}$ for all k, except $k = j$, then to achieve maximum sensitivity for isotope j, cooling time $T_D = 0$ must be chosen.

(*b*) If the measuring time is short compared to the half-lives, $4T < T_{1/2,k}$ for all k, then all accumulated counts increase linearly in time. The statistical error of any component is proportional to the square root of the counts, and from this it follows that its relative error is inversely proportional to the square root of the measuring time, $\dfrac{N_j}{\Delta N_j} \sim \dfrac{1}{\sqrt{T}}$.

(*c*) It $T_{1/2,j} \lesssim 4T \lesssim T_{1/2,k}$ (for all k, $k \neq j$), then the optimum measuring time, T_{opt}, depends on R_j, the activity ratio of the other disturbing activities to the activity of j at the beginning of the measurement. T_{opt} can be found by solving the equation [101]

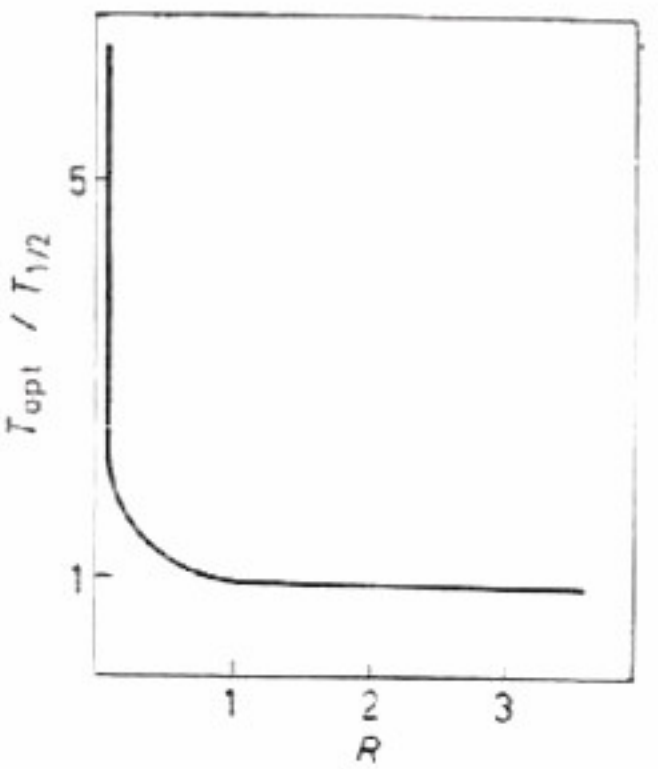

Fig. 25. Ratio of the optimum measuring time to the half-life of the isotope to be measured as a function of the activity ratio of the other disturbing activities to the activity to be determined at the beginning of the measurement. If $R_j \gtrsim 1$, then $T_{opt} \approx 2\,T_{1/2,j}$

$$\frac{1-\exp(-\Theta)}{\exp(\Theta)-2\Theta-1}=2R_j \quad \text{and} \quad T_{\text{opt}}=\frac{2\Theta T_{1/2,j}}{\ln 2}. \tag{8.10}$$

The numerical solution of Eq. (8.10) is shown in Fig. 25. For general use T_{opt} is expressed in 'half-life units'; $T_{\text{opt}}/T_{1/2,j}$ is given. If the disturbing activities are equal to or larger than the activity to be determined, then the optimum measuring time is approximately twice the half-life. The optimum measuring time increases rapidly when the ratio of the disturbing activities to the activity being determined decreases.

Some optimum time distributions have been discussed in Section 2.1 and solutions of several other optimization problems in activity measurements can be found in the book of Jánossy [13].

8.3 ACTIVATION ANALYSIS PROGRAMS

Activation analysis is one of the most sensitive analytical methods. With high resolution gamma spectrometry it can be automated and used for analysing samples on a large scale [102, 103]. For the principles and applications of activation analysis the reader is referred to the numerous excellent books [104–106]. Many methods used for evaluation of gamma-ray spectra have been developed and many computer programs written for the purposes of activation analysis. The computation of experimental results in activation analysis has been summarized by Yule [10] and by Gibbons [9] and the application of gamma-ray-spectrometry in this field by Heath [11].

In the most straightforward analysis, known amounts of each of the elements to be determined (the so-called standards) are irradiated and measured under the same conditions as the samples to be analysed. If A_j and a_j are the measured activities of element j in the standard and the sample, respectively, then the concentration, p, of this element is:

$$p=\frac{a_j}{A_j}\times\frac{M_j}{m}, \tag{8.11}$$

where M_j and m are the weights of the jth standard and the sample, respectively.

The input data contain besides the (repeatedly) measured spectra of the sample and the standards, their weights, the time elapsed between the end of the irradiation and the beginning of the measurement, the measuring time of each spectrum, the half-life of each component and information about the irradiation conditions and background. The a_j activities are determined either by peak area calculation or by least-squares resolution and are normalized to the same cooling time as the standards.

Equation (8.11) is valid only if the radioisotopes emitting the measured gamma-rays can be produced exclusively from one component of the sample. If this is not valid, then either several measurements must be taken on the same sample and the spectra combined into one spectrum to perform a least-squares resolution [67] (see Section 6.2), or the sample and the stand-

ards must be irradiated by fluxes with different energy distributions to utilize the energy dependence of the reaction cross-sections for the different reactions [107, 108].

The first automated computer-coupled activation analysis system was built by the Texas A. and M. group. Their first program identified spectral components and then evaluated peak areas to obtain quantitative results [103, 109].

Following the introduction of NaI(Tl) scintillation detectors and multichannel analysers, weighted least-squares resolution of the gamma spectra of the activated samples became more and more general. This technique was discussed in detail in Chapter 6.

High resolution Ge(Li) detectors have allowed the qualitative identification of numerous components in an activated sample. From the well separable full-energy peaks measured by these detectors, quantitative results are also obtainable. Since in conventional least-squares resolution, in contrast to peak area calculations, the spectra of all components must be known peak area calculations have regained importance in quantitative activation analysis in the last few years. Wainerdi *et al.* reported a general activation analysis data handling program which allows the analyst to choose between the peak area method, least-squares or quadratic fitting [109].

Together with simple pulse-height spectrum measurement, coincidence measurements can also be performed (see Section 9.3). For some elements the more precise results obtained from the coincidence data can be used to subtract their contributions from the complex spectrum, and the weighted least-squares resolution can be performed with less components to give higher precision [110]. This is especially advantageous if the detectors are NaI(Tl) crystals, where the spectra of gamma-rays differing only slightly in energy are very similar, but due to high efficiencies even the coincidence counts have relatively small statistical fluctuations.

If the conditions of both the irradiation and the activity measurements are highly reproducible, it is sufficient to use as standards spectra which were measured once with high precision and stored permanently on magnetic tape.

The first gamma-ray spectrum catalogue for activation analysis was prepared by Anders [111]. Using thermalized neutrons the generated spectra of the radioactive products were compiled for most of the activated stable, naturally occurring elements. The computer preparation of data for the catalogue included (*a*) smoothing of the experimental data; (*b*) correction for counting losses caused by dead-time; (*c*) background subtraction; (*d*) normalization to 1 minute measuring time and standard flux, and (*e*) a semi-logarithmic plot of each spectrum. In very accurate quantitative analysis neither this nor other spectrum catalogues [29, 55] can be used since there are no two completely matching detectors which have exactly the same characteristics.

For this reason the experimenter must always measure each standard or have his own carefully collected library. Once he has this and is convinced of the high reproducibility of his spectra, then the most advanced form of this evaluation method is when all spectra of the radioisotopes possibly

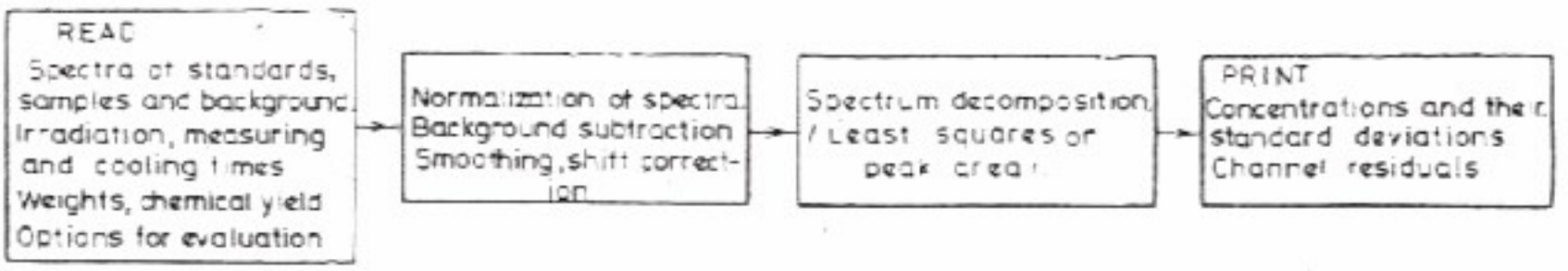

Fig. 26. Block-diagram of a general activation analysis program

present in any sample are stored on magnetic tape together with their other nuclear characteristics. Data are read from punched cards or tape or from magnetic tape. Invalid or suspicious data points are rejected or replaced by a special editing routine which examines the channel-by-channel variation in the measured counts. The presently existing programs locate the peaks in the gamma spectrum by the smoothed first derivative method (4.3), reject meaningless statistical fluctuations, Compton edges and backscatter peaks, determine the energies of the full-energy peaks, select from the energy the corresponding radioisotope from the library spectra of the standards and, by comparing the peak areas, perform a quantitative analysis [50, 112–114].

The block diagram of such a program is shown in Fig. 26.

Other checks, such as half-life determination, are also incorporated to avoid false identification of nearby peaks by inaccurate energy measurement. For isotopes emitting two or more gamma-rays the intensity ratios of these peaks serve as further checks. Gunnick, Levy and Niday [112, 113] worked out a six-step test to select the most likely radioisotopes from the possibilities corresponding to a given peak.

Cohen was the first to discuss the application of on-line computers to activation analysis [115]. A small digital computer collected the data from several different analog-to-digital converters, and performed some control functions and simple calculations. Since the first steps, other authors have also reported on using on-line coupled computers in activation analysis laboratories, e.g. [116, 117].

Several tables claim the excellent sensitivity of activation analysis. Most of them are based on the assumption that an element can be detected if its induced activity exceeds a certain limit. Tables giving the detection limits according to this definition are very misleading and should be entitled at least as "The sensitivity for activation analysis under ideal conditions which can very rarely be attained". Since titles should be short, the second part is omitted, but it must be understood. The reason that practical sensitivities can not be calculated in this way is that besides the interesting radioisotope others too are nearly always produced. Therefore, whether the counts due to the desired radioisotope are detectable or not depends on the natural background and on the other constituent of the sample. This problem will be discussed in detail in the next section.

In nuclear physics and chemistry it often occurs that a small intensity, I, must be determined in the presence of much higher ones. These disturbing background effects arise from the natural background and/or from other activities present in the measured sample. The problem is then either to determine what is the minimum I intensity which can be detected beside the background, B, within a given reasonable measuring time, T, or estimate the measuring time which is necessary to establish the presence of a given intensity above the background level. Since both problems can be treated in the same way, in this book only the first one will be discussed in detail.

In the simplest case two measurements are performed (or these are the averages of different measurements), one to measure the background intensity, B, and another one to measure the sum of B and I. (From the point of view of the calculations it is unimportant which one is carried out first.) As we assumed that I is small, $B \approx B + I$, and the optimum time division is obtained by dividing the total measuring time equally between the two measurements, $t = t_B = t_{B+I} = T/2$ (see Section 2.1). If both intensities can be regarded as constant during the measurements, then the presence of I is positively detected if

$$I = \left\langle \frac{N_{B+I} - N_B}{t} \right\rangle \approx \frac{N_{B+I} - N_B}{t} > 0 \tag{8.12}$$

significantly, where N_B and N_{B+I} are the total counts recorded in the first and second measurements, respectively. (The actual counts obtained in the two measurements due to the background need not be equal.)

The left side of Eq. (8.12) is positive with a probability $1 - \varepsilon$ if it is $\alpha(\varepsilon)$ times larger than its error, $\sigma(I)$, i.e.

$$I \approx \frac{N_{B+I} - N_B}{t} > \alpha(\varepsilon)\,\sigma(I) \approx \alpha(\varepsilon)\sqrt{\frac{2B + I}{t}} \tag{8.13}$$

from which the detection limit, $I_{\min}$, is

$$I_{\min} = \frac{\alpha^2(\varepsilon)}{2t}\left(1 + \sqrt{1 + \frac{8tB}{\alpha^2(\varepsilon)}}\right). \tag{8.14}$$

In practice $\alpha = 2$ (0.95 probability) or $\alpha = 3$ (0.997 probability) are chosen.

It should be mentioned that Eq. (8.14) can be used only as a guideline for estimating detection limits. In favourable cases the fluctuation can cause N_B to be smaller and N_{B+I} larger then their expected values, so a smaller intensity than that predicted from Eq. (8.14) can also be definitely established. On the other hand, in unfavourable situations N_B may be larger and

N_{B-I} smaller than their expected values. Then, even an intensity larger than I_{min} can not be positively identified.

Pauly and his co-workers gave a mathematical method to determine the detection limit for a radioisotope whose activity is measured within a complex gamma-ray spectrum [118]. A sensitivity spectrum can be derived from the measured gamma spectrum. In this sensitivity spectrum each channel content represents the minimum detectable gamma-ray counting rate of an isotope having a full-energy peak centred on the channel. From this the minimum detectable amount of any element in the particular sample can be expressed, knowing the nuclear data and the irradiation and measuring conditions.

The most sensitive way to detect the presence of a low activity in a complex spectrum is to find the full-energy peak of the corresponding radioisotope. The portion of the Gaussian shape peak which must be taken into consideration when determining the intensity depends on the peak to total ratio. The best signal-to-noise ratio is obtained in the peak channel, but this gives poor statistics and therefore the results have large relative scatters due to the small number of counts used for the intensity calculation. The maximum counts are accumulated with infinite (very wide) separated boundaries, but the statistical error is too large again, because the results are the differences of two nearly equal numbers.

The problem is similar to that discussed in Section 5.5 (selection of peak boundaries).

If the background is large compared to the peak, which is the case when detection limits are determined, then the smallest statistical scatter is obtained approximately when the channel contents are summed in the $[p - 0.6\Gamma, p + 0.6\Gamma]$ region, where p is the location of the peak and Γ is its full width at half maximum (FWHM). If the background is constant then the minimum detectable quantity becomes instead of Eq. (8.14).

$$I_{\text{min, peak}} \approx \frac{\alpha^2(\varepsilon)}{1.66t}\left[1 + \sqrt{1 + 8t \sum_{i=p-0.6\Gamma}^{p+0.6\Gamma} n_i/\alpha^2(\varepsilon)}\right]. \tag{8.15}$$

where n_i is the count rate in channel i.

If the full-energy peak of the element to be detected is superimposed on a visible peak of the composite spectrum, then the detection limit is greater than the value given by Eq. (8.15), since a part of the total peak area can be produced by radioisotopes having gamma-rays falling into this energy region. In this case, the detection limit is defined by Pauly *et al.* [118] such that the two gamma-rays separated by a given (energy) distance produce two distinct peaks, i.e. there should be a definite minimum between the peaks.

The results of their calculations are shown in Fig. 27 where the minimum amplitude ratio of two neighbouring peaks, separated by a minimum, is plotted vs. distance between the peaks measured in FWHM units.

If the energy difference is less than 0.86 times the FWHM, then the smallest peak which can be distinguished has an area (amplitude) equal to that

of the disturbing one.* When the energy difference is larger, this value decreases rapidly. When it becomes smaller than that obtained from Eq. (8.14) then the detection limit is again expressed by the latter expression.

The sensitivity spectrum of a $3\times3''$ NaI(Tl) scintillation detector and that of a 2.5 $cm^2\times0.3$ cm Ge(Li) semiconductor detector in the presence of a ^{137}Cs source are shown in Fig. 28 taken from ref. [118].

However, the detection limit for overlapping peaks defined as above is a cautious overestimation. If the detector resolution is stable, then overlapping peaks can be distinguished by least-squares techniques even if there is no observable minimum between them. This can be seen from Fig. 29, where the intensities of two unresolved peaks were determined with good accuracy by fitting two Gaussians by the non-linear least-squares method described in Section 3.1.

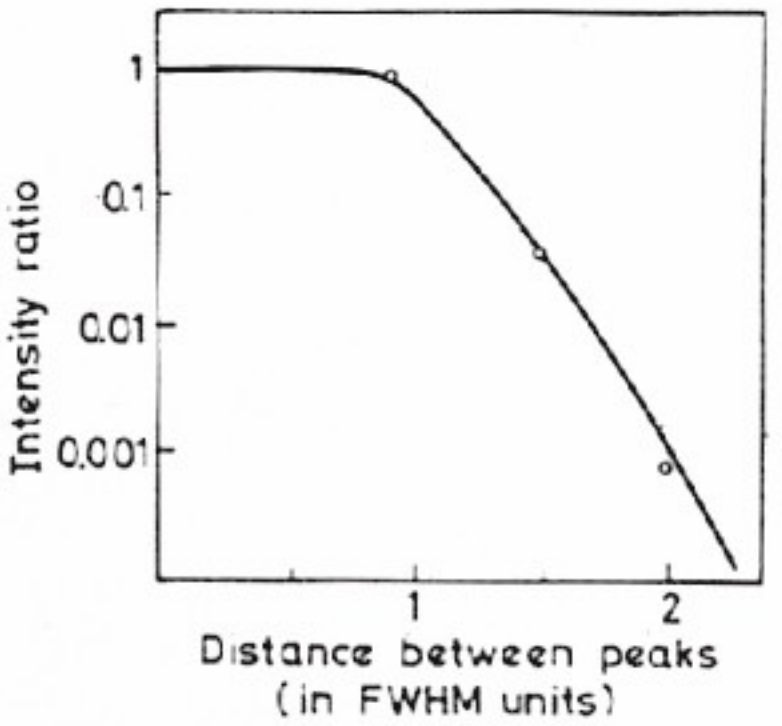

Fig. 27. Minimum amplitude ratio of two neighbouring peaks separated by a minimum vs. distance between the peaks measured in FWHM units

Wohlberg made calculations to predict what accuracy can be achieved by weighted least-squares techniques when decomposing complex spectra [84]. He approximated the response functions by a horizontal straight line until the Compton edge, then added a smooth connecting function which connected this to the Gaussian full-energy peak. The synthetized complex spectra were the sums of such components and the standard deviations were calculated as discussed in Section 6.2, i.e. they were the diagonal elements in the inverse matrix of the 'least-squares equations', Eqs. (6.3).

The errors were functions of (*a*) gamma-ray energies; (*b*) intensity ratios of gamma-rays; (*c*) absolute amplitude (total detected counts) of the composite spectrum, and (*d*) spectrometer parameters.

The parameters used in the calculations for (*d*), such as resolution and peak-to-total ratios, were those typical for commercial $3\times3''$ NaI(Tl) scintillation counters.

* In these evaluations as well as in Eq. (8.15) the activity is not obtained as the difference of two separate measurements but as the result of distinguishing the components in one complex spectrum.

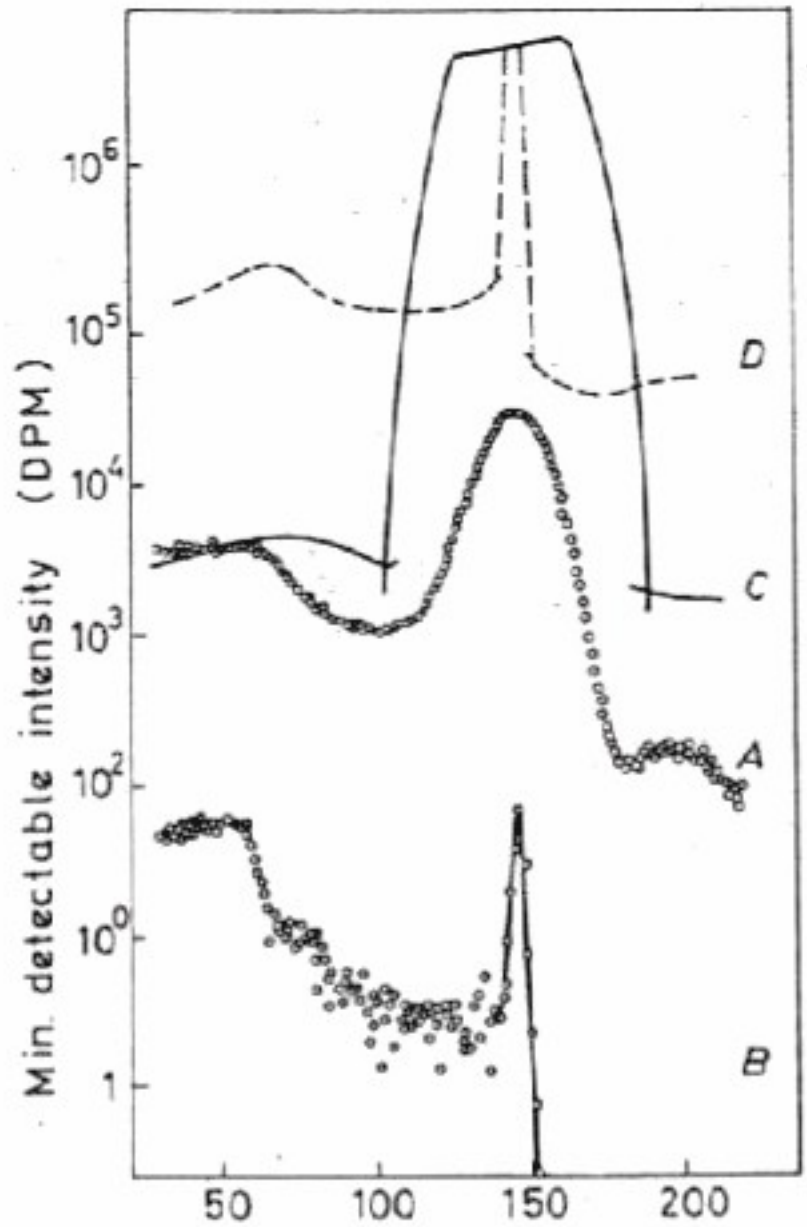

Fig. 28. Comparison of absolute gamma-ray detection limits in the presence of a ^{137}Cs source for a 3 × 3″ NaI(Tl) and 0.75 cm³ Ge(Li) detector [118]. Curves *A* and *C* represent the actual and sensitivity spectrum of the NaI(Tl) crystal and curves *B* and *D* that of the Ge(Li) detector

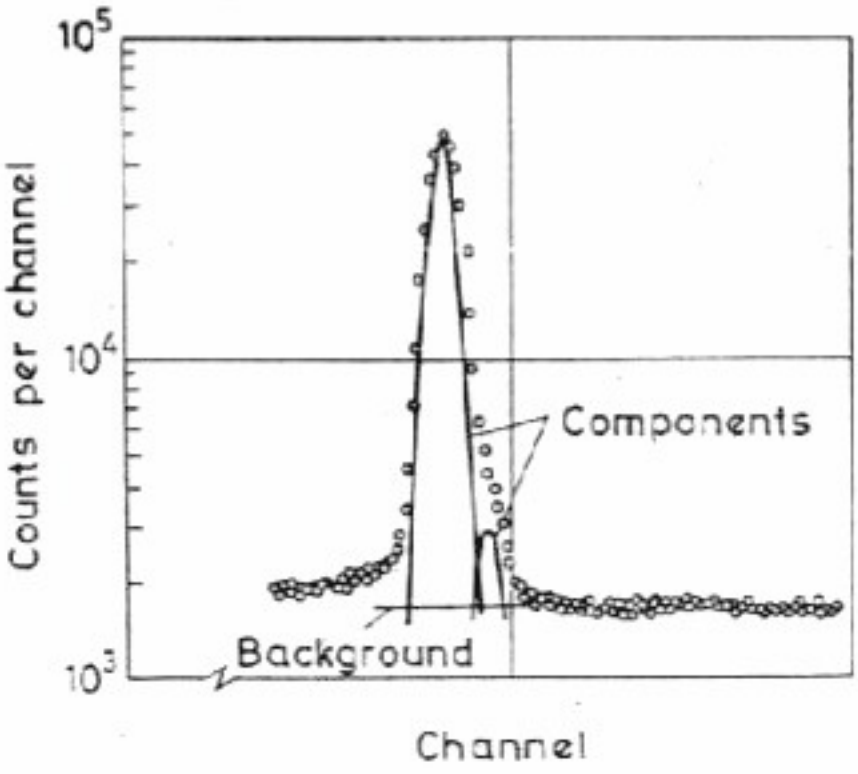

Fig. 29. Decomposition of a peak containing two components by least-squares techniques

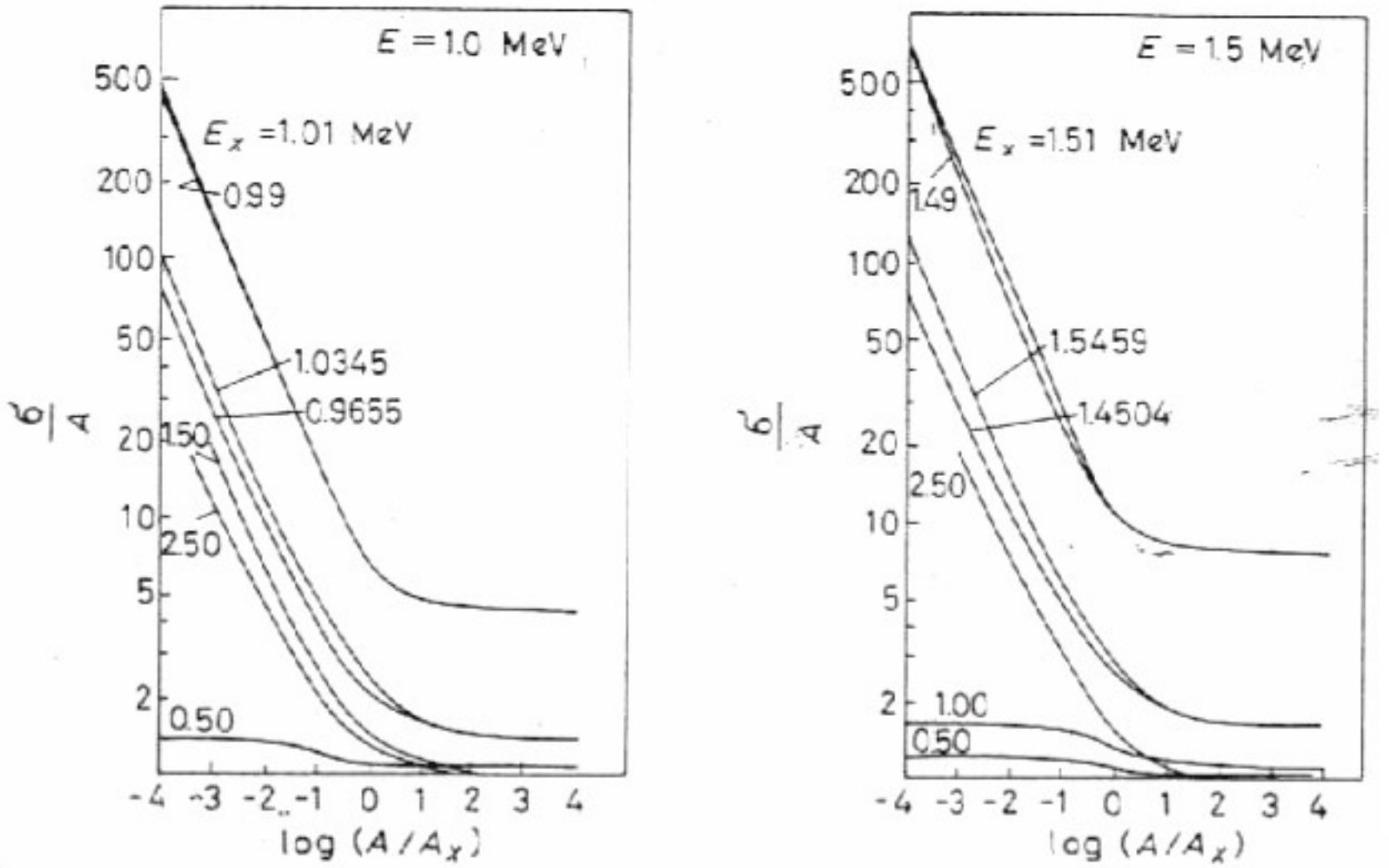

Fig. 30. Normalized scatter σ/A, of 1.00 and 1.50 MeV gamma-rays, respectively, in the presence of a second gamma-ray having energy E_x, as a function of the ratio of the total detected counts, A/A_x (after ref. [84])

To eliminate the dependence of the results on absolute intensity, so-called normalized scatters σ/A were introduced instead of scatters, where A was the amplitude (total detected counts) due to the component to be determined and σ its scatter.

Some of the results of these calculations for two-component systems are shown in Fig. 30. The normalized scatters, σ/A, are plotted as a function of amplitude (total detected counts) ratios for gamma-rays with 1 MeV and 1.5 MeV, respectively, in the presence of a second gamma-ray having energy E_x.

The following approximate general formulae can be derived, for $E_2 > E_1$:

When $A_1/A_2 \to \infty$, then $\sigma_1 \to \sqrt{A_1}$; $\sigma_2 \to \sqrt{\frac{A_2}{1-f}}$ where f is the fraction of the E_2 spectrum overlapped by the E_1 spectrum;

When $A_1/A_2 \to 0$, then $\sigma_1 \to C_1\sqrt{A_2}$; $\sigma_2 \to C_2\sqrt{A_2}$ where the constants can be determined from the graphs. The constant C_2 is significantly greater than 1 only when E_2 is approximately equal to E_1.

The more the energies differ, the faster the results approach their asymptotic values. It is interesting to note that σ_2 does not depend strongly on A_1/A_2.

When $E_2 \to E_1$ then $\sigma_1 \to \infty$.

In activation analysis it frequently occurs that during in-pile irradiation identical nuclides are produced from different elements by fast and slow neutron activation. Reactions of this type are, e.g., $^{27}Al(n, \gamma)\ ^{28}Al$, $^{29}Si(n, p)\ ^{28}Al$ and $^{31}P(n, \alpha)\ ^{28}Al$, or $^{59}Co\ (n, \gamma)\ ^{60}Co$, $^{60}Ni(n, p)\ ^{60}Co$ and $^{63}Cu(n, \alpha)\ ^{60}Co$. In

Section 6.2 it was shown how the spectra measured after different cooling times can be combined into one spectrum, from which unambigous results can be obtained by least-squares resolution even for the interfering elements.

However, it may occur that other activities present in the sample mask the small differences in the combined spectra, or, after chemical separation, the only remaining radioisotope is the very one which was produced from two (or sometimes three) elements.

In this case the problem is usually overcome by exposing the sample to neutron fluxes of different energy distributions, that is by irradiating them once with, then without a cadmium or boron filter. The energy dependences of the individual reaction cross-sections being appreciably different, both parent nuclei can be quantitatively determined from the activities produced in the same nucleus when irradiated with fluxes of different energy distributions.

In this case, however, the minimum detectable quantity can not be determined by the usual practice of activation analysis, requiring simply that the measurable activity should exceed the level determined by Eq. (8.14). This is quite obvious if one considers that, e.g., the ^{28}Al activity produced by the $^{27}\mathrm{Al}(n, \gamma)\ ^{28}\mathrm{Al}$ reaction even with minute quantities of aluminium, though well measurable individually, can not be identified in a sample with considerable silicon contamination because of the statistical error of the much higher ^{28}Al activity produced from ^{29}Si. Or, in the opposite case, since the cadmium ratio as a rule does not exceed two orders of magnitude, when using a cadmium filter the sensitivity to silicon will be considerably reduced by the presence of much aluminium.

It can be said in general that if the radioisotope C is produced from elements A and B the minimum detectable quantity for either will depend not only on background activity but also on their relative quantities present.

If the background was measured for a sufficiently long time, so that the error of its expected value during the actual measuring time (calculated from the separate long time measurement) can be neglected, then the minimum detectable quantity of A (x_A in μg) is given by the positive solution of the equation [108].

$$x_A^2(ab_f - a_f b)^2 - x_A \alpha_f^2(\varepsilon) \times (ab_f^2 - a_f b^2) - \alpha^2(\varepsilon) \times [x_B b\, b_f(b + b_f) + b_f^2 y + b^2 y_f] = 0, \qquad (8.16)$$

where a, b, a_f, b_f are the expected total numbers of counts during the actual measurement from radioisotope C produced by irradiating 1 μg of elements A and B separately without and with a cadmium or boron filter; y and y_f are the expected total numbers of background counts during the actual measurement from the natural background and from the sample irradiated without and with a cadmium filter; and $\alpha(\varepsilon)$ is the confidence parameter discussed earlier.

In Fig. 31 is shown the maximum sensitivity of activation analysis (for a given irradiation facility) for aluminium and silicon in tungsten as

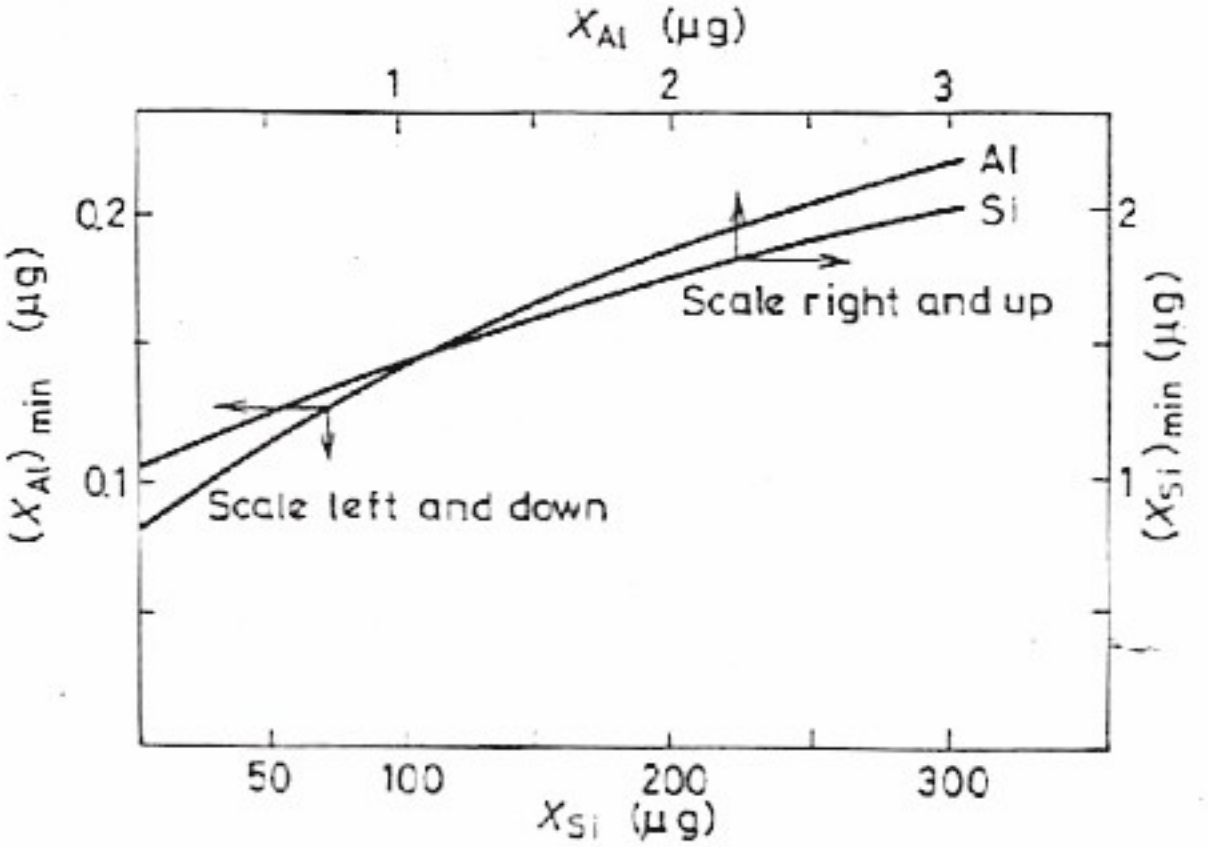

Fig. 31. Minimum detectable quantity of Al in 100 mg tungsten samples as a function of silicon concentration in sample (lower and left scale) and minimum detectable quantity of silicon as a function of Al concentration (upper and right scale)

evaluated from Eq. (8.16) with $\alpha(\varepsilon) = 3$ $(1 - \varepsilon = 0.997)$. From this it is apparent that for activation with pile neutrons the sensitivity to aluminium decreases only in the presence of large amounts of silicon, while that to silicon is markedly affected by even small quantities of aluminium.

8.5 ON-LINE APPLICATIONS

The wide variety and decreasing cost of computer systems available today have facilitated the automation of data collection and control functions for nuclear physics and similar experiments. The actual selection of a particular system has become increasingly difficult, since besides the numerous conventional characteristics, e.g. price, core memory size and speed, other factors especially aimed at satisfying the demands of the nuclear scientist, such as e.g. programming effort required, complexity of the experiment facility of experimenter interruption, the interrupt requirements and the availability of interface, the amount of on-line computation, etc., have won extreme importance.

The development of computers is so rapid compared to the preparation and printing of a scientific book that it would be useless to try to give a summary of all of the different types and their relative merits of computers applied for on-line measurements in nuclear physics, because by the time the book is published most of the compiled data would be out of date.

Without specifying any firm or model, on-line computers can be used in two ways, depending mainly on their sizes.

(*a*) Small digital computers are coupled by an appropriate interface to one measurement. By calling on different programs permanently present

in the core memory or stored on magnetic tape, the computer can solve different problems within the same type of measurement. With two directional interfaces, by feedback not only evaluation, but also control of the measurement, is possible.

(*b*) Large digital computers perform the same task for several experiments. The measurements are connected to interrupt channels and the computer works in time-sharing mode, and the highest priority interrupt is always served.

The on-line use of computers in nuclear physics has been discussed at several conferences [119, 120] and was excellently summarized in Lindenbaum's review paper.

In low-energy nuclear physics the prime use of computers has been as multi-parameter analysers. The conventional multi-parameter and multichannel analyser which could also be regarded as a computer having very limited programming capacity (i.e. which has been wired in by hardware) is continually being replaced by computers which perform mainly pulse-height analysis for one or more detectors.

The on-line system of the National Bureau of Standards (Washington, D. C.) installed in 1964–65 [121] has 80 interrupt lines, ordered according to the priority of the measurements, and can control the following experiments at the linear accelerator:

Electron scattering spectrometry
Heavy particle scattering spectrometry
Time of flight spectrometry
Single and multi-parameter pulse-height analysis
Multi-parameter analysis, such as the study of $(\gamma, p\gamma)$, $(\gamma, n\gamma)$, $(n, n'\gamma)$ reactions.

In gamma-ray spectroscopy on-line coupled computers perform the operations discussed in the previous chapters, either during or immediately after the measurements, e.g. [122, 123]. Several special macro instructions are written for rapid and easy data handling, e.g. for peak location, area calculation, background subtraction, etc. Depending on the results of these calculations various changes can be initiated in the experiment. The main difference between an on-line coupled computer and a computer-coupled multi-channel or multi-parameter analyser is that the digitalized data of the analog-to-digital converter are fed directly into the core memory of the computer instead of the core memory of the analyser. Therefore the data reduction can be started before accumulating all counts and after completing the measurement a data transfer (usually via magnetic or punched tape) is unnecessary.

An interesting method has been worked out by a group of physicists at the Central Research Institute for Physics, Budapest, to measure the half-lives of isomer states by an on-line correlation method [124, 125]. They exploited the fact that if the results of events A and B are recorded n times by two independent detectors for time Δ_t, then the correlation function

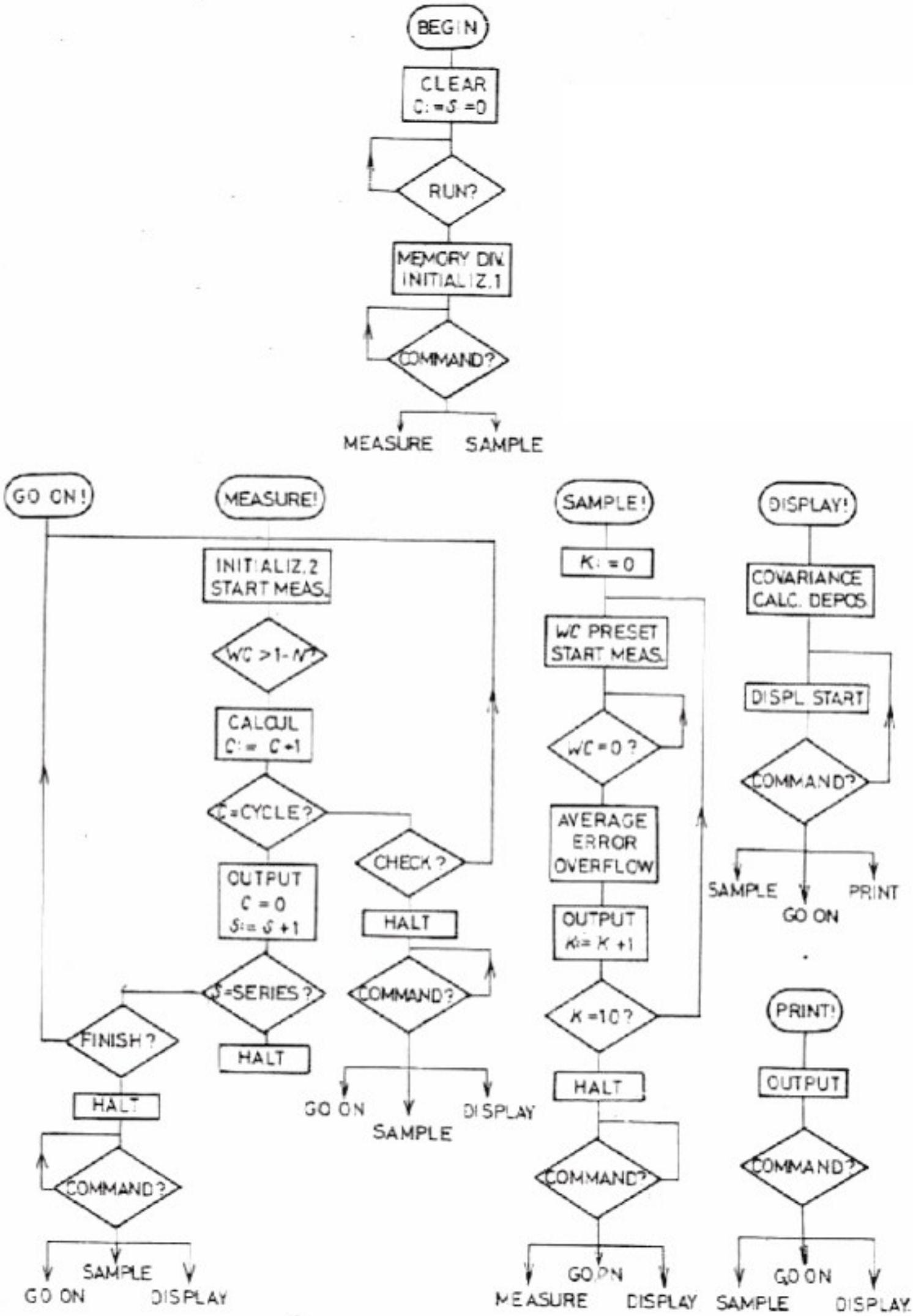

Fig. 32. Block-diagram of an on-line computer program measuring delayed coincidences by cross-correlation method (from ref. [125])

$$\varphi = \frac{1}{n}\sum_{i=1}^{n} A_i B_i - \frac{1}{n^2}\sum_{i=1}^{n} A_i \sum_{i=1}^{n} B_i$$

gives the expected number of the correlated events, i.e. the true coincidences which could be detected by the same experimental system equipped also with coincidence circuitry [126]. Here A_i and B_i represent the results of the ith measurement.

Uncorrelated events do not affect the value of φ but only increase its error.

Similarly, the correlation function

$$\varphi(T) = \frac{1}{n}\sum_{i=1}^{n} A_i B_{i+T} - \frac{1}{n^2}\sum_{i=1}^{n} A_i \sum_{i=1}^{n} B_{i+T}$$

gives the expected number of true coincidences occurring after a time delay T. Here B_{i+T} is the result of the measurement which started T later than the ith one.

A small, 8k memory word organized computer performed the calculation during the data acquisition. The block-diagram of the program is shown in Fig. 32. The command SAMPLE! served to calibrate the individual detectors, and the commands MEASURE! and GO ON! to start and continue, and CHECK! and FINISH! to stop the measurement, respectively.

The results of such a measurement for determining the half-life of the end-product of the ^{174}Yb (n, γ) ^{175}Yb reaction are shown in Fig. 33. They are in agreement with those obtained by other methods. The 20 ms half-life component is due to the activated sodium of the scintillator.

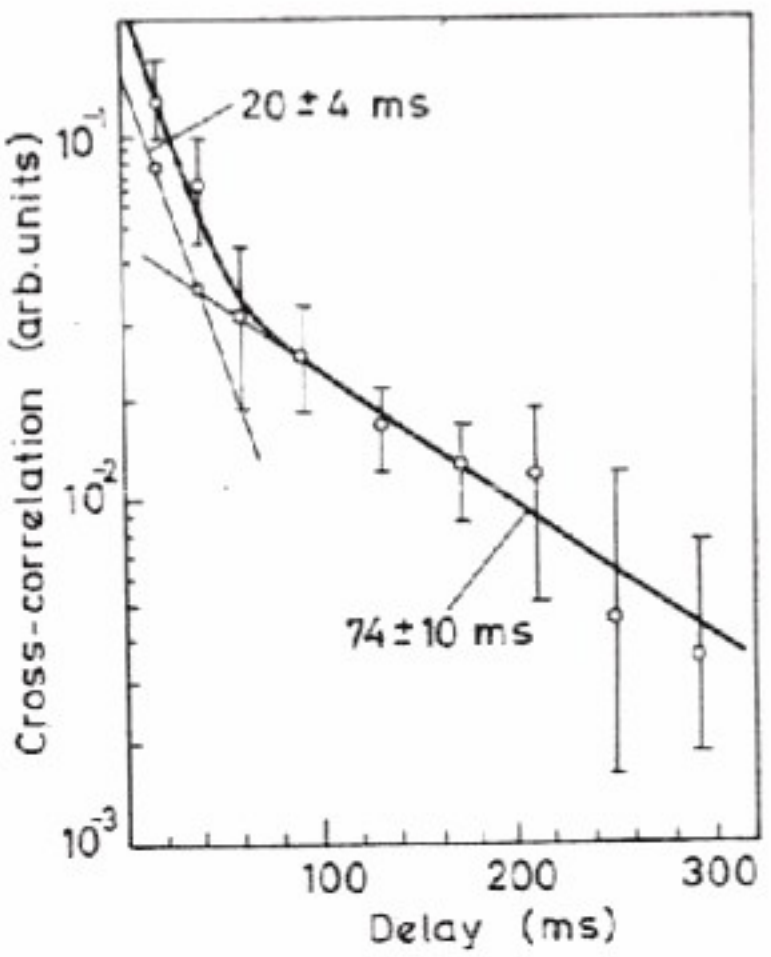

Fig. 33. Half-life of ^{175}Yb measured by the cross-correlation method. The 20 ± 4 ms component is due to the activated sodium of the scintillator (from ref. [125])

9. SPECIAL MEASURING APPARATUS

Till now it has been tacitly assumed that spectra are collected by single NaI(Tl) or Ge(Li) detectors. The shapes and the most significant features of these spectra were discussed in Section 3.1. Many nuclear textbooks give detailed information on the different physical processes contributing to the detector response function and on their effect on it (e.g. [21–23, 127, 128]). Several spectrometers, utilizing two or more detectors, have been built to improve on the peak-to-total or the signal-to-background ratio of the detector for the selected type of disintegrations or to establish time correlation between the emitted particles and by exploiting this correlation automatically increase the signal-to-noise ratio for the coinciding events. Multi-detector systems usually have higher selectivity but lower efficiency than single detectors. Although the additional detection conditions can improve the sensitivity and precision, sometimes by several orders of magnitudes, the concepts of spectrum evaluation remain the same for these more sophisticated devices as for single detectors. Naturally, either for monoenergetic gamma-rays or for coinciding radiations or for both, the response functions of multi-detector spectrometers differ substantially from those of the single-detector arrangements. As improvements are achieved either by coincidences or by anti-coincidences between the detectors, great care must be taken to estimate properly the contributions of chance coincidences; this is especially difficult when the counting rates are high and vary between different or during the same measurement.

Without going into the details we list the most often used multi-detector spectrometers and their main advantages. A complete summary of the different spectrometers can be found, e.g., in Chase's book [129].

9.1 ANTI-COMPTON SPECTROMETERS

The Compton continuum of higher energy gamma-rays is a disturbing background for lower energy photons. Most of the contribution of Compton scattered electrons can be removed from the spectra by anti-coincidence shielding techniques, called anti-Compton spectrometers [130, 131]. The main detector, serving for pulse-height spectrometry, is surrounded by a second large, high-efficiency detector in anti-coincidence. If a Compton scattered or an annihilation quantum, following the corresponding process in the principal detector, leaves it, there is a high probability that it will interact with the second detector. In this case the anti-coincidence condition is not fulfilled, and a pulse not falling in the full-energy peak is rejected.

For non-coinciding radiations the Compton continuum can be reduced 4–10 times without any significant loss in the full-energy peak. For Ge(Li) detectors, where multiple interactions are less probable than in large scintillators, the improvement is even more pronounced. Perkins and his coworkers reported on a 20 cc Ge(Li) diode incorporated near the centre of a 26 in. diameter by 24 in. thick NE-102 plastic phosphor anti-coincidence shield [132, 133]. The Compton edge was reduced by a factor of 10 and a peak-to-Compton edge ratio of 245 was achieved for the 661 keV ^{137}Cs gamma-rays. The Compton distribution was relatively smooth and void of a sharp Compton edge. The reduction in the full-energy peaks efficiency was less than 2%. Due to background suppression the improvement in sensitivity with anti-coincidence shielding is approximately a factor of 3 for single radionuclide sources. For complex mixtures it may be much greater (7–10) because in addition to reducing the natural background, the Compton interference is also significantly reduced (in favourable cases an 80—100-fold reduction can be achieved).

In Fig. 34 is shown the spectrum of ^{65}Zn measured with a $3 \times 3''$ NaI(Tl) detector with and without an anti-coincidence shield. Figure 35 shows the gamma-ray spectrum of ^{137}Cs measured by the Ge(Li) anti-Compton system of Perkins *et al.* [132], and Fig. 36 that of the muscle of a radioactive tuna fish collected in the region of the Bikini atoll [133].

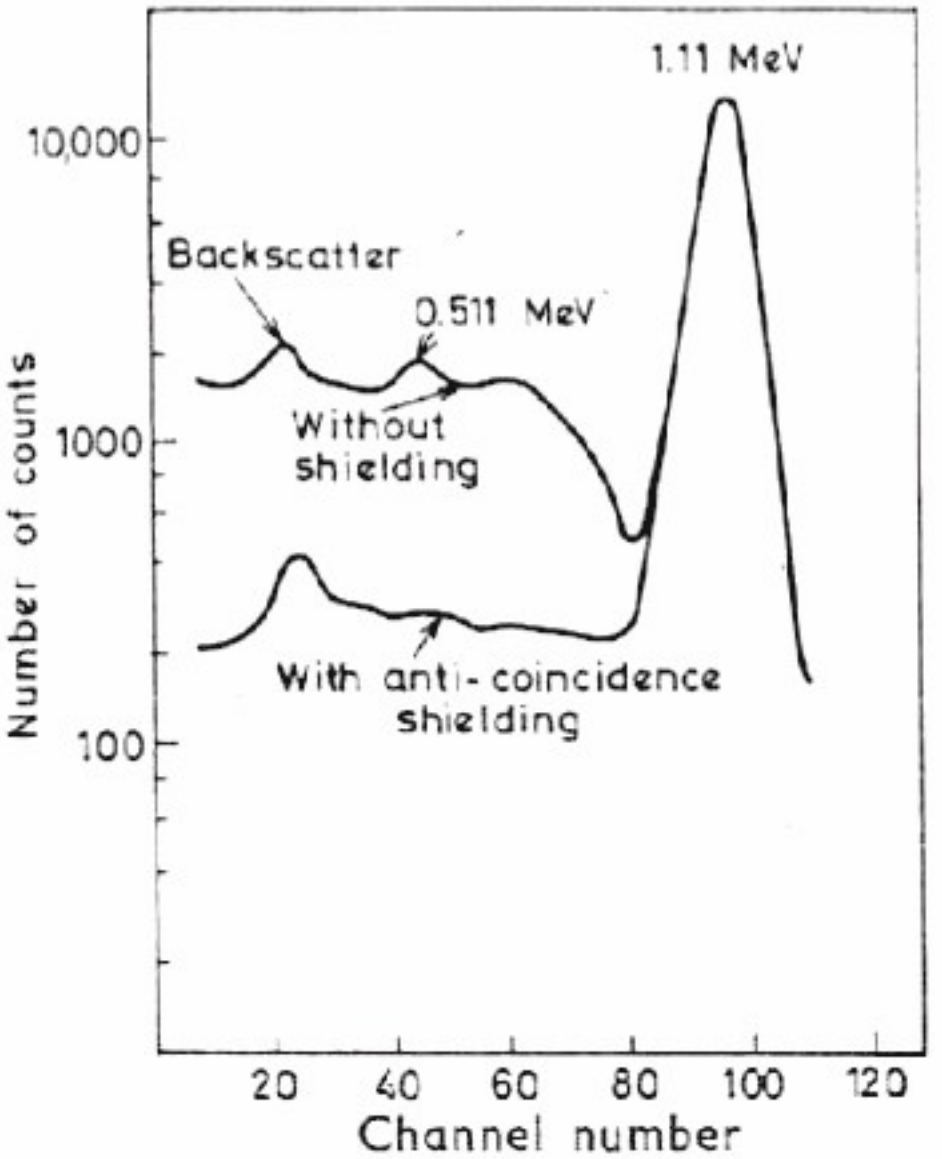

Fig. 34. Gamma-ray spectrum of a ^{65}Zn source measured with and without anti-coincidence shielding

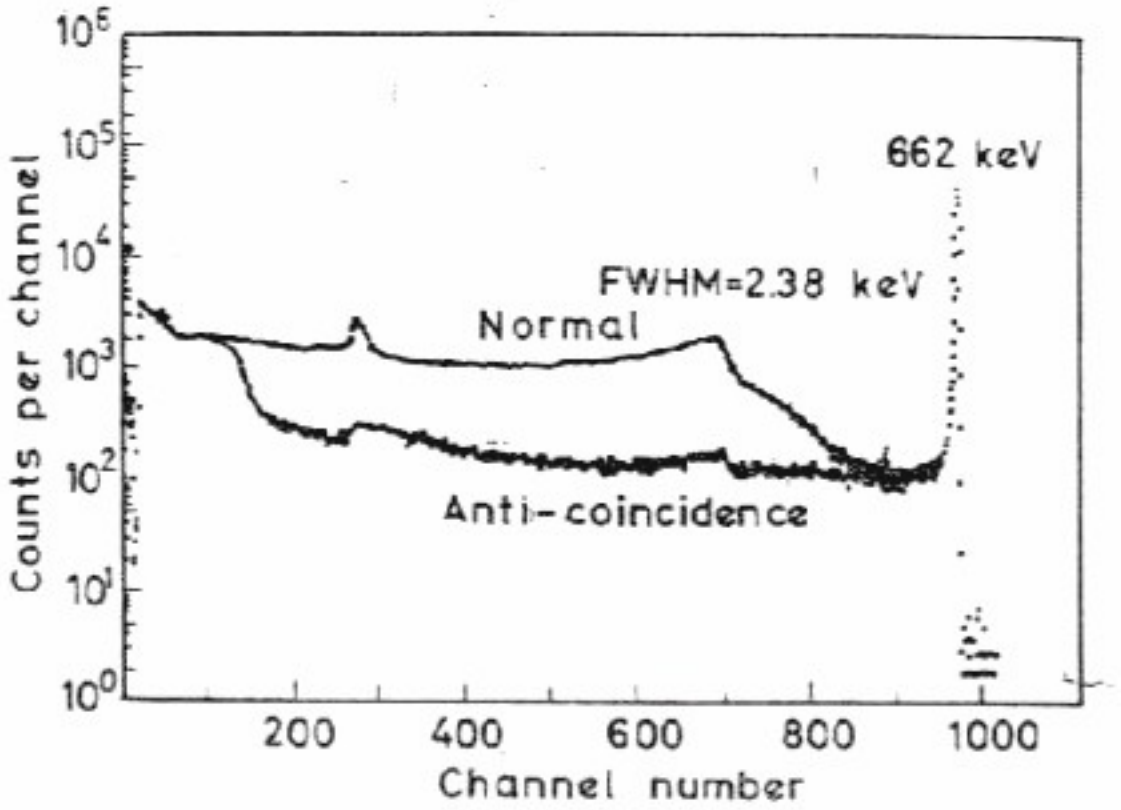

Fig. 35. Gamma-ray spectrum of ^{137}Cs recorded in the normal and anti-coincidence modes (from ref. [132])

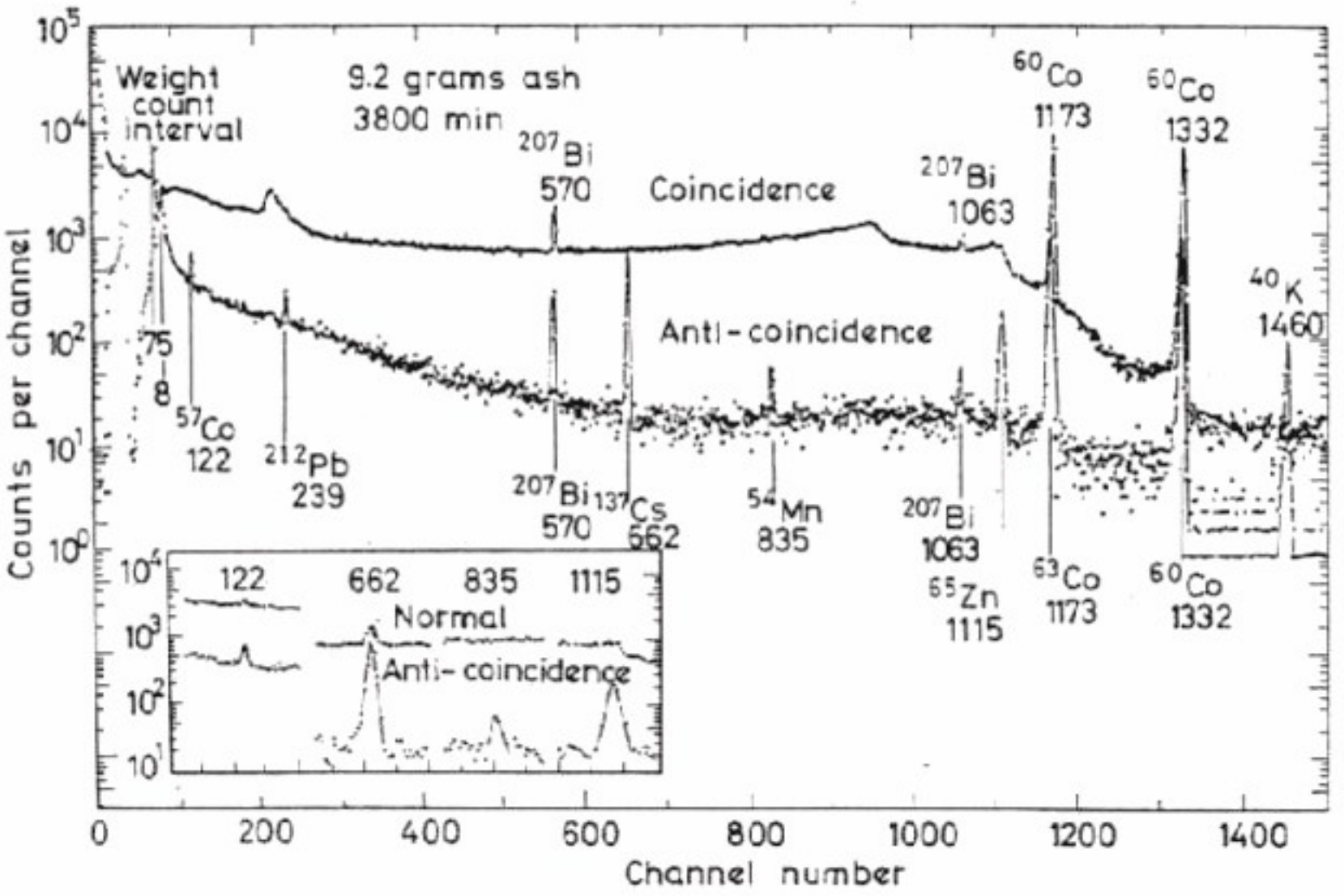

Fig. 36. Coincidence and anti-coincidence gamma-ray spectra of a sample of muscle tissue from a tuna collected in the region of the Bikini atoll (from ref. [133])

For sources emitting two or more gamma-rays simultaneously, the reduction in the full-energy peak efficiency can be considerable. When studying such decays, the advantage of a simple anti-Compton spectrometer is not so obvious and direct coincidence counting is usually preferable. Of course, it is advantageous to surround any of the detectors used for measuring the

coincidence radiations with an anti-Compton shield. To take full advantage of the information provided by the main detector without the anti-coincidence shield, the spectrum of coincidence events between the principal and Compton-scatter detector is recorded in one half of the memory of the multi-channel analyser, while the anti-coincidence events are stored in the second half of the memory [132]. The sum of these spectra gives approximately the same informations as the spectrum of the main detector measured without using any Compton reduction (see Fig. 36). Thus, the simultaneous storage of both coincidence and anti-coincidence spectra assures a high detection efficiency for gamma-emitting radionuclides with and without coincident gamma-rays.

For thin sources the contribution of bremsstrahlung can be reduced substantially by placing a thin plastic phosphor, viewed by a photomultiplier, between the detector and source to absorb the beta-rays. A coincidence between the main detector and the absorbing one indicates a bremsstrahlung photon, so the two detectors are in anti-coincidence.

9.2 PAIR SPECTROMETERS

For gamma-rays above a few MeV the most intense peaks of the spectra are the double-escape peaks. The energy, where the double-escape peak

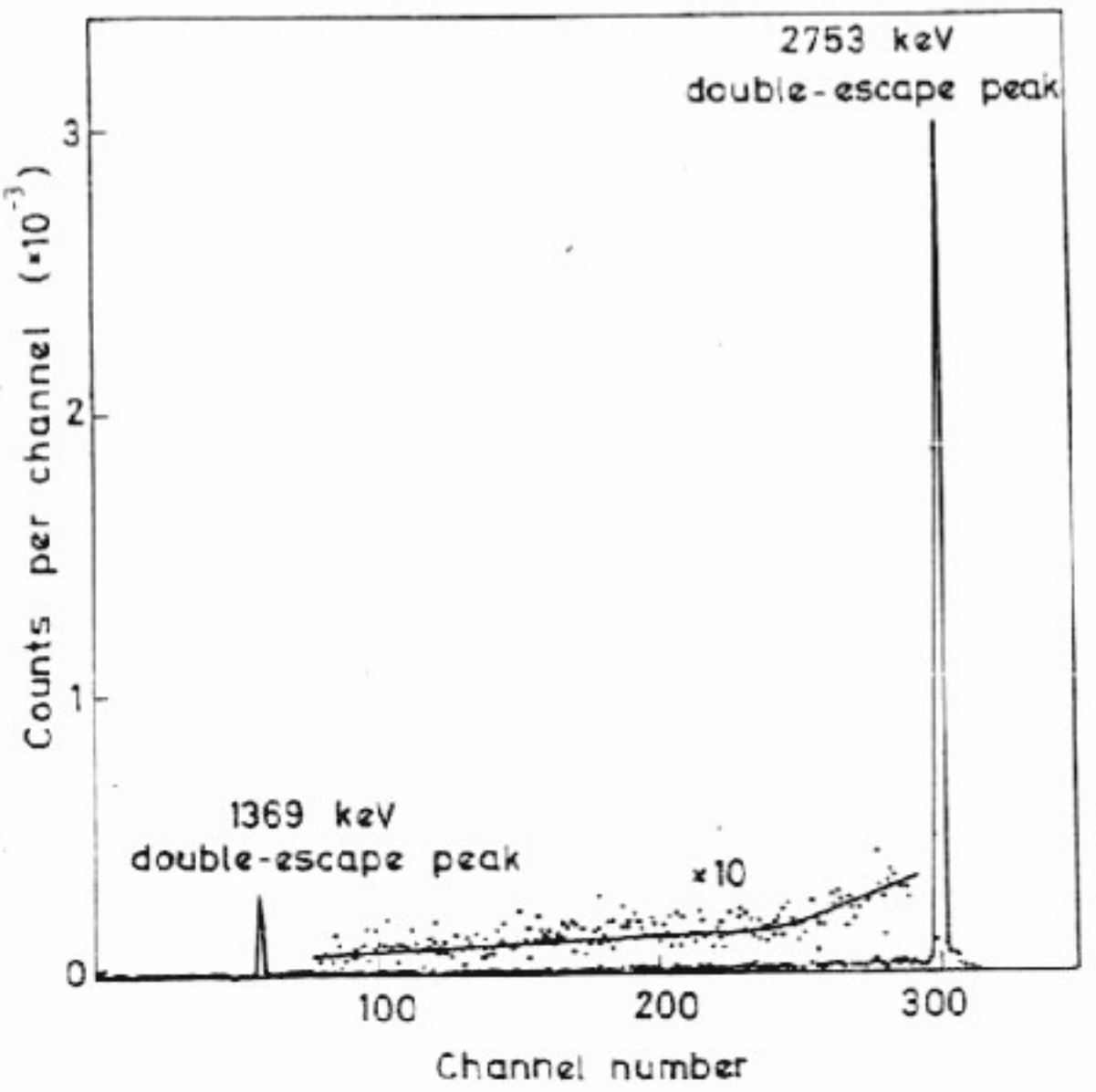

Fig. 37. Spectrum of ^{24}Na obtained by a pair spectrometer. The principal detector was a 4 cm^3 Ge(Li) detector. The annihilation quanta were detected by two 3 × 3″ NaI(Tl) crystals 6 cm from each other (from ref. [136])

becomes more intense than the full-energy peak depends on the detector type and size and is higher for large NaI detectors. If the main detector is surrounded in coincidence with two large scintillation detectors for measuring the annihilation quanta produced in the main detector, the spectrum of monoenergetic gamma-rays contains in principle only the double-escape peak [134, 135]. Although the total peak efficiency of a detector in a pair spectrometer is less than that of the same one used as a single detector, the portion of the spectra outside the double-escape peaks caused by chance coincidences is much more suppressed. The spectrum of ^{24}Na measured by a 4 cm^3 Ge(Li) principal detector and two $3 \times 3''$ NaI(Tl) crystals 6 cm from each other [136] is shown in Fig. 37. Other coincidence–anti-coincidence combinations are also possible between the three detectors.

9.3 COINCIDENCE MEASUREMENTS

The establishment of a time correlation between radiations emitted by the same isotope gives great help in understanding nuclear decay schemes. Utilization of the simultaneous emission of two or more quanta allows their measurement in the presence of a much stronger but not time-correlated background and other radiations. The coincidence technique may also be used for the absolute standardization of a radioactive source when its decay scheme is known. Excellent reviews on the principles and applications of the coincidence method have been given by De Benedetti and Finley [137] and more recently by Wapstra [138].

The most widely used coincidence arrangement is a one-dimensional multi-channel pulse-height analyser measuring the pulse height distribution of one of the detectors only if the pulse is in coincidence with a signal of the second detector. This coincidence or gating signal usually comes from a single-channel analyser, sensitive predominantly for one of the coincident radiations, i.e. having its window in the full-energy peak if it is gamma-ray. Besides the true coincidences, uncorrelated events occurring within the finite resolving time, τ, of the coincidence circuit in both detectors are also recorded. The rates of these chance coincidences and those of the true ones in channel i are (for $n_{\text{chance}}(i)$ only to a very good approximation):

$$n_{\text{chance}}(i) = 2n_1 n_2(i)\tau = 2n_0^2 \varepsilon_1 \varepsilon_2(i)\tau \tag{9.1}$$

and

$$n_{\text{true}}(i) = k n_0 \varepsilon_1 \varepsilon_2(i)\, f(1, 2). \tag{9.2}$$

where n_1 and $n_2(i)$ are the counting rates without coincidence condition in the fixed window single-channel analyser and channel i of the multi-channel analyser, respectively. n_0 is the source total disintegration rate and k its ratio to that of the coinciding radiation. ε_1 and $\varepsilon_2(i)$ are the total detection efficiencies, i.e. the probabilities that an emitted gamma-ray will hit the detector and undergo an interaction resulting in a pulse which will fall in the selected energy range. $f(1, 2)$ is constant for a given decay, describing the energy and angular correlation between the coinciding radiations.

Using Eqs. (9.1) and (9.2) it should be remembered that all n's represent counting rates and not total accumulated counts.

In a properly selected coincidence arrangement, the chance coincidences usually give the main contribution to the background.

From Eqs. (9.1) and (9.2) it can be seen that

$$n_{\text{chance}}(i) = \frac{2\tau}{kf(1,2)}\, n_0\, n_{\text{true}}(i).$$

This, together with Eq. (9.1), means that for a given type of source the spectrum of chance coincidences is (*a*) similar in shape to the single spectrum measured without any coincidence restriction (except for some very special cases), (*b*) its intensity increases with the square of the source strength, and therefore (*c*) its relative contribution compared to the true coincidences increases linearly with the source strength and is independent of the efficiencies of the detectors in any fixed energy interval, provided that there is no angular correlation between the coincident radiations. From (*c*) it follows that to obtain a good true/chance coincidence ratio for a given coincidence circuitry, the intensity of the source must be under a certain level.

To reduce the number of chance coincidences without losing true events, the resolving time of the coincidence circuit has to be shortened. For typical multi-channel analyser gating circuits $\tau \sim 10^{-6}$ s, but with modern fast coincidences 10^{-9} s can be achieved without any difficulties. In fast coincidence circuits not linearity but fast pulse rise time is important. Therefore the amplification of the detector is so large and the sensitivity of the fast coincidence circuit so low that it can be triggered even by the first few photoelectrons. Another method is the cross-overpick-off circuit which determines the amplitude-independent time when a pulse reaches its maximum. While in both cases the amplitude of the fast signal is not proportional to the energy loss in the detector, detectors used for nanosec coincidence measurements usually have a second output too, where the pulse-rise time

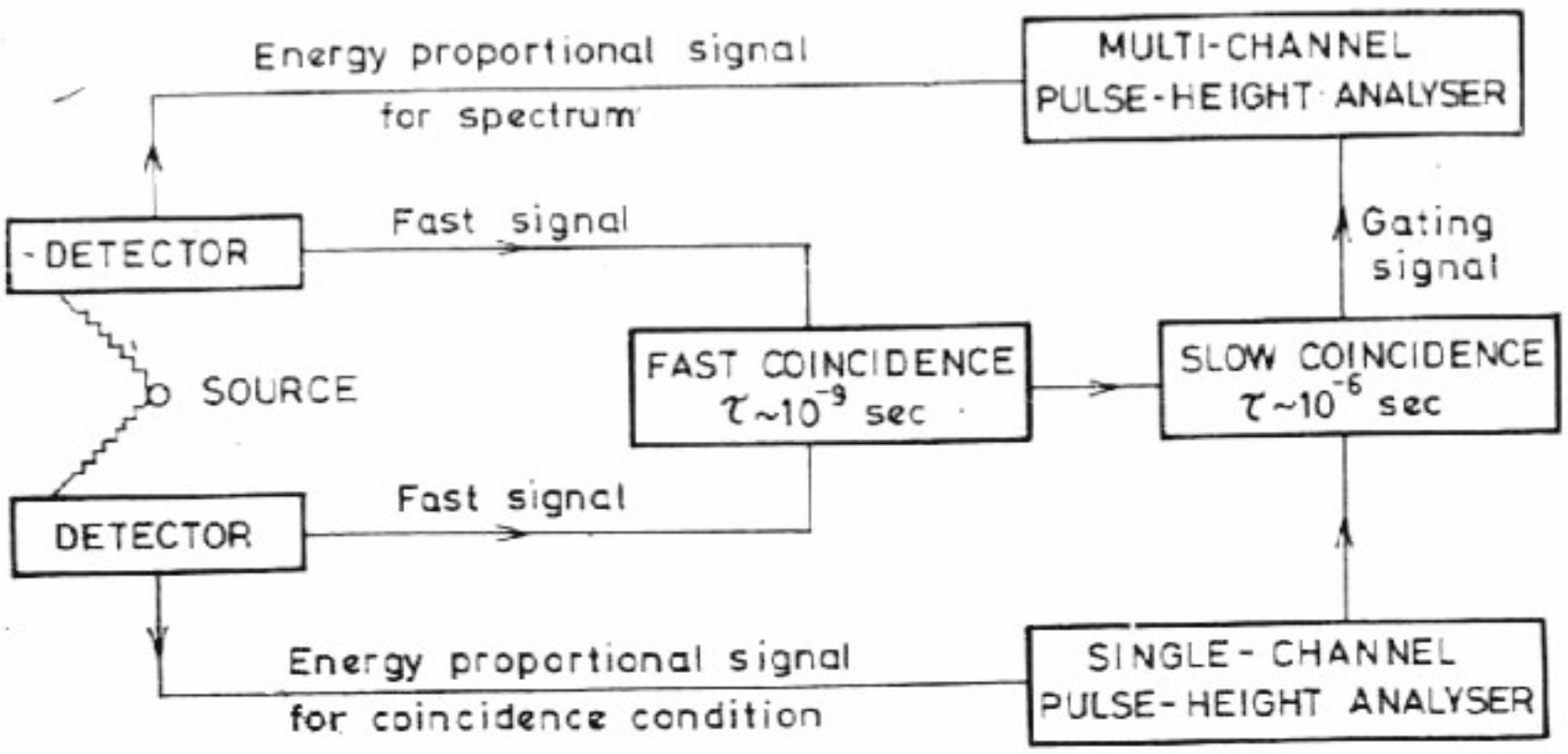

Fig. 38. Block-diagram of typical fast-slow coincidence arrangement

is not so fast but linearity is fulfilled. The energy measurement is performed further by the conventional slow electronics from the information coming from this second output and the fast coincidence circuit is used only to establish the simultaneity of the signals. The block-diagram of a typical fast-slow coincidence set-up is shown in Fig. 38. In this arrangement the resolving time of the fast coincidence circuit must be substituted into Eq. (9.1), but the approximation for the chance coincidences becomes less accurate. A detailed study of the different types of coincidence in fast-slow circuits has been given in ref. [139]. The efficiency of the coincidence method for selecting simultaneous radiation from a much higher background is illustrated in Fig. 39.

A natural extension of the multi-channel single-channel coincidence arrangement is the multi-dimensional analyser [131, 140]. In this case the energies E_1 and E_2 of both coincident radiations are measured separately and the result is stored as a count in the E_1, E_2 plane. The system response functions by which the measured data must be fitted are surfaces instead of curves.

The cost of magnetic storage becomes very high for more than a few thousand channels. Therefore, either the resolution of the individual detectors cannot be fully exploited or another type of storage must be used. Magnetic tapes with post-measurement playback and sorting allow only slow data acquisition. The other approach is to select only a part of the E_1, E_2 plane either from previous knowledge of the radiation or from the intensity of the incoming pulses into the various channels. In both cases the capability of the multi-parameter analyser to handle a large number of different data is considerably reduced. The most promising solution of the problem seems to be the use of computers on-line coupled to the converters

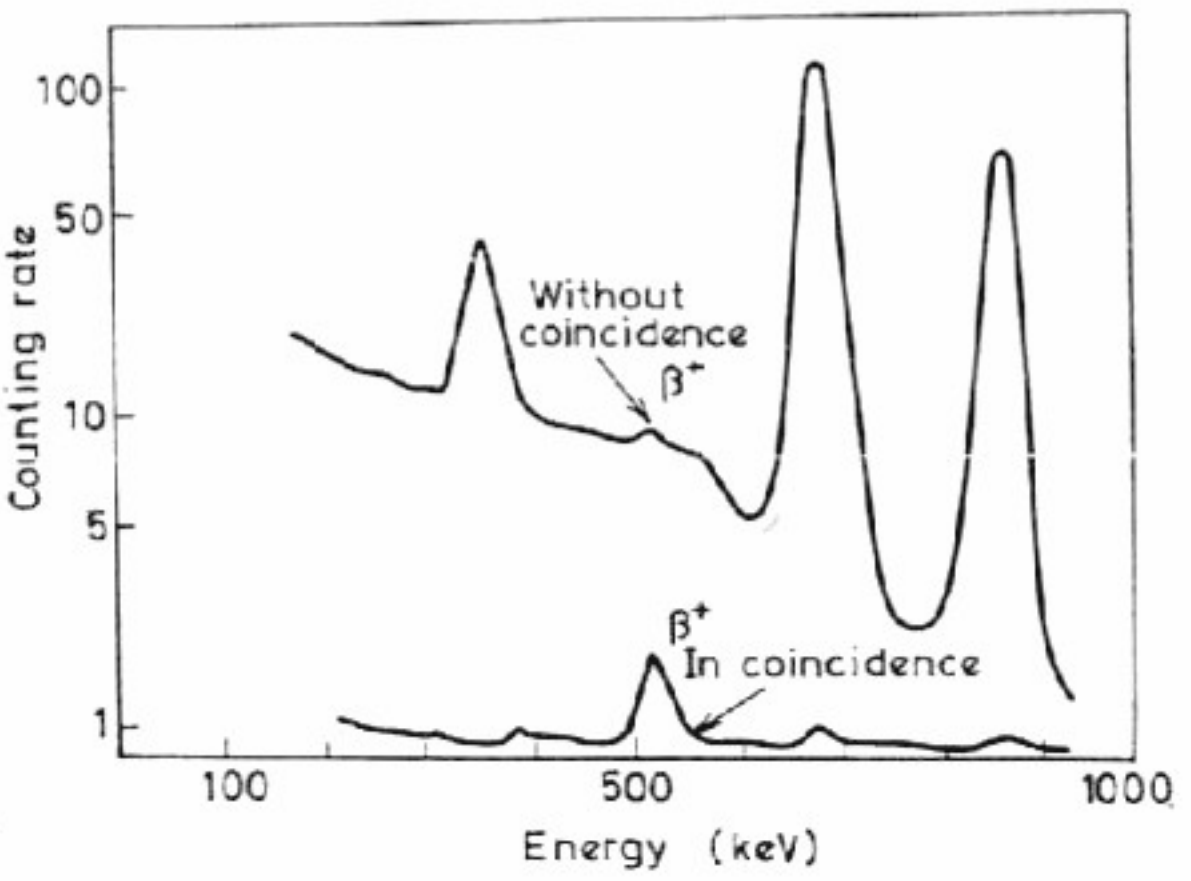

Fig. 39. The effectiveness of the coincidence technique. A complex spectrum measured with coincidence of the full-energy peak of the 511 keV annihilation photons and without coincidence

(see Section 8.5) digitalizing the energy proportional analog signals of the detectors, and to store the data in the memory of the computer which is used at the same time for data reduction as well. As was mentioned in Section 8.5, at present most of the on-line coupled computers perform only or mainly this task. The on-line use of computers in nuclear measurements being beyond the scope of this book, for further information the reader is referred to the review paper of Lindenbaum [5] and for the newest developments to refs [7, 120].

9.4 SUM-COINCIDENCE METHOD

A coincidence method, particularly useful in nuclear decay studies, where the total energy of the coincident gamma-rays is constant, has been developed by Hoogenboom [141]. The outputs of the two detectors are equalized to give the same energy-to-amplitude conversion. The signals of the detectors are summed. The multi-channel analyser measuring the pulse-height distribution of one or both detectors is gated by a single-channel analyser. The latter selects those signals of the summing circuit for which the total energy left in the two detectors is equal to the energy of the level to be studied. The measured spectrum contains only the full-energy peaks of those coincident radiations whose summed energy is equal to that selected by the single-channel analyser and from other true or chance coincidences only those for which this condition is accidentally fulfilled. The main advantages of the sum-coincidence method are the simple spectrum shape, improved resolution and relatively high efficiency. Denoting the individual resolutions of the detectors by Γ_1, Γ_2, their efficiencies by ε_1 and ε_2, and the channel width of the sum-coincidence detecting single-channel analyser by Γ_S, the width of a peak, Γ_{S1}, observed in the sum-coincidence mode is [141]

$$\Gamma_{S1} = \Gamma_1 \sqrt{\Gamma_1^2 + \Gamma_2^2} / \sqrt{\Gamma_1^2 + \Gamma_2^2 + \Gamma_S^2}$$

and the efficiency for this peak is

$$\varepsilon_{S1} = 2 \sqrt{\ln 2 / \pi}\, \varepsilon_1 \varepsilon_2 \Gamma_S / \sqrt{\Gamma_1^2 + \Gamma_2^2 + \Gamma_S^2} \,.$$

For gamma-rays having equal energies the resolution is improved by a factor of $\sqrt{2}$ and for the higher energy member of a cascade the reduction compared to a single crystal spectrometer is even greater. The practical limit for Γ_S is $\Gamma_S \approx \min(\Gamma_1, \Gamma_2)$, since further reduction in Γ_S causes only a loss in efficiency without significant improvement in resolution.

The relatively high efficiency compared to other coincidence methods is obtained because the individual detector efficiencies, ε_1 and ε_2, can be maintained relatively high since no collimation is necessary and both crystals can be placed in close proximity to the source.

The sum-coincidence spectrum of ^{60}Co measured by 2″ NaI(Tl) detectors is shown in Fig. 40.

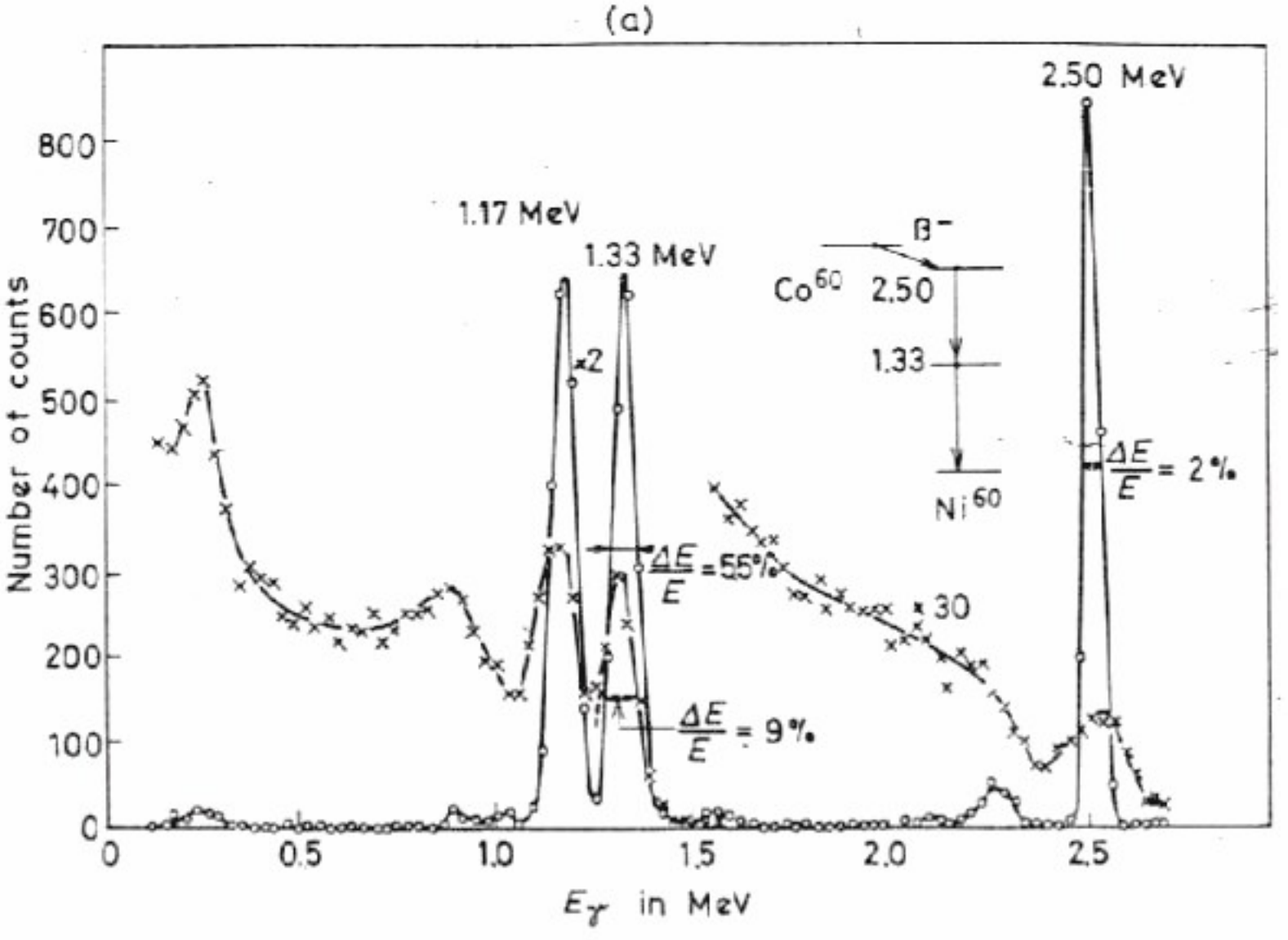

Fig. 40. (a) Single and sum-coincidence spectra of ^{60}Co using 2″ crystals. The single spectrum indicated by crosses is on an arbitrary scale. The sum-channel setting is at 2.50 MeV. The small peaks at 0.25, 1.0, 1.6 and 2.3 MeV are due to backscattering and can be removed by placing a thin lead shielding between the crystals. The sum peak at 2.5 MeV can be eliminated by putting a coincidence circuit between the output of the detectors (from ref. [141]) (b) Block diagram of the Hoogenboom coincidence circuit.

10. EXPERIMENTAL ERRORS

Computer-oriented scientists often forget that besides statistical errors there exist a lot of other hidden sources of errors connected with the actual collection of spectra. They try to reduce statistical fluctuations with smoothing and sophisticated filters, fit the data with more and more complicated functions, use repeated iterations, etc. But even the most sophisticated computer program cannot help in the case of erroneous measurements, unless it is incorporated in the program itself how to correct the errors unwillingly and often unnoticed committed by the experimenter.

In many cases one simply can not get rid of some disturbing effects. Sometimes their contribution can only be reduced. For instance, the variation in background intensity due to cosmic-ray showers, other nearby radiation sources, and the varying random content of the air, can be reduced by bulkier shielding and often repeated background measurements, but its disturbance in the measurement of weak radiations can not be completely eliminated. Computer programs can often indicate inconsistencies among the input data, but the last word must always come from the analyst. It is he who must decide in the knowledge of the experimental conditions of data acquisition what corrections to apply and how reliable the obtained results are. To be able to perform this task, he must know what errors can occur due to the detection process itself.

In this section a brief description is given of some artifacts and errors connected with the measurement of gamma-ray spectra. For more details the reader should consult the papers of Lyon *et al.* [143] and Lazar [144] and Section 3.2 of ref. [21].

10.1 ELECTRONIC INSTABILITIES

In Section 6.4 it has been shown how threshold and gain shifts can be corrected by programming. However, especially at high counting rates, these effects can lead to such serious spectrum distortion that to correct their effects only by software is impossible or at least unpractical. Since the stability of gain and zero intercept in a pulse-amplitude analysis system is most important for satisfactory performance of high resolution systems, modern multi-channel analysers are equipped optionally with a spectrum stabilizer (usually a digital one) to eliminate gain and sometimes baseline shift, and the pulse shaping circuits in some stage of the amplifier system have pole-zero cancellation and a baseline restorer to reduce baseline shift and fluctuation.

In the most widely used digital type spectrum stabilizer the position (pulse-height) of one or two peaks is stabilized in the spectrum. On the lower and upper sides of the peak to be fixed two digital windows are established. The positions and widths of these windows are selected such that in normal circumstances, i.e. in stable operating mode, their counting rates should be equal. Pulses falling into channels bounded by the windows are fed to an up-down scaler, from the lower position channels in additive, from the higher ones in subtractive, mode. Thus the total count in this scaler at any time provides a signed digital value which is proportional to the shift in the peak position. This digital value is converted into an analog error-signal by which the gain and/or the zero reference of the system is corrected.

Such systems can secure approximately $\pm 0.1\%$ stability. Difficulties arise when there exists no suitable peak for control in the spectrum, or the counting rate is low in this peak, when statistical fluctuations can lead to unwanted regulation. The one neglectable, only theoretical disadvantage of the digital spectrum stabilizer is the slight deterioration in system resolution due to the normal overshoot of such types of correcting method.

Operating at high counting rates without special precautions, serious shifts of zero and gain and degradation of resolution may occur. Most of these effects are the result of random fluctuation in the zero reference baseline at the input of the analog-to-digital converter. To achieve optimum signal-to-noise ratio for the pulses of the system, a monopolar pulse shaper with equal integration and differentiation time constants is generally employed. In this case the output pulses are followed by a negative undershoot with generally a few hundred microseconds recovery time constant. At low counting rates there is only a very slight probability that a pulse arrives before the undershoot of the previous one has finished. But at high counting rates several pulses will start from the 'undershoot level' which results from the point of view of the analog-to-digital converter in a reduced amplitude. The net effect of this will be a count rate-dependent asymmetry of the peaks: the low energy side will be broadened.

The pole-zero cancellation technique [145] quite effectively reduces the undershoot from monopolar pulses at moderate counting rates. In practice the complete pole-zero cancellation is limited by (a) the need for removal of low frequency noise by an additional differentiation, and (b) the difficulties of stabilizing the DC output level of an entirely DC-coupled amplifier.

At high counting rates (above 5000 counts/s) the residual undershoots will charge the coupling capacitors and so result in a long time shift in zero. The baseline restorer circuit forces the signal to return to the baseline immediately after each pulse [146–148]. Due to the restorer, small losses will result in resolution at low counting rates, because its performance can be optimized only for a given rate. Therefore, most recent DC restorers have switches for selecting the most suitable time constant to optimize for the counting rate expected in the experiment.

With pole-zero cancellation and baseline restoration the increase in resolution for ^{60}Co can be less than 0.4 keV, while the count rate increases from 1000 to 35,000 counts/s [11].

For spectrometers having a digital spectrum stabilizer, pole-zero cancellation and baseline restoration, gain and threshold corrections by programming (see Section 6.4) are often superfluous or need only one iteration step. The increase in χ^2 due to the still remaining electronic instabilities can be fairly well approximated by Fig. 21 and Eq. (6.4), or by Eqs. (6.5) and (6.6) [82].

10.2 SUMMING EFFECT

If two gamma-rays interact with the detector within the resolving time of the pulse-amplitude determining circuit, only one pulse will be stored with amplitude equal to the sum of the pulses. This pulse pile-up can be caused by the summing of true coincident gamma-rays, when both of the coincident radiations are detected by the same detector, and by random summing, when two independently emitted photons interact with the detector within the resolving time.

Theoretically, summing of gamma-rays can be avoided by a suitable choice of experimental conditions, but practically this is often not worthwhile. In experiments where the rate of data acquisition would be otherwise too slow, e.g. in coincidence measurements where the true coincidence rate would be too small, it is necessary to detect the gamma-rays very efficiently and to correct them for pulse summing. An easy experimental method to distinguish between single pulses and random or true sum-coincidences is that (*a*) the count rate of single pulses varies linearly with the efficiency, ε, (solid angle $\times$ intrinsic efficiency) of the detector, while that of the sum pulses varies quadratically, ($N_{\text{single}} = I\varepsilon$, $N_{\text{sum, true}} = I\varepsilon_1\varepsilon_2$, $N_{\text{sum, chance}} = 2I^2\tau\varepsilon_1\varepsilon_2$); (*b*) the measured rate of random sum-coincidences increases quadratically, and that of the true ones linearly with source strength. The effect is shown schematically in Fig. 41. Gamma-rays with energies E_1 and E_2 are emitted in coincidence while the emission of E_3 is independent of them. The peak-amplitudes at energies E_1, E_2 and E_3 vary linearly with both source strength, I, and detector efficiency, ε. The sum peaks at $E_1 + E_2$, $E_1 + E_3$ and $E_2 + E_3$ vary quadratically with ε, and the true sum peak at $E_1 + E_2$ decreases linearly, and the random sum peaks at $E_1 + E_3$ and $E_2 + E_3$ decrease quadratically with I.

If $y_1(E)$ and $y_2(E)$ are the detector response functions for two completely coincident gamma-rays, then the response function of the summed spectrum will be

$$y_s(E) = \int_{-\infty}^{\infty} y_1(E - x)\, y_2(x)\, f(1, 2)\mathrm{d}x \qquad (10.1)$$

$f(1, 2)$ being a correction factor for possible anisotropic angular dependence. If there is no angular correlation between the coincident photons, then $f(1, 2) = 1$, and for annihilation quanta originating outside the detector (even outside the well of well crystals) $f(1,2) = 0$. In the derivation of Eq. (10.1), all response functions are expressed in number of counts per energy interval per emitted gamma-ray, and corrections due to non-linearity in

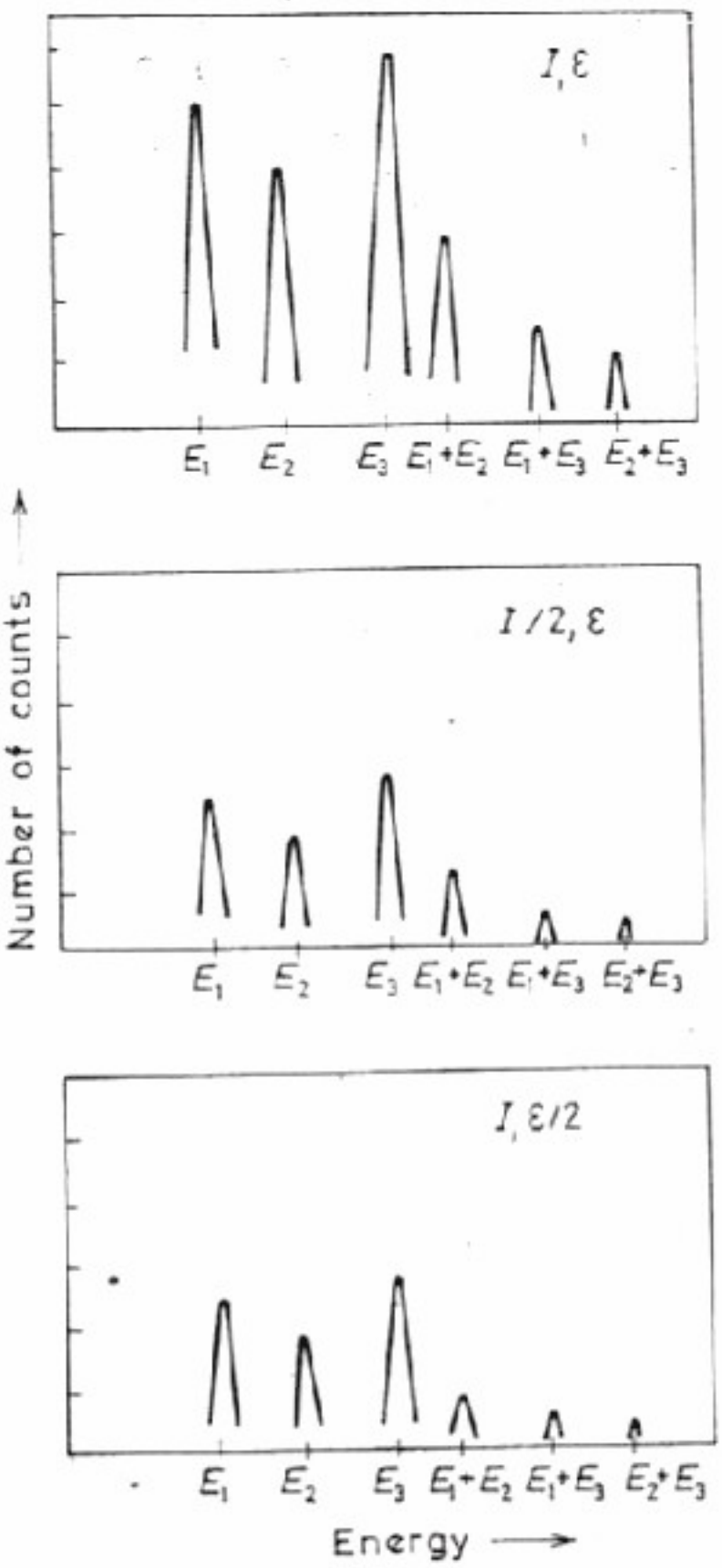

Fig. 41. The dependence of counting rates on source intensity, I, and detector efficiency, ε, for single pulses and true and random sum-coincidences

the energy-pulse-height conversion and counting losses are neglected. If intensities are to be determined by absolute peak area calculation (Section 5.1) the measured peak area must be divided by $[1 - \varepsilon_{T2} f(1, 2)]$ to correct for true coincidence summing losses. Here ε_{T2} is the total detection efficiency for the other coincident gamma-ray. For detectors having high total efficiency, this correction factor can be 0.8–0.9.

As the number of true sum-coincidences is independent of other radiations present, in relative evaluations, when the spectra of the standards are measured under the same conditions as the samples, their contributions are automatically incorporated in the response function. Using a calculated

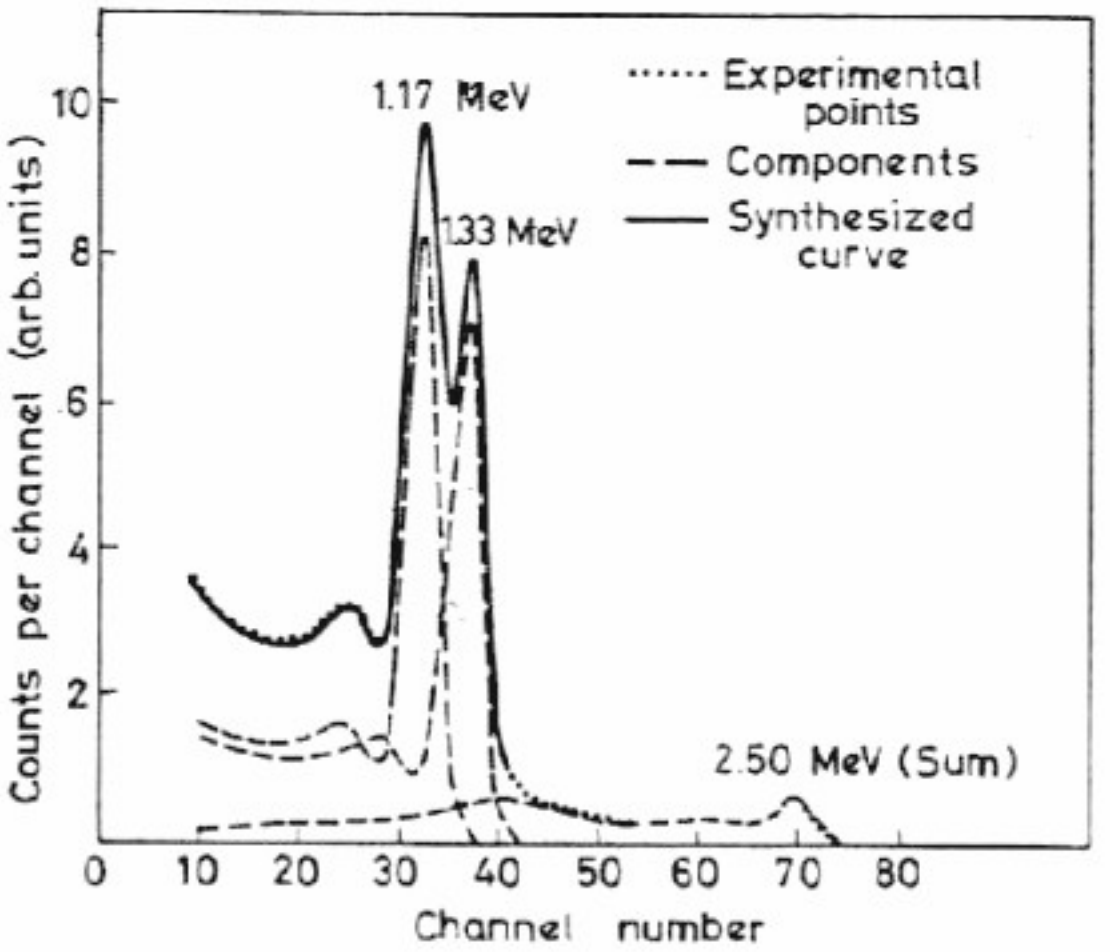

Fig. 42. Measured and calculated true sum-coincidence spectra of ^{60}Co 1.17 and 1.33 MeV gamma-rays. The source was placed centrally 3 cm from a 5" dia. by 4" long NaI(Tl) crystal [145]. The pulses above channel 41 are sum-coincidences.

response function in the evaluation, a true sum-coincidence component, calculated from Eq. (10.1), must be added to the spectra of coinciding radiations to prevent erroneous results and the discovery of non-existent gamma-rays from sum peaks. In Fig. 42 are shown the measured and calculated true sum-coincidence spectra of ^{60}Co gamma-rays [149].

10.3 RANDOM PULSE PILE-UP

The correct estimation of the random sum-coincidences (pile-up spectrum) is much more problematical. Measuring strong sources with high-efficiency detector pulse pile-up can cause serious errors if its contribution is not corrected appropriately. To simplify the discussion pile-up pulses are divided into two classes: (*a*) peak pile-up, which occurs when two pulses arrive within the time that the linear gate on the input of the analog-to-digital converter is open, and (*b*) tail pile-up, which happens when the ADC has completed the conversion but a second pulse comes before the tail of the preceding one has diminished. Tail pile-up effects are normally eliminated by a fixed dead-time, which ensures that pulses which are to be considered for amplitude measurement must have been preceded and followed by a fixed time period, longer than the overshoot recovery time, in which no detection event occurred. The number of random peak pile-up coincidences can be substantially reduced by special electronics without any significant loss in the single pulses [150–152]. The relative contribution to the spectrum of any type of pile-up can be lessened by reducing the source strength and/or the detector efficiency directly or by placing a thin lead absorber between

the source and the detector. The lead absorber is effective only when the attenuation for the principal gamma energy is less than the product of the attenuations of the lower energy photons seemingly giving the same energy by pulse pile-up.

Besides the spectrum distortion caused by pulse summing, there is a loss in the counting rate due to the finite dead-time of the spectrometer system. Due to tail pile-up this dead-time can not be very small (less than $\sim 10\mu s$ for multi-channel analysers) and relatively large losses may occur at high counting rates. If we denote by $n(E)$ the counting rate in the spectrum measured by a hypothetical ideal spectrometer with no random pile-up distortion and dead-time counting loss, then the counting rate in the observed spectrum is

$$n_{\text{obs}}(E) = n(E)\left[1 - (\tau_P + \tau_D)\int_0^{\bar{}} n(E)dE\right]$$

$$+ 2\tau_P \int_0^{\bar{}} n(E-x)\, n(x)dx\left(1 - \tau_D \int_0^{\bar{}} n(E)dE\right), \qquad (10.2)$$

where τ_D is the dead-time of the spectrometer (practically the dead-time of the multichannel analyser) and τ_P is the peak pile-up resolution time; two signals detected within this period will be summed. The term besides 1 in the first bracket is for dead-time counting correction and the second term is for random pulse summing.

Similar expressions can be written for all $y_{k,\,\text{obs}}(E)$, where $y_{k,\,\text{obs}}(E)$ and $y_k(E)$ are the response functions for the kth component measured (or calculated) individually with the real and the ideal spectrometer. If we denote by r_k the relative intensity ratio of component k in the complex spectrum compared to its standard, then

$$n(E) = \sum_{k\,=\,\text{all components}} r_k y_k(E)\,,$$

but as is obvious from Eq. (10.2), this is not true for the observed spectra,

$$n_{\text{obs}}(E) \neq \sum_{k\,=\,\text{all components}} r_k y_{k,\text{obs}}(E)\,.$$

Due to dead-time counting loss and coincidence summing, the individual components do not add linearly ! This means that one of the basic assumptions for least-squares resolution (assumption (b) of Section 6.1) is not fulfilled. As has already been mentioned, the error caused by this fact is negligible for low counting rates but increases quadratically with the counting rate.

Dead-time correction can be performed by calculation according to Eq. (10.2). The dead-time

$$\tau_D \approx \sum_{l\,=\,\text{all channels}} n(i)\ (A + Bi),$$

where $n(i)$ is the measured count in channel i and A and B are constants

for a given analyser. (For conventional multi-channel analysers $A \sim 10$–50 μs, $B \sim 0.04 - 1\mu$s.) Many multi-channel analysers have an optional built-in dead-time correction, giving the opportunity to measure in live-time instead of clock-time. If the measurement was performed in live-time, then $\tau_D = 0$ in Eq. (10.2).

The best way to correct for random pile-up, if it is necessary, is to do all measurements in live-time and determine the intensities, r_k, using the original standard spectra, $y_{k,\,\mathrm{obs}}(E)$, by any of the methods described in Chapters 5, 6 or 7. Then a new set of standards having intensities r_k times the original ones is created by

$$\bar{y}_k(E) = r_k y_{k,\mathrm{obs}}(E)\left[1 - \tau_P \int_0^\infty n_{\mathrm{obs}}(E)dE\right] + 2\tau_P \int_0^E n_{\mathrm{obs}}(E-x) r_k y_{k,\mathrm{obs}}(x)dx$$

and the spectrum is evaluated with $\bar{y}_k$'s as standards. In practice, the integrals are replaced by summing all over the channels. If necessary, the whole process can be repeated and a new set of standards can be calculated from the $\bar{y}_k$'s. If $\bar{r}_k$ is the relative intensity of $\bar{y}_k$, then the relative intensity of y_k will be $r_k \cdot \bar{r}_k$.

The effect of random pulse pile-up can be estimated by adding pulses of a pulse generator having well-known fixed amplitude and frequency to the spectrum. From the broadening of the peak and from the reduction of its area, the parameters necessary to construct the pile-up spectrum can be obtained.

It must be remembered that in all corrections it is assumed that the counting rate does not change rapidly during the measuring period. If this were not true, instantaneous corrections should be calculated and integrated over the measuring period. This would affect predominantly the results obtained for isotopes whose half-lives are shorter than or comparable to the measuring time.

10.4 MEASUREMENT OF ANNIHILATION GAMMA-RAYS

Positron emitters are most often identified by detecting one or both of the annihilation quanta. The strong angular correlation between the two photons can be exploited in coincidence measurements and provides a very sensitive method for detecting weak positron emitters in the presence of intense other radiations [110]. This is illustrated in Fig. 39 (Section 9.3). To distinguish between the different positron emitters and from the contribution of 0.511 MeV photons originating in the surroundings after the pair production process of high energy gamma-rays, the intensity determination is very often followed by a decay-curve analysis (Section 8.1).

In positron annihilation measurements the two main sources of errors are the summing effect and uncertainty in the place where the positron anni-

hilated. Less important is the variation in the energy of gamma-rays due to annihilation in flight [153, 154].

Summing effect was discussed in the previous paragraphs. To this it has to be added that when measuring positron emitters it is possible that one of the annihilation quanta will be detected in coincidence with the 180° Compton back-scattered gamma-ray of the other. This summing removes counts from the 0.511 MeV full-energy peak and results in a peak around ~0.7 MeV, whose magnitude can be relatively large in coincidence arrangements where scattering materials are near the detectors.

Most of the annihilations take place after the stopping of positrons. If the source is not sufficiently thick, only a small fraction of the positrons will be stopped in the source itself. The solid angle subtended by the detector depends on the place of annihilation, and varies with source thickness. It was shown [143] that depending on the thickness of the positron emitter and the absorber around the source the uncorrected results deviated by $\pm 20\%$ from the true positron activity. To avoid this it is best either to surround all sources with sufficient absorber (usually Be, or other light Z elements) or to use sources with the same thickness to assure that annihilation quanta will always be produced in the same volume.

To distinguish between annihilations taking place in the source (and in the sample holder) and in the surroundings (mainly in the shielding) two measurements are performed. In the first the source is on the straight line connecting the detectors, while in the second one it is outside it. The difference between the two measurements gives the positron activity of the sample. Special care must be taken that when moving either the source or a detector the solid angle of the detectors from the source should remain exactly the same, and their relative position to the shielding should not alter considerably. The same method can be applied when measuring weak positron emitters in the presence of other strong (coincident) but not β^+-emitting radiations.

10.5 CROSS-TALK COINCIDENCES

In coincidence measurement a photon after being Compton-scattered in one detector can reach the other one and produce a false coincidence. The relative intensity of this effect to the true coincidences can be reduced neither by shortening the resolving time, nor by reducing the efficiencies of the detectors. However, they can easily be recognized, because the peaks in cross-talk coincidence spectra are geometry-dependent and at the usual 180° geometry at the backscatter peaks and at the Compton edges of the gamma-rays present in the source. If they are disturbing, their relative contribution can usually be lessened by placing sufficient lead or lead collimator between the detectors to absorb the lower energy photons. Naturally, this additional lead increases the number of photons scattered into the detector from the surroundings.

Some possible geometrical arrangements to reduce cross-talk coincidences are shown in Fig. 43. The geometry shown in (b) considerably reduces

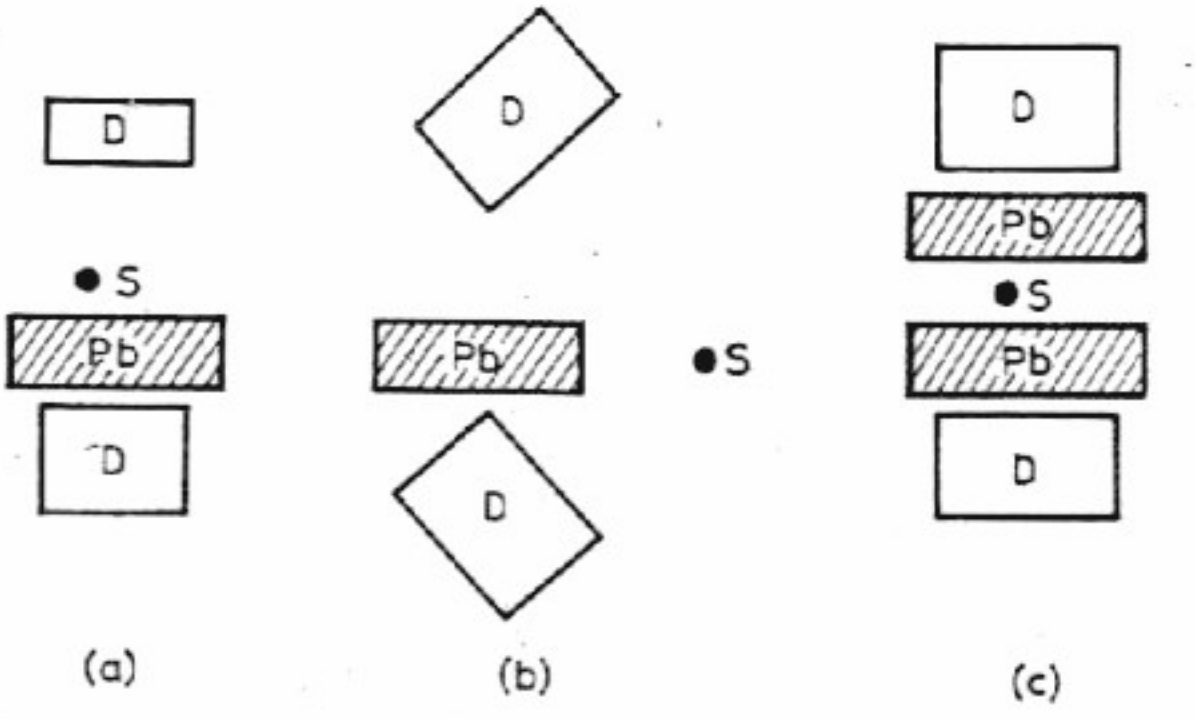

Fig. 43. Different geometrical arrangements to reduce cross-talk coincidences

cross-talk coincidences but gives much lower efficiency than normal coincidence arrangements without any lead absorber. For favourable energies the (a) geometry can give less cross-talk without reducing the coincidence efficiency too much. When measuring coincidences between gamma-rays in the energy region of backscatter radiation the geometry shown in (c) can be advantageous.

11. REFERENCES

1. *Applications of Computers to Nuclear and Radiochemistry, USAEC, NAS-NS.* 3107 (1962).
2. *Symposium on Radiochemical Methods of Analysis, Applications of Computers to Activation Analysis,* Vol. II. pp. 125–195, IAEA, Vienna, 1965.
3. J. R. De Voe, (Editor), *Modern Trends in Activation Analysis,* NBS Special Publications, No 312, Vol. II. pp 959–1259, (1969).
4. *Proc. Conf. on Computer Systems in Experimental Nuclear Physics, Skytop,* Penn. USA, 1969.
5. S. J. Lindenbaum, *Annual Review on Nuclear Sciences,* **16,** 619 (1966).
6. H. Gelertner, *Advances in Computers,* **6,** (1965).
7. K. A. Matalin, S. I. Csubarov and Zs. Náray, *Methodi Registracii i Obrabodki Dannih v Jadernoj Physike i Technica,* Atomizdat, Moscow, 1968.
8. P. Quittner and R. E. Wainerdi, *Atomic Energy Review,* **8,** (1970).
9. D. Gibbons, *Computer Methods in Activation Analysis; Principles and Applications,* Ch. 15., J. M. A. Lenihan and S. J. Thomson (Editors), Academic Press Inc. Ltd., London, 1965.
10. H. P. Yule in [3] pp. 1155–1204.
11. R. L. Heath in [3] pp. 959–1031.
12. E. Schonfeld, A. H. Kibbey and W. Davis, Jr., *Nucl. Instr.,* **45,** 1 (1966).
13. L. Jánossy, *Theory and Practice of the Evaluation of Measurements,* Clarendon Press, Oxford, 1965.
14. A. Rényi, *Wahrscheinlichkeitsrechnung mit einem Anhang über Informationstheorie,* Deutscher Verl. Wissenschaften, Berlin, 1962.
15. H. Cramer, *The Elements of Probability Theory,* J. Wiley & Sons Inc., New York, 1955.
16. B. L. Van der Werden, *Mathematische Statistik,* Springer Verl., Berlin-Göttingen-Heidelberg, 1957.
17. P. Quittner and A. Montvay, *Acta Chim. Hung.,* **51,** 37 (1967).
18. L. E. Fite, E. L. Steele and R. E. Wainerdi, *Investigations in Automated Activation Analysis,* TEES-2671-2, Cat. No. UC-23 Ch. 8. Section IV (1962).
19. A. Savitzky and M. J. E. Golay, *Anal. Chem.,* **36,** 1627 (1964).
20. H. P. Yule, *Nucl. Instr.,* **54,** 61 (1967).
21. K. Siegbahn (Editor), *Alpha-, Beta- and Gamma-Ray Spectroscopy,* North Holland Publishing Company, Amsterdam, 1965.
22. C. E. Crouthamel (Editor), *Applied Gamma-Ray Spectrometry,* Pergamon Press, London, 1960.
23. E. Segré (Editor), *Experimental Nuclear Physics,* J. Wiley & Sons Inc., New York, 1953.
24. C. D. Zerby and H. S. Moran, *Nucl. Instr.,* **14,** 115 (1961).
25. C. D. Zerby, A. Meyer and R. B. Murray, *Nucl. Instr.,* **12,** 115 (1961).
26. N. V. de Castro Faria and R. J. A. Levesque, *Nucl. Instr.,* **46,** 325 (1967).
27. V. J. Orphan and N. C. Rasmussen, *IEEE Trans. Nucl. Sci.,* NS-14 544 (1967).
28. C. M. Lederer, J. M. Hollander and I. Perlman, *Table of Isotopes,* Sixth Edition, J. Wiley & Sons Inc., New York, 1967.
29. R. L. Heath, *Scintillation Spectrometry, Gamma-Ray Spectrum Catalogue,* IDO-16880, TID-4500 (1964).
30. J. H. Neiler and P. R. Bell, in [21] Vol. I. Ch. V.
31. R. van Lieshout, A. H. Wapstra, R. A. Ricci and R. K. Girgis, in [21] Vol. I. Ch. VIII. B.

32. B. R. Kowalski and T. L. Isenhour, *Anal. Chem.*, **40,** 1186 (1968).
33. R. L. Heath, R. G. Helmer, L. A. Schmittroth and G. A. Cazier, *Nucl. Instr.*, **47,** 281 (1967).
34. R. G. Helmer, R. L. Heath, M. Punam and D. H. Gibson, *Nucl. Instr.*, **57,** 46 (1967).
35. D. P. Donelly, H. W. Baer, J. J. Reidy and M. L. Wiedenbeck, *Nucl. Instr.*, **57,** 219 (1967).
36. G. T. Evan and A. J. Tavendale, *Can. Journ. Phys.*, **42,** 2286 (1964).
37. D. Engelkemir, *Rev. Sci. Instr.*, **27,** 589 (1956).
38. R. L. Heath, *IRE Trans Nucl. Sci.*, NS-9, **3,** 294 (1962).
39. L. Salmon, in [2] p. 125.
40. B. J. Allen, J. R. Bird and S. Engström, *Nucl. Instr.*, **53,** 61 (1967).
41. J. Kopeczky, W. Ratynski and E. Warming, *Nucl. Instr.*, **50,** 213 (1966).
42. K. M. Kaino and G. F. Knoll, *Nucl. Instr.*, **44,** 213 (1966).
43. E. S. Fry, J. M. Palms and R. B. Day, LA-3456 (1966).
44. J. R. Morrey, *Anal. Chem.*, **40,** 905 (1968).
45. H. P. Yule, in [3] p. 1256.
46. G. Guzzi, J. Pauly, F. Girardi and B. Dorpema, *EUR-3469e* (1967).
47. F. Girardi, G. Guzzi and J. Pauly, *Radiochem. Acta*, **7,** 202 (1967).
48. W. E. Kuykendall and R. E. Wainerdi, *Proc. IAEA Conf. on the Use of Radioisotopes in Physical Sciences and Industry*, Copenhagen, 1960.
49. H. P. Yule, *Anal. Chem.*, **38,** 103 (1966).
50. H. P. Yule, private communication.
51. M. A. Mariscotti, *Nucl. Instr.*, **50,** 309 (1967).
52. A. Ádám, P. Quittner and P. Zentai, *KFKI Közl.*, **9,** 293 (1961).
53. W. R. Kane and M. A. Mariscotti, *Nucl. Instr.*, **56,** 189 (1967).
54. J. M. Freemand and J. C. Jenkin, *Nucl. Instr.*, **43,** 269 (1966).
55. C. E. Crouthamel, C. Gatrousis and S. J. Groslovich, in [22] Appendix III.
56. C. C. Grossjean and W. Bossert, *Table of Absolute Detection Efficiency of Cylindrical Scintillation Gamma-Ray Detectors*, Computing Laboratory, University of Ghent, 1965.
57. B. Angström, A. H. Wapstra, S. Thulin and I. Bergström, *Arkiv Fysik*, **7,** 247 (1954).
58. R. L. Heath, in [3] p. 959.
59. D. F. Covell, *Anal. Chem.*, **31,** 1785 (1959).
60. H. P. Yule, *Anal. Chem.*, **40,** 1480 (1968).
61. W. Schulze, *Z. Anal. Chem.*, **234,** 401 (1968).
62. S. C. Choy and R. A. Schmitt, *Nature*, **205,** 758 (1965).
63. P. Quittner, *Anal. Chem.*, **41,** 11 (1969).
64. P. Quittner, *Nucl. Instr.*, **76,** 115 (1969).
65. J. D. Reber, and J. K. Major, *Nucl. Instr.*, **23,** 162 (1963).
66. F. B. Hildebrand, *Introduction to Numerical Analysis*, McGraw-Hill Book Co., New York, 1956.
67. P. Quittner and R. E. Wainerdi, *Nucl. Instr.*, **74,** 33 (1969).
68. E. Schonfeld, *Proc. Conf. Modern Trends in Activation Analysis*, p. 279, College Station, Texas, 1965.
69. L. Salmon, in [1] p. 165.
70. P. Quittner, to be published.
71. P. Müller, *IKF-10*, 1963 (German Federal Republic).
72. L. Salmon, *Nucl. Instr.*, **14,** 193 (1961).
73. E. Schonfeld, *Nucl. Instr.*, **42,** 213 (1966).
74. W. L. Nicholson, J. E. Schlosser and F. P. Bauer, in [1] p. 254.
75. W. L. Nicholson, J. E. Schlosser and F. P. Bauer, *Nucl. Instr.*, **25,** 45 (1963).
76. P. D. Drew, L. E. Fite and R. E. Wainerdi, in [1], p. 127.
77. J. I. Trombka, in [1] p. 183.
78. L. Salmon, in [2] p. 125.
79. H. Münzel, in [2] p. 141.
80. G. Perneczky and P. Quittner, *KFKI preprint* No. 5. Budapest, Hungary, (1967).
81. R. A. Dudley and A. Ben Haim, in [2] p. 69.

82. P. Quittner, *Nucl. Instr.*, **51**, 273 (1967).
83. W. R. Burrus and D. Bogert, in [1] p. 127.
84. J. R. Wohlberg, *Proc. Conf. Modern Trends in Activation Analysis*, p. 13., College Station, Texas 1965.
85. R. M. Parr and H. F. Lucas, Jr., *IEEE Trans on Nucl. Sci.*, NS-11, 349 (1964).
86. J. I. Trombka and R. L. Schmadebeck, *Nucl. Instr.*, **62**, 253 (1968).
87. R. L. Heath, R. G. Helmer, L. A. Schmittroth and F. A. Cazier, *IDO-17017*. (1965).
88. P. Paatero, *Nucl. Instr.*, **31**, 360 (1964).
89. J. J. Steyn and D. G. Andrews, in [3] p. 1231.
90. E. Schonfeld, *ORNL-3975* (1966).
91. G. Perneczky, private communication.
92. R. van Lieshout, A. H. Wapstra, R. A. Ricci and R. K. Girgis, in [21] § 5, p. 524.
93. O. V. Anders and W. H. Beamer, *Anal. Chem.*, **33**, 226 (1961).
94. W. Lee, *Anal. Chem.*, **31**, 800 (1959).
95. O. Kempthorne, *The Design and Analysis of Experiments*, J. Wiley & Sons Inc., New York, 1952, p. 55.
96. J. B. Cuming, in [1] p. 25.
97. D. G. Gardner and J. C. Gardner, in [1] p. 33.
98. D. G. Gardner, J. C. Gardner, G. Laush and W. W. Meinke, *J. Chem. Phys.*, **31**, 978 (1969).
99. T. L. Isenhour and G. H. Morrison, *Anal. Chem.*, **36**, 1089 (1964).
100. T. L. Isenhour, *Proc. Conf. Modern Trends in Activation Analysis*, College Station, Texas, 1965, p. 123.
101. P. Quittner and A. Montvay, *Acta Chim. Hung.*, **51**, 37 (1967).
102. R. E. Wainerdi, L. E. Fite, D. Gibbons, W. W. Wilkens, P. Jimanez and D. Drew, in [2] p. 149.
103. L. E. Fite, D. Gibbons and R. E. Wainerdi, TEES-2671-1 (Texas) (1961).
104. W. S. Lyon (Editor), *Guide to Activation Analysis*, D. van Nostrand Publishing Company, Princeton, 1964.
105. D. Taylor, *Neutron Irradiation and Activation Analysis*, George Newnes Ltd. London, 1964.
106. J. M. A. Lenihan and S. J. Thomson (Editors), *Activation Analysis: Principles and Applications*, Academic Press Inc. Ltd., London, 1965.
107. C. Engelman, in [2] Vol. I. p. 341.
108. P. Quittner, *Acta Chim. Hung.*, **54**, 127 (1967).
109. W. E. Kuykendall and R. E. Wainerdi, *Proc. IAEA Conf. The Use of Radioisotopes in Phys. Sci. and Industry*, Copenhagen, Denmark, 1960.
110. J. Bogáncs, P. Quittner and E. Szabó, *Magy. Kém. Folyóirat*, **73**, 346 (1967).
111. O. V. Anders, *Dow Chemical Co. Publ.*, (1961).
112. R. Gunnick, J. B. Niday, in [3] p. 1244.
113. R. Gunnick, H. B. Levy and J. B. Niday, *UCID-15140* (USA) (1967).
114. H. P. Yule, in [3] p. 1108.
115. M. D. Cohen, *Proc. Modern Trends in Activation Analysis*, College Station, Texas, 1965.
116. T. B. Pierce, R. K. Webster, R. Hallett and D. Mapper, in [3] p. 1116.
117. F. Girardi, G. Guzzi, G. Di Cola, W. Becker and A. Terminani, in [3] p. 1111.
118. J. Pauly, G. Guzzi, F. Girardi and A. Borella, *Nucl. Instr.*, **42**, 15 (1966).
119. *Proc. of the Karlsruhe Conf. on Automatic Acquisition and Reduction of Nuclear Data*, Karlsruhe, German Federal Republic, 1964.
120. *Proc. Conf. on Computer Systems in Experimental Nuclear Physics, Skytop*, Penn. USA, 1969.
121. *Nucl. Spec. Rep. Nucl.*, **22**, Ns-12, December, 1964.
122. C. J. Thompson, in [3] p. 1121.
123. J. I. Trombka, R. L. Schmadeback, in [3] p. 1097.
124. Z. Seres, private communication.
125. Z. Zámori, B. Kardon, Z. Seres, J. Biri and L. Somlai, *XX. Ezhegodnoe soveshchanie po yadernoi shpektroskopii i struktura atomnogo yadra, 28. Jan. — 5. Febr. 1970*, Leningrad.

126. V. I. Goldanskii and M. I. Podgoreckii, *ZsETPH* **29,** 559 (1955).
127. G. Bertolini and A. Coche (Editors), *Semiconductor Detectors,* North-Holland Publishing Company, Amsterdam, 1968.
128. G. T. Evan and A. J. Tavendale, *Can. Journ. Phys.*, **42,** 2286 (1964).
129. R. L. Chase, *Nuclear Pulse Spectrometry,* McGraw-Hill, New York, 1961.
130. C. C. Trail and S. Raboy, *Rev. Sci. Instr.*, **30,** 425 (1950).
131. N. A. Wogman, D. E. Robertson and R. W. Perkins, *Nucl. Instr.*, **50,** 1 (1967).
132. J. A. Cooper, L. A. Rancitelli, R. W. Perkins, W. A. Haller and A. L. Jackson, in [3] p. 1054.
133. J. A. Cooper, L. A. Rancitelli and R. W. Perkins, *J. Radioanal. Chem.*, to be published.
134. A. J. Tavendale, *IEEE Trans. Nucl. Sci.*, NS-11, No. 3, 191 (1964).
135. G. T. Evan and A. J. Tavendale, *Nucl. Instr.*, **26,** 229 (1964).
136. P. Suominen and J. Kantele, *Nucl. Instr.*, **58,** 229 (1968).
137. S. De Benedetti and R. W. Finley, *The Coincidence Method,* in *Handbuch der Physik,* **45,** Springer Verlag, Berlin, 1958, p. 222.
138. A. H. Wapstra, in *Alpha-, Beta- and Gamma-Ray Spectroscopy,* K. Siegbahn (Editor), North Holland Publishing Company Amsterdam, 1965. Vol. I. Ch. VIII. C.
139. E. B. Sheba, K. J. Casper and B. L. Robinson, *Nucl. Instr.*, **24,** 482 (1963).
140. *Proc. Conf. Utilization Multi-parameter Analysers,* Columbia University Report, C. U. (PMPL)-227 (1960).
141. A. M. Hoogenboom, *Nucl. Instr.*, **3,** 57 (1958).
142. J. Kantele and R. W. Fink, *Nucl. Instr.*, **15,** 69 (1962).
143. W. S. Lyon, J. S. Eldridge and P. Crowther in [2] p. 33.
144. N. H. Lazar, *IRE Trans. Nucl. Sci.*, NS-5, No-3, 138 (1958).
145. C. A. Knowlin and J. L. Blankenship, *Rev. Sci. Instr.*, **36,** 1830 (1965).
146. R. L. Chase and L. R. Poulo, *IEEE Trans. on Nucl. Sci.*, NS-14, 83 (1967, February).
147. L. B. Robinson, *Rev. Sci. Instr.*, **32,** 1057 (1961).
148. E. A. Gere and G. L. Miller, *IEEE Trans. on Nucl. Sci.*, NS-14, 89 (1967, February).
149. G. Bradford, R. B. Galloway, R. M. Silitto and D. G. Vass, *Nucl. Instr.*, **52,** 93 (1967).
150. R. Rozen, *Nucl. Instr.*, **11,** 316 (1961).
151. Gy. Máthé, *Nucl. Instr.*, **23,** 261 (1963).
152. M. G. Strauss, *Rev. Sci. Instr.*, **34,** 335 (1963).
153. R. A. Ricci, R. K. Girgis and R. Van Lieshout, *Nuovo Cimento,* **11,** 156 (1959).
154. J. B. Gerhart, B. C. Carlson and R. Sherr, *Phys. Rev.*, **94,** 917 (1957).

AUTHOR INDEX

SUBJECT INDEX